Toward a better Understanding of Europa Crevasses

Application of Linear Elastic Fracture Mechanics to Europa

Mattia Poinelli

TUDelft
Delft
University of
Technology

Challenge the future

Toward a better Understanding of Europa Crevasses

Application of Linear Elastic Fracture Mechanics to Europa

by

Mattia Poinelli

in partial fulfillment of the requirements for the degree of

Master of Science
in Aerospace Engineering

at the Delft University of Technology,
to be defended publicly on Monday November 13th, 2017 at 5:00 PM.

Supervisors:	Prof. Dr. L. L. A. Vermeersen,	Technical University Delft
	Dr. Ir. E. Larour,	NASA Jet Propulsion Laboratory
	Dr. J. Castillo-Rogez,	NASA Jet Propulsion Laboratory
Thesis committee:	Dr. S. Cazaux,	Technical University Delft
	Ir. P. P. Sundaramoorthy,	Technical University Delft

This thesis is confidential and cannot be made public until November 13, 2017.

An electronic version of this thesis is available at `http://repository.tudelft.nl/`.

-"Sal, we gotta go and never stop going 'till we get there."
-"Where we going, man?"
-"I don't know but we gotta go."

Jack Kerouac, On the Road

ACKNOWLEDGEMENTS

ABSTRACT

Europa is one of the most interesting celestial world that has been ever observed. The habitability condition, met for the liquid water layer covering the moon, yields to astonishing speculations concerning what might exist in the interior of the tiniest moon of Jupiter. The *Voyager* and *Galileo* programs detected a frozen and brittle layer, deeply battered by lineament features. These lineament formations have been distinguished in the literature in terms of ridges, strike-slips and cycloids. The majority of the features is suggesting the presence of fractures that can resemble linear patterns such as the ones observed. The observed crevasses on the moon's icy surface can be considered as results of a strong and variating stress field applied to the brittle icy shell that eventually reaches critical deformation conditions locally, and lead the process of crevasse propagation. Stress components acting at different timescales can be found on Europa, and these could be modelled with the usage of potential theory, among others. Non-zero eccentricity of the Europa orbit, together with the non-zero obliquity and the possible physical libration of the ice crust induce stress sources that work at a short timescale, namely one orbital period of Europa around Jupiter. These short-term components are called diurnal tides. On the other hand, the estimated non-synchronous rotation of the moon, the true polar wander and the progressive thickening of the ice shell deform the surface of Europa at a timescale that is several orders of magnitude higher that the diurnal components and can be termed as secular contributors. The superimposition of secular widening to diurnal components is the source of stress that continuously deforms the brittle surface of Europa and induces the ice to crack, similarly to the processes observed with crevasses in large terrestrial ice sheets.

The current research's aim is to improve the existing models of fracture propagation for the Europa ice shell, dealing with analogs observed in Earth's crevasses on large ice shelves, by the implementation and the usage of linear elastic fracture mechanics (LEFM). The numerical technique has been already applied to Europa in order to determine whether or not the fractures crack the entire ice layer. The current project aims to improve the models already developed in order to produce a global estimation of potential vertical critical depth for surface crevasses and critical heights for bottom crevasses, using a model designed for terrestrial fractures on ice sheets. Tidal stress, coupled with ice overburden pressure and water-pressure filling the crevasses are the deforming sources at the tip of an existing crack. Two different LEFM approaches are included in the document, one dealing with the estimation of global areas on the moon that are more favourable to host propagation and one dealing with the estimation of fractures' lengths for specific observed features. Results describe the existence of critical and non-critical areas centred in the equatorial zone which are respectively prone or not to present vertical propagation. Maximum critical depths reaches maximum values of 120 meters while critical heights touches values of 1.5 kilometers, around ten orders of magnitudes higher than the former. Additionally to the outcomes of the vertical simulation, a mathematical manipulation of the LEFM analysis allowed the determination of horizontal propagation events. Knowing the aspect of an observed fracture, the current research calculated fracturing events that reach propagation rates of kilometers per second. These are almost instantaneous events that are similar to what happens to terrestrial crevasses on large ice sheets, such as the recent calving event of the Larsen C on July 2017. A comparison between the two approaches indicates that the non-critical areas seem to arrest the horizontal propagation of the lineament features, beside discouraging the vertical growth of the same crevasses.

The outcomes of the current research are interesting when seen in relation with the future exploration missions to Europa: ESA's *JUICE* and NASA *Europa Clipper*. These are planned to reach the Jovian environment at the end of the 2020's and will enormously improve the actual knowledge of dynamics and geology of the satellite. Additionally, NASA is considering the idea of hosting a lander in the *Clipper*'s spacecraft. Having already a preliminary determination of potential interesting landing sites could be very helpful. Additionally, the extremely large dimensions for the observed lineament features on the moon would imply a tremendous and detectable release of energy when fractured. The current research tries to deal with these issues, in order to give preliminary helpful estimation to the missions' design. In more general terms, new numerical models that can simulate the propagation events on the surface of Europa and that will result as output of the current research, will yield to a further and more accurate understanding of the dynamics for the interior of one of the most promising celestial object, in term of searching for a biosphere, hence extraterrestrial life.

CONTENTS

LIST OF FIGURES

LIST OF TABLES

LIST OF ACRONYMS

FEM	Finite Element Methods
GIS	Geographic Information System
GEM	Galileo Europa Mission
GMM	Galileo Millennium Mission
GPS	Global Positioning System
Hemi	Hemisphere (Function)
IAU	International Astronomical Union
IR	Infrared
JPL	Jet Propulsion Laboratory
JUICE	Jupiter Icy Moons Explorer
LEFM	Linear Elastic Fracture Mechanics
NASA	National Aeronautic and Space Administration
NSR	Non-Synchronous Rotation
SSI	(Galileo) Solid State Imager
TPW	True Polar Wander
US	United States (of America)
VDV	Van der Veen (Model)
2D	Two Dimensions
3D	Three Dimensions

To those who love me

1

INTRODUCTION

More than 400 years after the first observation of the Jovian moon by Galileo Galilei, an Italian astronomer, a new beginning for the exploration of the so-called Galilean satellites is about to start, by the end of the next decade. Probably one of the more successful NASA mission, named after the discoverer of the moons *Galileo*, was directly focussed to the understanding of Io, Europa, Ganymede and Callisto in the Jovian environment. After the team of scientists and of engineers started to analyse data and images coming from Europa, a full extension of the *Galileo* mission was entirely directed to complete flybys of the tiny satellite of the gas giant, since people started to realise how scientifically promising was the moon. One of the first astonishing findings emerged from the analysis of Europa, is that a global water ocean is covering the satellite. In the absence of a proper atmosphere and given the large distance with the Sun, the extreme outer layer is supposed to be totally frozen. Pictures coming from *Galileo* showed an outer ice crust that is deeply battered by extremely long lineaments and by chaotic regions. The presence of lineament features is generally linked to the existence of fractures on the brittle ice shell. The deformation of Europa in form of rifts and faults, is considered to be the most evident result of a strong stress field that is continuously varying in amplitude and orientation and that is also applied to the fragile icy surface of the moon. Tides on Europa are several orders of magnitude larger than the ones observed on Earth, where these are one of the most important element that stimulate the ocean to be as biologically variegate as possible. Mixing of different chemical components are due to currents circulations produced by tidal effects, among others. Beside the potential analogue effects that can be produced on the subsurface ocean the moon, one of the key consequences is that large tidal dissipation would produce an amount of heat, assumed to be enough to maintain the water layer in a liquid state for the majority of its status. Liquid water is naturally one of the fundamental element needed to sustain life as we know.

More than 10 years after the official end of the *Galileo* mission which dived into the atmosphere of Jupiter, new projects are about to initiate the new era of the exploration of the Medicean moons. The new *Jupiter Icy Moons Explorer* mission (*JUICE*) is estimated to be launched around 2022, according to ESA and is going to target the Galilean moons. Besides, NASA is considering to launch the *Europa Clipper* mission, with the specific focus of Europa, just a few years after the *JUICE* mission. In particular, the possibility of placing a lander, contemplated by the *Clipper* design team on the crust of the moon, would be a gigantic step toward the global understanding of the dynamical and geological processes on the satellite. For instance, one or more seismometers would definitely allow a complete characterisation of the moon's stratification that is still an argument of discussion. The new data and the intriguing outcomes that these missions would eventually bring to our knowledge of Europa are elements that keep the attention toward researches and studies concerning the Jovian moon. Among others, the condition of habitability[1] is considered to be met for an ocean that is globally covering the satellite's core. Therefore, theoretically speaking life could potentially form. In its outer portion, the water layer is considered to be frozen, fact that would protect the potential life forms

---

[1] The definition of a planet's habitability is not universally defined, but the majority of the set of requirements are requiring the presence of water.

from the deadly radiation field coming from Jupiter. The fractures that are deforming and creating disconti-
nuities in the potential flow of ice on the surface could be suitable to host biological material themselves, in
the case that these are somehow in contact with the global ocean. As natural consequence of the fascinating
discoveries of *Galileo*, the focus of scientific community is concentrated on continuously new speculations
concerning the tiniest moon of Jupiter. Nevertheless, there is still a lot to do and a few characteristics and
physical parameters are effectively considered to be known for sure. The necessity of obtaining new data is
continuously suggested by the majority of the people involved with planetary sciences. This gap of observa-
tions should be filled with the measurements of *JUICE* and *Europa Clipper*.

Questions concerning the physical reasons of the existence of crevasses on Europa, dealing with the pos-
sibility of comparison with terrestrial features observed on large ice shelves are few of the aspects that could
be enlightened by future exploration missions. Hundreds of article and researches have been published since
the first direct observations of the surface and numerical models have been based on the (limited) amount
of data available. As consequence, for the same physical phenomenon, multiple physical explanations and
apparently several valid models have been proposed. Among the most interesting application of numerical
analysis to the investigation of the dynamical behaviour of the crevasses, a few works successfully applied
linear elastic fracture mechanics in order to mainly determine whether or not the fractures are cracking the
entire ice layer. The described scenario is very interesting, particularly when related to the possibility of hav-
ing an active lander on the surface of the moon. Indeed, in the case of a connection between the ocean and
the outside surface, a probable possibility is that material from underneath the moon is ejected to the sur-
face, thus easier detected and analysed by lander's potential instruments. Linear elastic fracture mechanics
is a numerical analysis that investigate the conditions around the tip of an existing crack, in order to de-
termine whether or not the material reaches the eventual propagation threshold. Estimation of thicknesses
and of potential length of fractures are seeing completely different scientific points of view, and more data
are needed to actually determine what is the dynamical behaviour of such large fractures. Furthermore, the
actual determination of areas of the moon that are more prone to present fractures would be an enormous
help in the preliminary selection of potentially interesting landing sites. Areas that are more favourable to
host horizontal and/or vertical propagation would be the preferred target zones to place the lander. The aim
of the current research is to improve the existing models of vertical and horizontal rifts propagation for the
Europa ice shell, dealing with analogs observed in Earth's ice shelves, by the implementation and usage of
a linear elastic fracture mechanics analysis. The project adopts a model that was successfully developed for
the investigation of terrestrial crevasses observed on the large terrestrial ice sheets in order to tune it with the
physics known for Europa and to find estimation of depths for surface crevasses and of heights for eventual
bottom crevasses together with the calculation of horizontal propagation rates for the fractures themselves.
In particular, the last concept can be assuming the description of different scenarios, where cracks are prop-
agating in a very slow way or with almost instantaneous fracturing events. The solutions of the numerical
simulation, presented in the document, opted for the second scenario with a similarity to what happens on
terrestrial crevasses on large ice sheet, such as the recent rupture of the Larsen C ice shelf in Antarctica.

The current report represent the technical presentation of the numerical model built with the aim of in-
vestigating vertical and horizontal propagation of Europa's crevasses. The document is divided into three
different Parts with the key purpose of schematise the presentation of the current research. Part I aims to
present what is known already about the generality of Europa. Being the research aim specifically focussed
on the investigation of propagation events on the surface of the moon, the icy crust of Europa finds central
focus. Additional sections are based on the qualitative presentation of the stress sources, analysed via tidal
potential theory and limited to the effect of non circularity of the Europa's orbit around Jupiter, the tilt of the
moon's rotation axis and the physical libration of the crust, together with the non synchronous rotation of the
crust with respect to the interior core. This part also presents, describe and tries to catalogue the lineament
features observed on the crust. Ridges, strike-slips and a type of feature only observed on Europa and named
cycloids are some of the lineaments observed on the surface and here these are described in details, by keep-
ing a particular attention to the introduction of terrestrial analogues. The reader is encouraged to view this
Part of the document to have a global view of the state of the art for the most important findings concern-
ing Europa with a specific focus on the description of the crust environment. Part II wants to describe the
theoretical and mathematical methodology behind the building of the numerical routines. The description
of the brittle fracture of Europa via linear elastic fracture mechanics requires basics of elasticity theory, since
the material is assumed to be purely elastic. The framework of the numerical model, firstly applied to terres-
trial crevasses by a Dutch glaciologist C. J. Van Der Veen is presented in this part of the document, together
with other models applied to crevasses propagation. The stress field that is required to be acting on the tip

of the fracture is also shown in its analytical details in this Part. Readers not interested in the full mathematical description of the model and the theoretical background for the research can freely skip this purely mathematical Part. Finally, Part III aims to present the built numerical model in its technical details. This is distinguished between vertical and horizontal propagation, depending on the different results obtained. A validation section is added in this Part with the main scope of defining the range of validity of the current routines. Of course, the mentioned lack of observational data for Europa does not allow a directly validation of the satellite's results. Nevertheless, one of the few experimental work focussed on the measuring of terrestrial crevasses' depths is used to positively validate the numerical model. The most important results, always presented with a critical discussion and with a comparison with the past literature on the moon are also presented in this Part of the document.

Outcomes of the current research allows a better understanding of how propagation works on Europa. Key results for the vertical approach are surface and bottom crevasses critical depths and heights. Additionally, areas that are more prone to host the two direction of propagation are also delimited. On the other hand, horizontal propagation routines allow the estimation of the fracturing event's amplitude for propagation rates. Propagation rates and the discretisation of a set of target features observed on the surface produced an evaluation of the number of orbital cycles needed to fully develop the lineaments. The outcomes of the numerical model are particularly interesting when seen in relationship with the potential measurements that future exploration missions, such as *Europa Clipper* or *JUICE* could bring. These could potentially corroborate or reconsider the estimations found in the current research. A further improvement in the analysis of Europa's crevasses is a further step in the understanding of one of the most promising satellites in the Solar System, when speaking of search of a biosphere, hence of life.

I

EUROPA

2

HERITAGE

The story goes that Galileo Galilei was the first man that decided to point his brand new telescope toward the sky. Among the wonders that he had the chance to stare at, he discovered and kept track of four mysterious stars that were dancing around the path of Jupiter through the night sky. Their peculiar pattern intrigued the Italian scientist so much to let him thinking that they were actually orbiting Jupiter itself, something completely against the heliocentric and religious view and mentality of the time. The *Sidereus Nuncius*, published in 1610 when Galileo was professor at the University of Padua, Italy, records the first scientific publication concerning the four new Medicean satellites around Jupiter. These satellites were named after Lorenzo de Medici, archduke of Florence at the time. Io, Europa, Ganymede and Callisto were part of the astronomical records henceforth.

Around 400 years after the discoveries of Galileo, a man-built spacecraft named after the Italian scientist was launched with the purpose of reaching Jupiter and its satellites. The investigation of the two gas giants of the Solar System, Jupiter and Saturn, have been one of the most ambitious and rewarding goal of space exploration. The main findings that the human kind evinced from the planets are results of the investigation of the two *Voyager* spacecrafts in the late '70s, followed by the *Galileo* and *Cassini* missions, launched in the late '90s and in the early '00s, respectively. Probably, these missions and their findings have been the most intriguing and though challenges of the human scientific research. Nowadays, given the promising habitable conditions of one the four Medicean moons, Europa, the focus of the scientific community is constantly kept pointed toward the tiny icy satellite. Therefore, one of the next big challenge of space exploration is the further investigation and studying of the Europa, by new and exciting NASA and ESA missions. The ESA's *Jupiter Icy Moons Explorer* (JUICE) and the NASA's *Europa Clipper* are scheduled to be launched in 2022 and have as main target Europa and its neighbour moons.

Galileo noticed that these 'erratic stars' were moving in the sky with an intriguing pattern. Modern science knows that these moons are orbiting in a resonant state which leads to a perturbation of their orbital parameters [54]. Io, Europa and Ganymede are orbiting in a so-called 1:2:4 orbital ratio, meaning that while Ganymede completes one cycle around Jupiter, Europa ends his second orbit and Io its fourth. In other words, Io orbits Jupiter 2 times more frequently than Europa, which orbits 2 times more frequently than Ganymede. The particular type of orbital resonance that characterises to the Medicean satellites in the Jovian environment is called mean motion resonance and is particularly frequent phenomenon in the Solar System. Resonance occurs when a dynamic system is forced by perturbation with a frequency that is commensurable with the natural frequency of the system [54]. The amplitude of the response of the system to such perturbation is amplified, and the effects are often easy to see. Resonant forcing might lead to forced eccentricities, obliquities or inclinations. Orbital resonance of asteroids with Jupiter is considered to be the main reason for the generation (and the sustenance) of the Kirkwood gap in the asteroid belt.

The current chapter aims to give the general background and the key findings on the Jovian moon Europa, obtained by the various missions to Jupiter combined with astronomical observations and numerical models that produces a complete literature survey. As previously mentioned, the satellite's shape and behaviour is

mainly influenced by the massive and disturbing presence of Jupiter, together with the orbital perturbations of the other neighbour moons. In section 2.1, the state of the art for the description of Europa is summarised. This part includes different estimation of the vertical stratification of the moon together with the geological processes that are supposed to be influencing the shape of the surface. On the other hand, a first (and mostly qualitative) description of the stress that is deforming the brittle surface is presented in section 2.2. A more quantitative description of the stress that is used in the current research is given in Chapter 4, when the tidal potential is introduced in the analysis.

A detailed description of Europa in its general aspects is a key aspect in the analysis of its cracks. A lot have been published although the amount of data to corroborate the results is limited. The *Galileo* mission which represents the most substantial source of data for Europa, completed around 12 flybys, counting no more than 150 photos. Therefore, the speculations about the moon are often not showing confirmation in the reality. The reader is referred to the review book Pappalardo et al. [71] for a global and detailed overview of the findings for the moon in all its investigated details.

2.1. AN OCEAN WORLD

The state of the art for the description of the Europa's interior is a silicate core that is covered by a global H_2O liquid ocean. The upper part of the ocean is thought to be far enough from the moons' internal heat sources and it is basically formed by ice. Additionally, this extremely cold and brittle ice layer shields and protect the ocean from the deadly radiation of Jupiter. Europa revealed to possess a curious surface shape already by studying data coming from the *Voyager* mission in the late '70s [99]. The *Voyager* team observed that a substantial amount of the surface shows lineament pattern which have been interpreted as cracks. Already since the very early stages of the Europa investigations, these cracks have been assumed as result of a continuous deforming tidal effects. Tides on Europa are strong, considering the massive influence of the host planet Jupiter. The relative absence of impact craters lead the scientists to assume a fast resurfacing surface and the possible presence of water. Furthermore, IR absorption spectrum revealed a strong signal in H_2O [75] which began to speculations on the possibility of habitability.

Figure 2.1 shows one of the first pictures that the Jet Propulsion Laboratory (JPL) internal televisions were transmitting live [71] from the *Voyager* spacecraft. Already in this coarse image, the lineament patterns are evident and they immediately began to rise up questions and speculations about their characterisation and origins. After *Voyager*, the two proposed successful extensions for the *Galileo* mission had as main target Europa, and a lot more was discovered, henceforth. *Galileo* first extended mission from late 1997 to late 1999 was named *Galileo* Europa Mission (GEM), while the second one is the *Galileo* Millenium Mission (GMM), performed until the controlled dive of the spacecraft into the gas giant in 2003. In total, the prime mission and the two extensions allowed the spacecraft to complete 12 close encounters, with a joint operation with the *Cassini* mission for the GMM. The total amount of pictures that were taken by the *Galileo* Solid State Imager (SSI) for the Europa surface are around 150, with best resolution of 21 m/pixel. Such a small amount of optical data has definitely under-constrained the evaluation of the several and in-

Figure 2.1: One of the first images that the *Voyager* 2 spacecraft of the Europa surface. Image taken on July 9, 1979. Image credit: NASA/JPL.

triguing problems that raised with the first observations of the moon. Nowadays, two new ESA and NASA mission, JUICE and the *Europa Clipper*, respectively, are planned to be launched in the early 2020 with main target Europa. The successful outcomes for the two missions will definitely help to constrain and to solve more questions that Europa is posing to the scientific community, beside finding new puzzling findings.

The most relevant evidence for the presence of a subsurface ocean underneath the brittle icy shell is the fact that the magnetometer mounted on the *Galileo* spacecraft recorded an induced magnetic field. During

the extension mission GEM, the two flybys E4 and E14 were specifically designed to capture evidence of a magnetic field on Europa [48]. The data coming from the magnetometer confirmed that the moon is not generating a proper magnetic field itself, but some disturbances with the background magnetic environment (associated with Jupiter) allowed the *Galileo* team to first speculate abut an induced magnetic field, instead. It is known that a static magnetic field is decaying and vanishing with the passing of time. On the other hand, in order to maintain a magnetic field, some energy is required to be constantly added to the system. A possible physical configuration that allows a magnetic field to be maintained is the Faraday disk dynamo [54]. Assuming that a magnetic field exists and that its stream lines pass through a conductive spinning disk, the Lorentz force would produce currents flowing outward the disk. If this conductive disk is somehow connected to a decoupled and non-rotating rim (e.g. a shell connected to the conductive disk rotor), a magnetic field in the same direction of the original one is created, and therefore sustained. The key elements for the Faraday disk dynamo are a rotating conductive material and a decoupled/non-rotating outer shell. As consequence, if an induced magnetic field is present on Europa, the outer frosted shell should be somehow decoupled from the interior by a conductive and rotating layer. The scientific community explains this with the existence of conductive global ocean underneath the icy crust. The data of the two flybys E4 E14 were taken in the northern hemisphere and a further measurement in the southern hemisphere was needed in order to confirm the induced nature of the field. The pass E26 in early 2000 was specifically designed for that and confirmed the supposition of the previous magnetic measurements of E4 and E14 [49]. To present, the evidence of an induced magnetic field on Europa is the key proofs that corroborate the presence of a subsurface ocean for the moon.

The implications for the actual existence of a subsurface ocean on Europa are multiple and very intriguing. Among others, the habitability condition for this ocean is claimed to be met. Habitability means that the environment can potentially host life. Ingredients to host life are one of the key factors that have been continuously investigated by the scientific community, but complete and universal definitions are difficult to formulate [61]. Possible dominant factors are the presence of liquid water, energy, nutrients and temporal stability [54]. Europa is an ocean world that is heated by tidal dissipation from the host planet Jupiter [19]. Nutrients might be given by underwater volcanism that is very likely to be happening on the moon [84], given the observations of water plumes from the surface [86, 96].

The characterisation of the Europa's layers is one of the most debated aspect of the moon. The main information about the vertical stratification came from the *Galileo* radio doppler data and optical images [11]. In particular, since the first flybys of the moon by the GEM and GMM, the evidence of a layered object, with an exterior cover of H_2O. The first stratification of Europa presents an highly dense metallic core, surrounded by a silicate rocky mantle is interfacing with the global salty water ocean [1]. Linking data coming from the Deep Space Network facilities in Goldstone, California, near Madrid, Spain and Canberra, Australia, the *Galileo* radar doppler team succeed in evaluate the third degree coefficients in the standard spherical harmonics representation of the Europa gravitational potential[1]. Among other outcomes, information constrained the evaluation of the normalised axial moment of inertia which dominates the global distribution of mass in an object. The value was calculated as 0.3466, lower than 0.4, threshold for a constant density sphere. This result imply a moon with a density that increases closing to its centre [54], which was aligned with the claim of an ice layer as well. Nevertheless, the gravity experiment presented in Anderson et al. [1] could not distinguish between liquid or frozen water, given the extremely close density value for the two matter state.

The evidence of an ice layer mainly comes from optical observations, beside the necessity of decouple the liquid interior from the surrounding space, in order to sustain an induced magnetic field [48, 49]. As it has been said several times already, the presence of lineaments on the surface has been interpreted as cracks on ice since the first images of *Voyager* (e.g. Figure 2.1). The wide catalog of features that are characterising the surface of the moon require a global ocean in connection with a frozen upper layer in order to be explained [70]. In general, the studies of Europa found evidences of ridges, rifts, chaotic regions, cryovolcanism, lenticulæ, which are strongly supported by the presence of material arising from the subsurface ocean. The topographic features allowed a rough estimation of the surface age as 50 Myr which is well aligned with the crater technique analysis that produced a value of 60 Myr [116].

After the missions provided insights in the definition of a vertical stratification for Europa, a lot of numerical models were generated, in order to investigate the behaviour and the characterisation of surface and subsurface. Although the scientific community is almost agreeing in the explanation of the stratification proposed by Anderson et al. [1], the rheological parameters that describes the moon are still poorly constrained.

---

[1]More details on the spherical harmonics representation of the gravitational potential are given in Chapter 4. Potential theory will be used as key mathematical tools for the current research project.
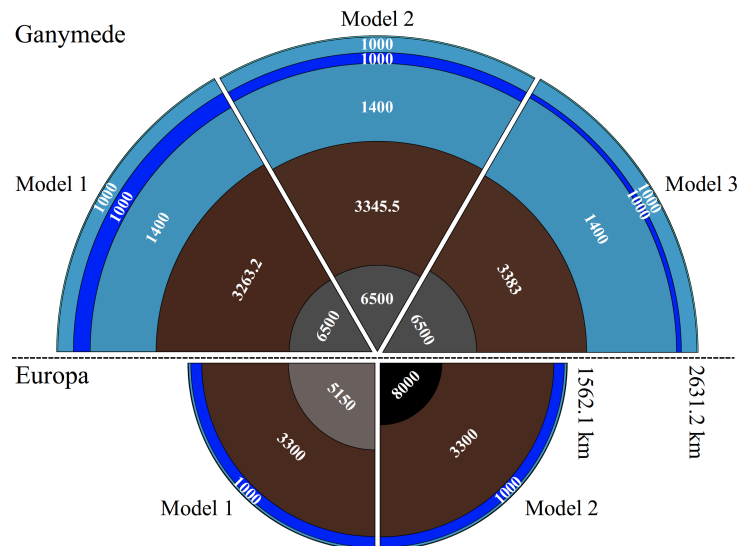
Figure 2.2: Europa and Ganymede vertical stratification as produced by the heat balance analysis of [36–38]. The three different models for Ganymede (upper picture) and the two ones for Europa (lower picture) are differentiated by a different values for the silicate mantle or the iron core. In particular, Ganymede is assumed to be formed by an iron core (grey sector), a variable silicate mantle (brown sector), an high pressure ice shell (light blue sector), an ocean (blue sector) and a further elastic shell (light blue sector). On the other hand, Europa shows an high variable iron core (black and grey sector), a silicate core (brown sector), an ocean (blue sector) and a global ice-I layer (light blue sector) of almost fixed dimensions. Black numbers are the estimated radii of the two moons. Figure taken from Hussmann et al. [38].

Values such as thickness of the ice layer, local viscosity and rigidity have large error bars that do not allow a precise characterisation of the moon. Besides, the numerical models available for Europa shows a huge sensitivity for these key parameters. A method that allowed an estimation of the ice thickness and of the vertical stratification of the moon is a implementation of an energy balance in the moon, taking into account the different energy source that are known to be present for Europa, such as the tidal heating. A common issues between glaciologists is the investigation of the freezing process on glaciers and on ice sheets, and in particular of the spatial and time scale. This process is studied by the so-called Stefan problem.

The implementation of a 3 to 5 layers viscoelastic Maxwel body allows Hussmann and Spohn [36], Hussmann et al. [37] and Hussmann et al. [38] to produce estimation of the ratio between liquid and frozen water. In the models, energy sources are radiogenic heat from the silicate core and tidal dissipation. heat is transferred from the central part of the moon toward the outer layers and the different mechanism of transfer (convection and conduction) are taken into account, depending on the rheological properties of the specific layer[2]. For Europa, the silicate core's dimension plays a key role in the tidal heat dissipation, given the fact that the tidal forces acting on Europa are order of magnitude higher than the ones on Ganymede [38]. This particular heat source is the main factor that explain the presence and sustenance of a liquid ocean [65]. It has been shown that the Rossby tidal waves generated by the tilted rotation axis of the moon are energetically sufficient to maintain a 100 km liquid water [107]. Results of the heat balance problem present the thickness for the ocean of a range between 70 to 100 km. Figure 2.2 represents the different interiors model that [36, 37] obtain by the energy balance for the two Galilean moons. In the current research, particular weight is given to the superficial ice thickness for Europa.

Nevertheless, for sake of the current research, the dimension of the iron core and of the silicate mantle will not be taken into account, so the important value to extract from the past numerical models is the ice thickness. Using the data that are available for Europa, it is still not possible to precisely estimate the thickness of the outer icy layer. Numerical models extrapolate this value by numerous and, sometimes debatable, limitations. A current review for the several attempts of estimating the vertical dimension of the ice layer is referred as Billings and Kattenhorn [5]. The work contains the summary of the most important papers that debate

---

[2]The a-dimensional parameter that governs the transfer mechanism is the Rayleigh number, function of density, viscosity and spatial scale.

Layer	Outer Radius [km]	Density ρ [kg/m^3]	Rigidity μ [GPa]	Viscosity η [Pa s]
Lithosphere	1562	937.0	3.487	10^{21}
Asthenosphere	1557	937.0	3.487	10^{14}
Ocean	1532	1000.0	0	0
Silicate Mantle	1432	3453.6	65.0	10^{19}
Core	600	5565.8	0	0

Table 2.1: 5 layers Maxwell viscoelastic model for Europa, proposed by Jara-Orue and Vermeersen [42]. Brittle ice layer (lithosphere) measures 5 km, consistent with the review paper of [5].

the thickness of the layer and the simplification/assumptions that the various authors had to face. Beside the already mentioned thermal models, flexural analysis is an other common method that has been applied to Europan rifts in order to estimate thickness and elevation of the ridges. On average, the thickness of the ice layer is estimated to be between 1 and 30 km, depending on the location and on the material characteristics of the ice [5]. The scientific community is still debating on the composition of the outer layer and the current data are definitely not sufficient to provide constraints. The extreme outer layer is considered to be extremely cold and brittle, with an average temperature of 100 K [98]. Thus, the outer layer can be considered as elastic and this will play a key role in the development of the current research. Considering the elastic behaviour of the outer layer, the common nomenclature for this portion of Europa is lithosphere, in alignment with the brittle rocky layer of the Earth. Below, a relatively warm and viscous layer is though to be the interface with the liquid ocean, although the scientific debate is still on Pappalardo and Barr [68]. This layer is also called as astenosphere.

For sake of the current research, some parameters had to be constrained. The rheological and physical properties for the vertical layers of Europa have been reported in Table 2.1, taken from Jara-Orue and Vermeersen [42]. Important difference between lithosphere and astenosphere is the viscosity, that might be linked to the temperature via the Arrhenius equation [37]. In Table 2.1 the thickness of the lithosphere (ice layer) is fixed to 5 km as common value found in the literature [5]. The current research will take as basis these value but some modifications will be introduced in order to generate a sensitivity analysis for the various outcomes presented.

2.2. STRESS AND TIDES

The relative proximity of Jupiter to its four inner moons implies a massive perturbation of their environment. Since the early explorations of the Jovian environment it was clear that the tides produced by the gas giant were the key factor for all the geological implications of the surface, evinced by observations. Tides are the results of the differential gravitational attraction of the moon itself and of the host planet. Tides on Earth can be easily seen in the oscillation of the sea level, more evident in particular areas rather than others. On the Galilean satellites' surfaces there are no visible free water layer, therefore the results of tides are more evident in geological phenomena on the crust[3]. Several other stress sources are acting on the brittle surface of Europa and the scientific community is continuously debating on them. Depending on the different methods or data used, the implication of different stress source has to be evoked.

A particularly useful mathematical tool that can describe tides is the potential theory. A complete analytical study for tidal effects is included in Chapter 4 and will be the basis for the implementation of the tidal stress background for the surface of Europa. For a complete mathematical representation of tides in astrodynamics problems, the reader is encouraged to look at Souchay et al. [95]. Purpose of the current section is to present the literature findings that concern stress on the surface of the moon, rather than a pure methodological approach, which will be addressed in Part II instead. The stress sources that are supposed to continuously acting on the moons can be divided according to their time scale, as it has been done in Sabadini et al. [88], among others. Short time scale sources are due to non-zero eccentricity of the moon's orbit, to the obliquity of the moon's rotation axis and to the libration of the ice shell, decoupled from the interior core by the salty ocean. Short time scales are considered to be acting every orbital period, meaning the order of days. Longer time scales are related to more complex orbital phenomena that might reach orders in the time scale of thou-

---

[3]Tides are also influencing the moon's subsurface ocean. For sake of the current research this part will not be treated.
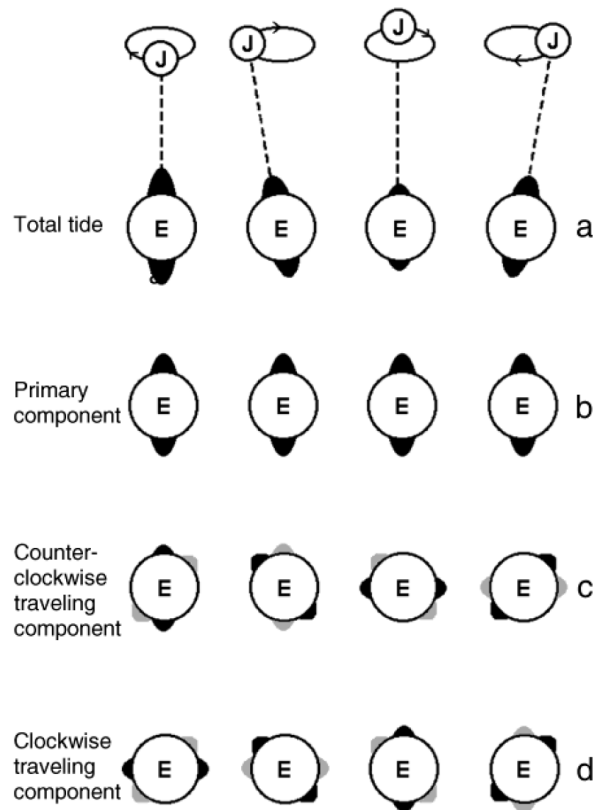
Figure 2.3: Image taken from Greenberg et al. [18], representing a schematisation of the different tidal components for Europa (E), generated by the presence of Jupiter (J). In case of a circular orbit, the tidal bulge (black bulge) is constantly facing the host planet (b). In case of perturbations in the orbital parameters, it is possible to observe migrations of the tidal bulge with respect to its fixed position (c) and (d). The components that characterise the total tide can be summed up in order to find the full determination of the tidal bulge (a).

sands of years. Nevertheless, the error bar on this value is definitely large and completely dependent on the method used to calculate it. Long-time or secular stress sources are produced by non-synchronous rotation of the crust and to true polar wander. As it will become clear in the next sections, secular stress components are assumed to influence the general environment of the moon by different observational studies that are not able to understand the presence of certain features otherwise. Purpose of the next sub-sections is the presentation of the key aspects of the five stress sources, both diurnal and secular.

2.2.1. NON-ZERO ECCENTRICITY

Io, Europa and Ganymede move around Jupiter in a 1:2:4 locked orbit. In other words, the three revolution periods around the host planet are integer of the orbital frequency of Io, the closest satellite to Jupiter. A complex dynamical system, such as the described Jovian environment is subjected to a wide number of perturbations produced by different sources. If these perturbing sources sum up coherently, the outcome's amplitude can increase of several order of magnitude [54]. In physics, this phenomenon is called resonance and the easiest way to picture is with the spring analogue. It is known that physical springs have an internal frequency, called natural frequency. If one perturbs the springs with an oscillating force acting with a frequency that is an integer of this characteristic frequency, the amplitude of the spring's oscillation show a large amplification, eventually leading to the destruction of the spring itself. The analogue with an orbiting system is pretty straightforward. Each moon is experiencing the gravitational attraction of the other Galilean moon, beside the one of Jupiter. Therefore, resonating pattern occurs, given the forcing sources' characteristics. Orbital resonance is a particularly complex case to study but the consequences are generally easy to observe. In the Solar System, resonance is assumed to be the cause of the Kirkwood gap in the asteroid belt, for example. The asteroids occupying this space of the Solar System are forced to reach large eccentricities that eventually lead to hyperbolic trajectories. Europa's eccentricity is forced to be slightly different than zero

(around 0.0094) by the resonating influence of the other Galilean moons [18, 58]. Given the eccentric orbit, the distance moon-planet varies every orbital cycle, leading to a varying gravitational attraction hence the so-called tidal effect.

The stress background due to non-zero eccentricity is historically the first one to be thought of acting on the surface of the moon. The influence of the neighbour moons prevent them to assume circularised orbits, as expected by tidal theory [18, 88]. As it will become clear from the mathematical formulation of the tidal stress, the non-zero eccentricity breaks the longitudinal stress symmetry. If the orbit was circular, the stress would distribute in a symmetrical shape with respect to the meridian passing by the sub-jovian point. It is possible to distinguish between fixed and variable tides. The first tidal component is indeed represented by a fixed tidal bulge that arise in case of a circular orbit[4]. Variations in the orbital parameters (such as eccentricity) implies a migration of the tidal bulge Souchay et al. [95]. Figure 2.3 represents the different types of tides that a moon can experience. Tidal potential theory expects that in case of non-zero eccentricity, the tidal effects are proportional to the value of the eccentricity itself. The effects that are induced by the non-zero eccentricity are acting on a diurnal timescale, meaning that the outcomes are potentially observed within the Europa orbital period around Jupiter. Europan features that require the presence of non-zero eccentricity are the strike-slips, which need to be formed by a variating stress source. More on strike-slips on Europa will be presented in the next chapter. Concluding, non-zero eccentricity will be key acting sources in the development of the current research project.

2.2.2. NON-ZERO OBLIQUITY

Additionally to the diurnal stress induced by the non-zero eccentricity, non-zero obliquity is assumed to influence the stress pattern over the surface of the moon. Instead of introducing a longitudinal stress redistribution, the inclination of the rotation axis causes a latitudinal asymmetry with respect to the equator. Nevertheless, the amount of axis inclination is still poorly constrained. The reasons why a slightly tilted rotation axis needs to be considered for Europa, as well as for the other Galilean moons can be found in both theoretical and observational works.

On the observational point of view, the presence of non-zero obliquity was shown to be key in order to understand the presence of cycloids, for example [35, 82]. On Europa, cycloids are peculiar features that assume the shape of a multiple serie of arches. More on cycloids will be presented in next chapter. Non-zero obliquity and the related asymmetry in the latitudinal plane help the explanation of the curious cycloidal pattern of several features. The influence of inclined rotation axis on strike-slips is still argument of discussion [82]. Fitting the observation with the numerical models that include non-zero obliquity, it has been possible to induce an amount of inclination that ranges from 0.2° to 1.35° [83]. Nevertheless, as observed in Baland et al. [3] these assumption are merely related to the specific cycloidal features under investigation and does not imply that the moon is actually tilted that much. The dynamical history of Europa can be very complex and the features observed can be heritage of a past configuration of the moon.

Theoretically speaking, the non-zero obliquity can be derived by a mathematical study built on a simple secular variation model for the Jovian system, that includes Io, Europa and Ganymede [6]. The outcome of this analysis shows small forced obliquities for the satellites. Small non-zero obliquities are expected also by the analysis of the so-called Cassini state model [3]. In 1693 an Italian scientist, Giandomenico Cassini studied the motion of the Moon around the Earth. The Cassini state-model describe the motion of a satellite that satisfy three general laws: it orbits the host planet in a tidally locked pattern (also known as synchronous rotation), the inclination of the rotation axis is a constant value with respect to the orbital plane and the rotation axis itself belongs to the intersection between the plane perpendicular to the ecliptic and the one perpendicular to the satellite's orbital plane [73]. More studies, such as Peale [73] included variation in the orbital parameters for the Cassini state-model (an example is the addition of the physical libration of the crust) and therefore extended the validity of the model to satellites other than the Moon. Baland et al. [3] used the Cassini model in order to calculate the eventual obliquity of the rotation axis. The results are slightly different from the ones obtained by observational fitting techniques such as Rhoden et al. [82, 83], as already mentioned. The amount of rotation axis according to Baland et al. [3] reaches an order of magnitude of around 0.04° in case of no-ocean and of 0.055° in case of a global ocean. The discrepancies between theoretical and observational point of view can be due to the different orbital state used by Rhoden et al. [83] and Baland et al. [3]. Nevertheless, for the sake of the current project an inclination of 0.5° was chosen, being a compromise between the different opinions encountered in the literature review.

---

[4]Excluding natural oscillation from the equilibrium position, phenomenon that is also called as physical libration.

A further theoretical work that investigates the outcomes of a potential non-zero obliquity is Tyler [107]. According to the paper, the inclination of the rotation axis would produce large Rossby waves in the subsurface ocean. These would be one of the key actors that keep the ocean in a liquid state. The kinetic energy of these waves is theoretically a thousand times higher than the one of the flow induced by primary tidal components. The heat produced by their dissipation is already enough for small values of non-zero obliquity (around 0.1°).

2.2.3. LIBRATION OF THE DECOUPLED SHELL

The variation in the gravitational attraction that occur within the orbital cycle due to non-zero eccentricity has effects that go beyond the pure variation of stress, phenomenon addressed already in the previous sections. The tidal bulge of the icy moon is forced to oscillate in longitude[5] as it happens to every system that tends to reach equilibrium. This oscillation, that would also happen even in a circular orbit, is called physical libration of the crust and it is composed by a free and a forced component [34, 80]. Free libration depends on the shape of the satellite's interior and it is supposed to be damped if its frequency is not commensurable with the orbital period. The forced libration is linked to the gravitational torque of Jupiter, hence the forced frequency of libration is the orbital motion itself, while the amplitude depends on the physical properties of the moon. Particularly useful in the investigation of the satellite's physical libration is the studying of amplitude and phase of the different components that induce the tidal bulge to oscillate in longitude. A complete mathematical formulation for the dynamical response for the libration of the crust is included in Rambaux et al. [80]. The work uses the mathematical setup of a solid shell that cover a global ocean. The modelled satellite is spinning in a synchronous rotation around Jupiter. Results are the frequency spectrum in the libration response of Europa that characterise short and long period librations. The former has frequency that are close to half the orbital motion (twice the orbital period) and characterises the interior parameters of the satellite while the latter are substantially independent from the stratification properties.

Among others, Rhoden et al. [82] used geological features in order to constrain the parameters that characterise the physical libration of the crust. This work presents an approach that is completely different from the just mentioned Rambaux et al. [80], since it uses observations to fit the dynamical parameters. Results are other sets of phases and amplitudes based on single cycloids mapped on the surface. The discrepancies that emerged with the comparison with the mathematical model of Rambaux et al. [80] need to find validations and proofs that can only come from new missions's data.

2.2.4. NON-SYNCHRONOUS ROTATION

So far, the current section has described deforming sources that are acting on Europa on a short timescale, meaning that stress variation can be observed within one orbital period of the moon around Jupiter. From this observation, these sources are called diurnal effects. Since the very early stages of the investigation of Europa's surface, already with the images and data coming from the *Voyager* spacecraft, a long term component in the stress has been evoked. Indeed, a long-term, also known as secular, component in the deforming field would allow the stress to reach higher values and eventually lead to the failure of the cold ice [17, 23]. If one considers the ice on the moon as a cold and brittle material, the tensile strength, the ultimate threshold for the failure of the structure can be considered to be 100 KPa [18, 20]. Tidal theory that takes into account diurnal timescale stress provides that the maximum stress limit reached by the surface is of 30 times lower than the tensile strength, i.e. around 40 KPa [18, 44]. This large gap between the ice failure and the stress reached by the diurnal effects lead the scientific community to speculate about the potential presence of longer timescale deforming actors, that together with the fatigue induced by multiple orbital cycles would permit the ice to break.

A large number of satellites in the Solar System are trapped in the gravitational lock of their host and massive planet. If the satellite is always facing the planet with the same side, this behaviour is called tidal locking[6]. A moon is tidally locked to the planet because the tidal bulge that is arising from the differential gravitational attraction (tide) tends to accelerate or slow down the rotation of the satellites itself in order to balance the different torques that are generated [54]. The result is that the revolution of the satellite around

---

[5]Of course, assuming a non-zero obliquity would imply the tidal bulge to slightly oscillate in latitude. For the majority of the case this can be simplified as zero [80]

[6]Clear example is our Moon facing the Earth with the same side. The other side of the Moon is also known as Dark Side of the Moon for this reason.

NS rotation	Reference
25° − 50°	McEwen [58]
60°	Greenberg et al. [18]
60° − 95°	Geissler et al. [15]
360°	Geissler et al. [14]
360° − 720°	Figueredo and Greeley [13]
720° − 900°	Kattenhorn [44]

Table 2.2: Non synchronous rotation amount as expressed in the literature. The huge discrepancy has been pointed out by Kattenhorn [44] and it is due to the different geological features that have been studied in the addressed works.

the planet and the its self rotation assume the same period. This phenomenon is also called synchronous rotation of the satellite with its host planet.

The Laplace resonance that has been already mentioned when talking about the forced eccentricities assumed by the Galilean satellites, is thought to be one of the main theoretical reasons why Europa might have a rotation around its axis that is slightly faster than its revolution around Jupiter. The modified inertia tensor that is generated by the eccentric orbit, would force the moon to rotate faster, on average, than a synchronous motion [17]. This would mean Europa rotates non-synchronously with Jupiter, from where the terminology non-synchronous rotation (NSR).

Beside the theoretical argumentation that would prove the non-synchronous rotation of the exterior crust with respect to the orbital revolution, some insights that can confirm this phenomena come from the observational point of view. The stronger evidence of NSR is seen in the northern hemisphere, where the features in the so-called Bright Plains region can be better explained with a secular clockwise rotation of the stress field [44]. In more specific, a couple of features[7] passing by the Bright Plains and the Conamara Chaos region need at least a couple of complete reorientation of the tidal stress on the crust, in order to fit the models. A couple of cycle of reorientation means that the NSR can be measured as at least 720°. This value is definitely higher than the ones proposed in the literature before Kattenhorn [44], because of the peculiar configuration of the Bright Plains region. The differences between the actual amount of NSR that have been encountered in the literature survey are summarised in Table 2.2 which was rearranged from the paper of Kattenhorn [44]. As it can be seen in the table, the amount of crust reorientation slightly varies from a quarter of a full cycle to a couple of them, by taking into consideration different areas of the moon.

In addition to the clear uncertainties that are mining the correct estimation of the amount of crust reorientation that has occurred on Europa, there are multiple open discussions when defining the actual reorientation rate; in other words the effective difference in the spinning of the crust with respect to the (tidally locked) interior. According to the milestone papers about the dynamical study of Europa e.g. Hoppa et al. [28] and Greenberg et al. [18], the NSR period is estimated to be of around 10^4 years. As a matter of fact, several observational investigations have been proposed in order to validate this number, but more geological data are needed and the rate of NSR is still heavily doubted. In the current research, the rate of NSR will be included in the sensitivity study of the model produced.

2.2.5. TRUE POLAR WANDER

True polar wander has been firstly assumed to be a relevant phenomenon for the Earth dynamics at the end of the 19th century by astronomical observation [87]. Two periodic drifts were in fact calculated from astronomical data, which were immediately related to the free nutation of a rotating and deformable body such as the Earth. On the other hand, any potential connection to continental drift was discarded. The filtered periodic drift can be seen as a secular movement of the rotation axis of the Earth, from here the name polar wander. The secular drift that is not corrected from the mentioned continental motion is also called as apparent polar motion while the corrected polar wander is called true polar wander (TPW). The motion is always calculated with respected to fixed terrestrial hot spots[8]. Hot spots are assumed to be results

---

[7]Agave and Asterius Lineæ.

[8]One of the most notorious hot spot on Earth, is the Hawaiian archipelago in the middle of the pacific ocean. In particular, The hot-spot is located below the Big Island of Hawaii.

(a)   **(b)**
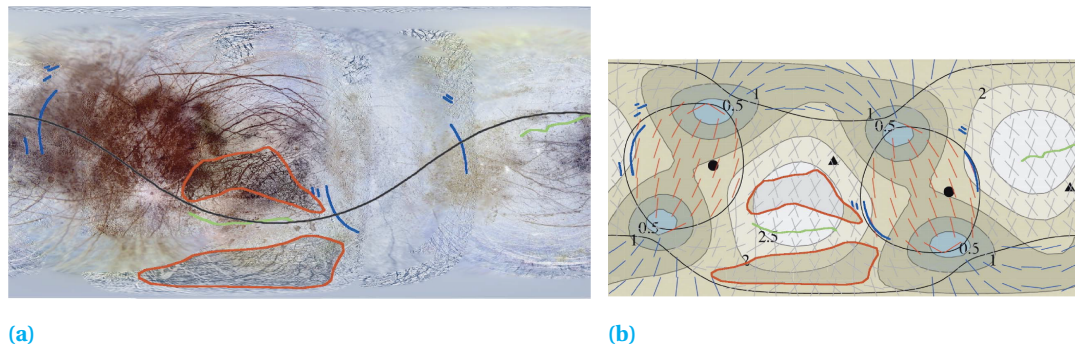
Figure 2.4: Global colour mosaic for the surface of Europa and stress map that accounts for TPW, taken from Schenk et al. [92] as a digital elaboration of *Voyager*, *Galileo* and *New Horizon* images. In Figure 2.4a, the areas within orange lines are containing strike-slips or pulled apart features used to match the observation with TPW models. The heavy black line roughly divide the two areas of the moon containing the two orange sectors. Blue and green lines are small circle depression and wavy lineaments, respectively. Figure 2.4b represents a stress map with an addition of 80° of crust reorientation due to TPW. Palaeo-pole locations are marked with solid dots while initial tidal axis are marked with solid triangles. The short red lines, grey crosses and blue lines indicate directions of the expected normal, strike-slip and thrust faulting, respectively. Again, black lines separate these tectonic regions. Shaded regions and contours correspond to deviatoric stress in units of MPa.

of the shallow upper mantle activities and these are usually assumed to be crossing the upper layer of the Earth relatively undisturbed, reversing material directly to oceans or to continents [87]. Therefore, these can be considered as fixed points with respect to the migrating oceanic and continental plates. Subduction of terrestrial plates, mantle convection and the redistribution of surface load are thought to be the key factors that drive TPW. Example is the post-glacial rebound which is assumed to be a lithosphere reaction to the melting of the large ice sheets that once covered large parts of the northern hemisphere. Such a relatively rapid loss of surface load is considered to trigger a counter effect of the lithosphere that in some parts of the world is constantly changing its height with respect to the geoid. A complete analysis of TPW goes beyond the scopes of the current research and the reader is referred to Sabadini and Vermeersen [87] or Peltier [74] for further details.

Key finding that is taken from the TPW description is that a redistribution of loads on the surface of a deformable planet can trigger the rotation axis to migrate. Similarly to what happens on the Earth, Europa tidally deformed figure is assume to experience masses redistribution. The evidence comes from observations obtained for the icy surface which contains features that could be only explain with a polar migration theoretically described by TPW theories [53, 66]. More in specific, a progressing thickening (or thinning) of the ice crust would induce a variation in the moon's inertia tensor followed by a reorientation of the rotation axis. The work of Schenk et al. [92] represents the most recent development in terms of TPW analysis deduced from observational data. In 2007, on his way to Pluto, the *New Horizon* mission transmitted the most recent images for the surface of Europa. A certain amount of features, mapped on a combination of *Voyager*, *Galileo* and *New Horizon* images, allowed the research team to match the geometry with a 80° reorientation of rotation axis due to TPW stress. Figure 2.4a shows these areas with an orange contour, separated by a rough division of the two hemispheres (black solid line). On the other hand, Figure 2.4b represents the Europa stress map with an addition of 80° of crust reorientation due to TPW, over a global colour map of the Europan surface. Solid dots are palaeo-poles while initial tidal axis are marked with solid triangles. The short red lines, grey crosses and blue lines indicate directions of the expected normal, strike-slip and thrust faulting, respectively.

Concluding, TPW similarly to what happens for NSR, is thought to induce a crust reorientation and a following stress redistribution. Timescales of this two source are not known but considered to be orders of magnitude higher than diurnal effects.

3

OBSERVING THE ICY SURFACE

In the last chapter the most recent description for the interior characterisation and the stress condition on Europa has been addressed in details. Key finding is that an icy shell covers a global H_2O ocean. The brittle crust is continuously deformed by the effects of tides and other stressing sources, that act at different timescales. Diurnal tides and secular stressing phenomena are the key actors that force the icy surface to change shape (e.g. in terms of tidal bulges) and, eventually, to initiate and propagate rifts.

During the years of Europa's exploration by the *Voyager* and *Galileo* missions, images and data have shown a curious aspect of the Europa's surface. Lineament features and other surprising patterns have been observed on large areas of Europa's crust. Their aspect suggests unambiguously the presence of fractures in the ice, which are likely to be intimately linked to the lineament patterns. In other words, lineament features on Europa seem to be related to tensile stress and presumed to be resembling rifts of the ice. It is logical to imply that extension of the lithosphere might lead the brittle ice to reach tensile strength and hence to fracture. A little amount of features that resemble compression of the lithosphere have been also observed on Europa (e.g. in the work of Prockter and Pappalardo [77]).

As substantially described in Greenberg et al. [18], stress due to non-synchronous rotation of the crust, together with diurnal tidal effects (non-zero eccentricity) are sufficient to explain the several major lineaments observed on the surface of Europa. Nevertheless, by assuming the effects of non-zero obliquity, physical libration of the crust and true polar wander, further insights and more accurate models can be produced, especially if taken as basis for the proposed numerical analysis of crevasses on Europa. Moreover, potential theory will be presented in chapter 4 as a good analytical and numerical tool for the stress field build up and, as consequence, for the crack propagation.

The current research will apply the necessary constraints that the stress field, caused by the different contributors, pose on the brittle surface. After that, a fracture mechanics analysis will be issued in order to explain the mechanisms of deforming the crust, until reaching the point where the ice cracks eventually propagate. Additionally, diurnal tides will act on the opening generating oscillating phenomena, whose dynamical description is also part of the simulations. An important first step toward the research goal has been already carried out in chapter 2 where stress contributors and Europa's stratification have been analysed in their qualitative details. The following chapter will summarise the key aspects of the characteristics shown by the different observed lineament patterns on Europa. Generally speaking, rift formations on Europa can be distinguished in ridges, strike-slips and cycloids. The first two categories have several similarities with terrestrial formations and will be described in section 3.1 and 3.2, respectively. The third category is intimately linked to the curious Europan stress conditions and its characteristics will be presented in section 3.3. These three groups have been distingushed in order to clarify predominant characteristics of specific features of the moon. In reality, it is very rare to find perfect examples that belong to a single group. More likely the features have properties that combine the formation of ridges, lateral displacement and cycloidal shape at the same time.

An accurate attempt of explaining the formation of the different features that *Galileo* and *Voyager* cap-
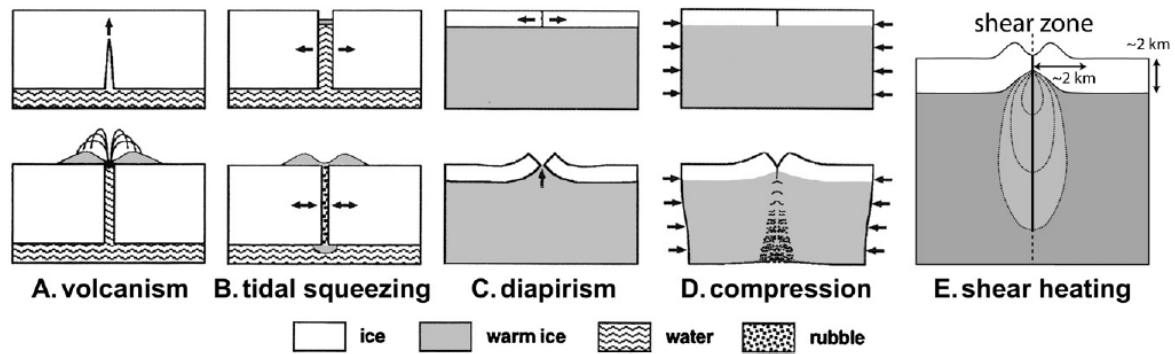
Figure 3.1: Current models for explaining the formation of the cracking features observed on the brittle surface of Europa [2]. A-D from Pappalardo et al. [70]. E represents the effects of heat generated by friction due to shear stress, from Nimmo et al. [64]. In particular, B is the effect of diurnal tides as explained in Greenberg et al. [18] and Pappalardo and Coon [67] and in section 2.2 of the current work. Further details in the text.

tured on the surface of Europa is given in Pappalardo et al. [70], enriched by Aydin [2] and schematically represented in Figure 3.1. In the image, Figure 3.1A shows the cryovolcanism model, firstly proposed by Kadel et al. [43]. The model describes the formation of rifts and fractures with the several explosions due to the low temperature volcanic mechanism termed as cryovolcanism. Differently to Earth volcanism, driven by extremely high temperature characteristics of silicates in the mantle, the water, ammonia and other volatiles are at very cold states. Hence, a small variation in the temperature could lead the materials to flow and pressurised volatiles' chamber can be ejected at very high speed [110]. The latter are supposed to be the cause of the plumes that have been observed in the icy moons in the Solar System such as Enceladus [10]. Just recently Europa showed plumes from equatorial and southern regions that might confirm the presence of cryovolcanism on the Jovian moon [86, 96]. Figure 3.1B represents the relatively opening and closure of a crack generated by alternation of tensile and compressional stresses produced by diurnal tides and already addressed in section 2.2. The mathematical representation of this process will be presented in chapter 4. It has also been proposed that some features could be explained with the solid-state convective process called diapirism, firstly proposed for Europa by Pappalardo et al. [69] and schematically shown in Figure 3.1C. This phenomenon consist in the geological intrusion of warm and relatively low density material that arises buoyantly above the surrounding colder environment. The assumption that this model is valid for Europa would positively explain the presence of pits, domes and spots, which are common on the surface [18, 19, 68, 69]. The acceptance of diapirism may have the consequence of refusing the effective presence of a liquid water ocean, assuming a global solid-state convection. Nevertheless, since the first proposal of such a model for the H_2O layer [69], these implications have been strongly contested and discussed. Other researches, produced models that strongly require presence of a water layer in order to form diapir formations, e.g. Nimmo [62], Pappalardo and Barr [68], Rathbun [81]. It is important to notice that Chaos regions are assumed to be mainly formed by diapiric extrusion [91] or, in any case, by effects of convective phenomenon. Diapiric formations such as pits and domes will not take place in the current research. Figure 3.1D represents the generation of folds or wedge ridges, mainly due to compressional forces, also addressed in Prockter and Pappalardo [77]. This group represents the minority of the features observed on the surface, surpassed in amount by large presence of extension mechanisms on the surface, which will be presented throughout the development of this chapter. Figure 3.1E represents the deformation of the crust that might be due to the shear heating as proposed by Nimmo et al. [64] and better explained when talking about strike-slips (section 3.2), where shear stress is dominant. Despite the wide catalogs of models that have been proposed in the history of the discovery of Europa, the current literature review concentrates the focus on tidal stress, superimposed to the secular forcing due to reorientation of the crust as presented in section 2. The reason is that tidal stress can be studied by using relatively simple mathematical tools such as the potential theory. The models presented so far are useful to understand the full variety of features observed on the surface but will not be used in the current research.

Additionally, the geological analysis of ridges and in general, of all the fracturing patterns on Europa, have been the major contributor for the validation of the ice shell vertical dimension, which can only be calculated by theoretical models. Examples are Billings and Kattenhorn [4, 5], which confirmed the average range of 1-30

Feature Name	Length [km]	Central Coordinates
Agave Linea	1440	273.1°W, 12.8°N
Agenor Linea	1496	213.5°W, 43.8°S
Alphesiboea Linea	1438	175.9°W, 25.1°S
Asterius Linea	1943	122°W, 14.9°S
Belus Linea	2437	231.4°W, 9.3°N
Cadmus Linea	3584	191.7°W, 38.7°N
Drizzlecomb Linea	1500	111.7°W, 7.7°N
Euphemos Linea	1250	45.7°W, 11.4°S
Harmonia Linea	1154	171.7°W, 28°N
Hyperenor Linea	2996	324.4°W, 12.1°S
Mehen Linea	1500	236.7°W, 56°N
Minos Linea	2170	195.2°W, 47.2°N
Pelorus Linea	1535	188.3°W, 19.8°S
Phineus Linea	2004	319.9°W, 29.8°S
Rhadamantys Linea	1747	200.5°W, 19.3°S
Sparti Linea	1600	245.5°W, 59.3°N
Telephassa Linea	777	177.2°W, 0.8°S
Tormsdale Linea	875	258°W, 47.7°N
Udaeus Linea	2050	239.4°W, 48.6°N
Yelland Linea	186	196°W, 16.7°S

Table 3.1: List of a selection of 20 lineament features observed on the surface of the moon, including their length and their central longitude and latitude. Data from IAU.

km present in the rest of the literature on Europa. The corroboration mainly comes from geological study of ridge flexure of flanking cracks. It is clear how the study of the lineament features that Europa shows is a key aspect in the description of the global environment of the Jovian moon, since ridges, strike-slips and cycloids are the visible effects of the huge oscillations of stress on the icy surface.

It is important to highlight that several terrestrial analogs with Europan features have been proposed throughout the years, and these will be pointed out in the developing of the following sections. The reasons of giving large importance to the Earth analogs are principally two. First of all, it is easier to drawn general conclusions for geological formations that the scientific community is familiar with. Thousand of papers and researches are investigating Earth rifts, under different aspects, while for Europa a lot of work is still lacking. Secondly, the proposed research will use a fracture mechanics model that have been developed exclusively for Earth ice shell and it has strong capabilities of model terrestrial cracks. The idea of the proposed research is to tune this Earth model with boundary conditions for Europa, and to investigate the dynamical behaviour of cracks.

Voyager, *Galileo* and *New Horizon* images picturing the surface of the moon have been digitalised in one single map that is now representation of the highest quality aspect of Europa. The current research and in particular the numerical algorithm that is produced in order to find critical depths for the crevasses, takes as basics this map, also reported in Figure 3.2. The map is a product of the International Astronomical Union (IAU)[1]. As it can be seen from the map, the lineament features presents extremely large dimensions for the crevasses. Many features cross more than half of the surface dimension, meaning values larger than the radius of around 1500 km. The list of a selection of features that are also used as target for the simulations of the next Part are included in Table 3.1 also taken from IAU data[1]. Maximum crevasses length are of 3500 km and at such spatial scales no analogues with terrestrial crevasses can be drawn.

---

[1] http://planetarynames.wr.usgs.gov/Page/EUROPA/target, last view on October, 15th 2017
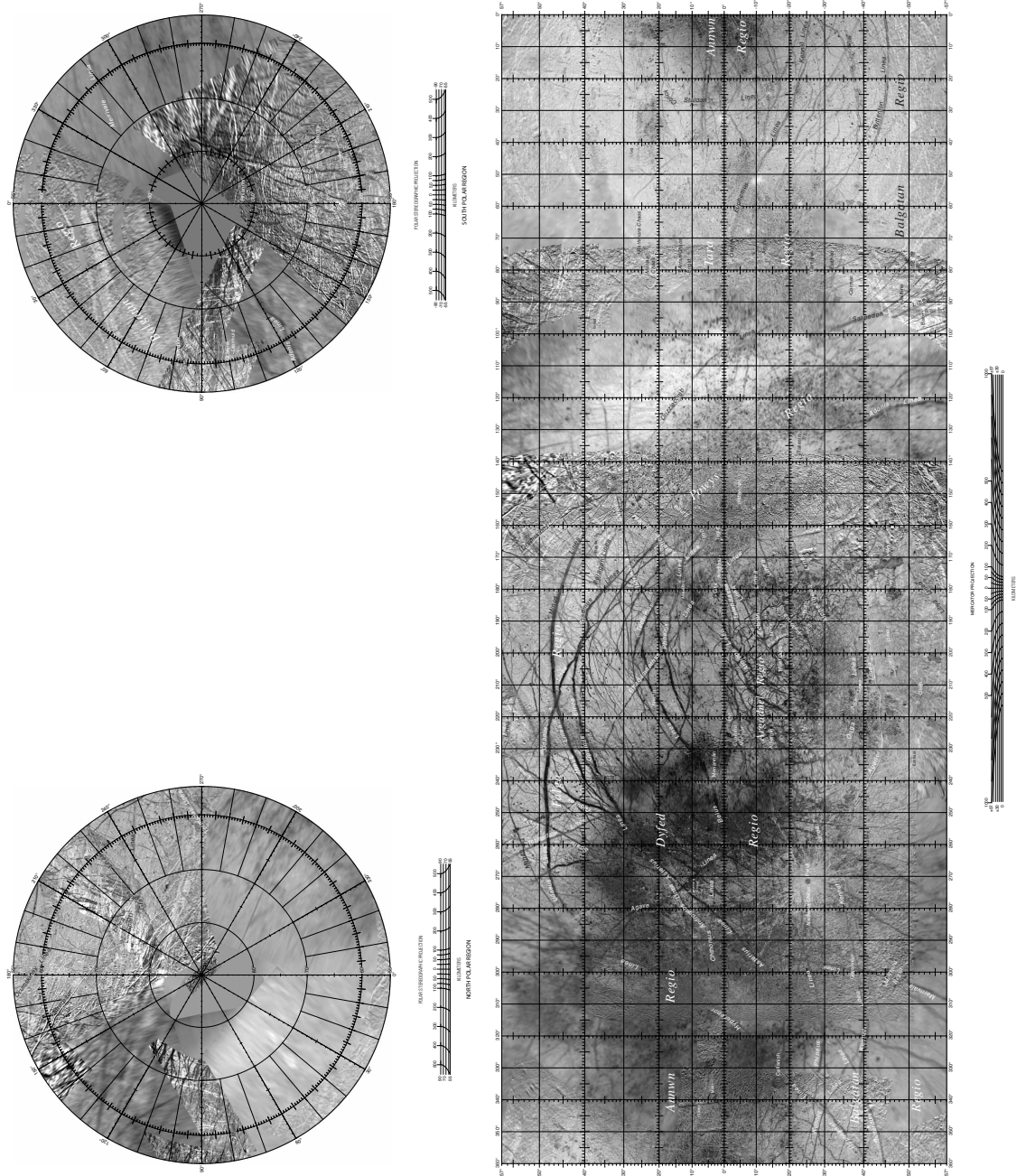
Figure 3.2: Global Map of Europa, where the main lineament features have been labeled in white. This map is the latest version for the Europan surface aspect and it has been produced by images of *Galileo* and *Voyager*, with elaboration of the International Astronomical Union. Free access to the interactive map of Europa and lineaments nomenclature on the website of IAU.

3.1. RIDGES

Ridges are probably the most common group of features that have been observed on the surface of Europa by *Voyager* and *Galileo* programmes. An useful definition, though qualitative, can be that a ridge is an accumulation of material due to some sort of forced extrusion or ejection of material from an icy rift. On Earth, common types of ridges are the one generated when large plates of ice shelves are compressed and/or sheared among each others. Examples can be observed in the large shelves of Antarctica, where terrestrial tides force a relatively thin chunk of ice to impact and compress again an other. Besides, an other common phenomenon that is associate to material ejection from a rift can be see at the bottom of the Atlantic Ocean, where the so-called mid ocean ridges continuously produce new lithospheric material coming from underneath the ocean floor. Terrestrial mid ocean ridges are associated with volcanic episodes that occur at the boundary between two tectonic plates in phase of separation from each other. On Europa, the formation of ridges is strongly related to the tidal stress field build up on the surface, but most importantly to its frequent variation in time (also known as diurnal tides). In chapter 2, it has been shown that secular components contribute to the process of deformation. Differently to what happen in the large ice shelves on Earth, Europa has no open ocean where the ice chunks can float. Therefore, the global ice layers are forced to be continuously compressed and stretched, maintaining approximately the same geographical position[2].

Talking about experimental works, it is interesting to report the paper of Manga [56], who built a wax experiment, with the purpose of simulating the formations of cracks on a test closed domain. The experiment is based on the cooling of a wax layer until it reaches the solidification point. After that the layer is deformed cyclically, allowing the simulation of diurnal tides effects and secular components, such as NSR. Once the generation of a frozen shell above a liquid layer is complete, the analogs with the Europan global description is set. A moving plate perpendicular to the layers plays the role of the deforming source. Introducing scaling a-dimensional parameters, the research could observe similarities between the wax cracks and the Europan rifts, in particular with ridges and dilatational bands, by playing and tuning these coefficients. An important a-dimensional parameter is the dilation coefficient which will be reported in the following equation and used in the development of the section. This coefficient has been firstly proposed by Tufts et al. [106].

$$\gamma_D = \frac{\text{net secular dilation during one cycle}}{\text{amplitude of diurnal opening during one cycle}} \tag{3.1}$$

The coefficient γ_D in the ratio between the secular dilation[3] rate during one Europan day and the amplitude of opening rate due to diurnal tidal effects. The wax experiment proposed by Manga [56], though the obvious limitations in terms of simulating the complex deformation sources on Europa, achieved positive outcomes in the contribution of crust reorientation due to NSR on ridges and on dilatational bands. Additionally, the usage and the variation of the dilatation parameter, together with other a-dimensional numbers (e.g. the Rayleigh number which governs the distinction between conduction and convection), allows a sensitivity study about how the layer deforms with changing the key rheological characteristics.

A consistent and useful classification of ridges on Europa, which is still the baseline for the most recent researches related to the analysis of superficial features, is the one proposed by Greenberg et al. [18]. The classification is qualitatively based on the optical aspect of the ridge. Indirectly, this is linked to the age of the feature, as it will become clear later. According to Greenberg et al. [18], on Europa it is possible to detect simple pair of ridges (Class I), multiple subparallel lines of ridges (Class II) and formations consisting of mutually crossing ridge complexes (Class III). Figure 3.3a represents a typical Class I ridge in the area of the Bright Plains, imaged by *Galileo* during the flyby E6. This lineament has been named Androgeos Linea (14.7°N, 273.4°W). This type of ridge should have been generated in a period of 30000 years approximately. The accumulation of material has assumed to be largely influenced by the frequent effects of oscillating diurnal tides. In particular, a proposal for the generation of ridges consists in the continuous opening and closure of the fracture which leads to the ejection of material from the ocean to the surface [67]. That would cause the formation of an accumulated amount of material at the top of the rift. Figure 3.3b represents a typical Class II ridge (4.7°N, 325.7°W). The difference with the former type of ridge is only given by the fact that Class II presents an evolution in terms of extension, that has occurred for the surrounding lithosphere. Multiple crack lineaments have formed parallel to the central though, due to the relatively large time period of diurnal tide action. Finally, Figure 3.3c shows a Class III type of ridge which is assumed to be the oldest of the three

---

[2]Not considering reorientation of the crust, namely true polar wander and non-synchronous rotation. These phenomena deeply modify the shape of the crust.

[3]In the current document, the term dilation and dilatation have the same meaning and will be both used.
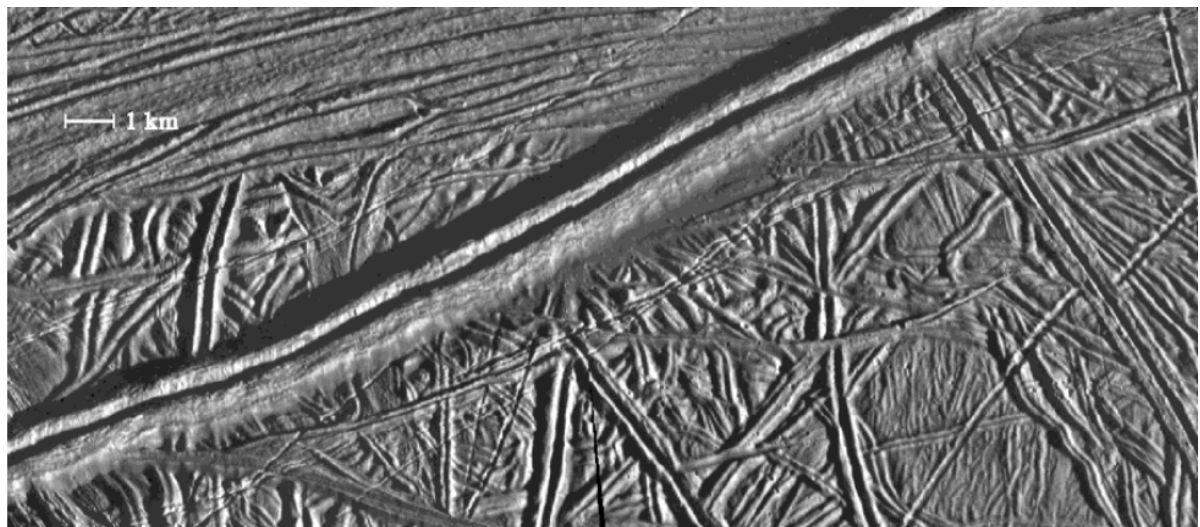
(a)
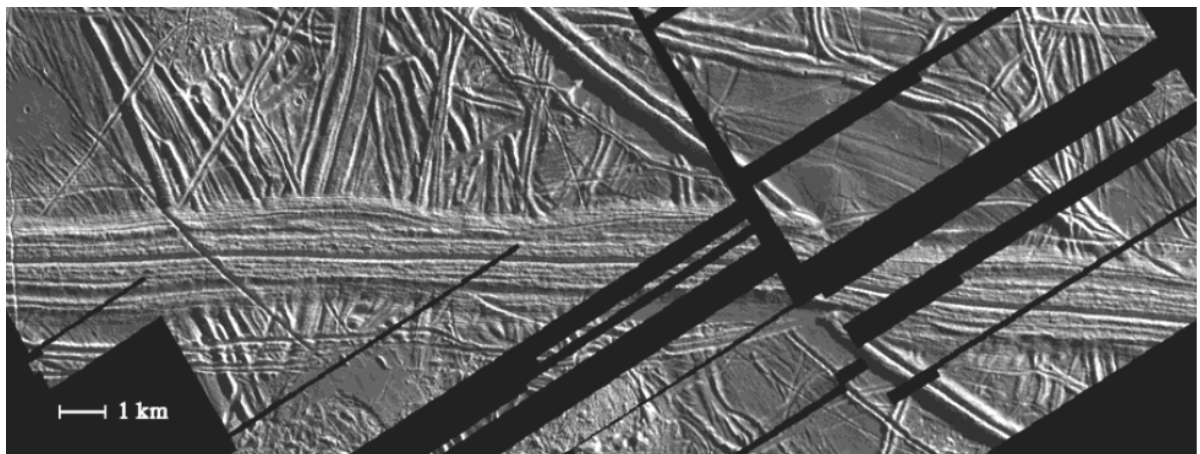
(b)
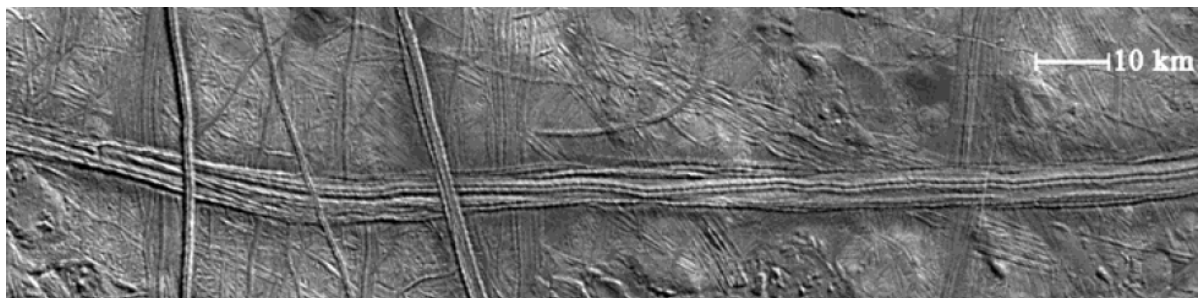
(c)

Figure 3.3: Classification of Europan ridges introduced by Greenberg et al. [18]. Further information and geographical coordinates of the lineaments in the text. (a) Class I ridge in the area of Bright Plains, from *Galileo* images taken during the flyby E6. A central rift is surrounded by accumulated material, due to the progressive opening and closure of the fracture. Several other Class I ridges can be seen in the same picture. (b) Large Class II ridge. The central rift represents a spreading centre. Dilatation processes generate multiple subparallel lineaments which resemble further cracks, surrounded by smaller ridges. (c) Class III type of ridges. The picture shows Agave Linea, nearby Conamara Chaos region, as imaged from the *Galileo* E6 flyby. The presence of intersecting lineaments suggests that this kind of ridges is the oldest of the three classes. It is possible to notice other dated Class 3 ridges crossed by Agave Linea.

groups. This image represents a mature Europan lineament named Agave Linea (12.8°N, 273.1°), which is crossed by relatively younger features, and crosses, itself, relatively older features. Due to the prolongated time under the effects of diurnal tides, water and material from the deeper layer of Europa might have found the possibility of flowing on the surface, generating multiple intersecting patterns and features that are similar to secondary canals. The reddish colour that these features shows in true color images, might be due to silicates or even organic material coming from the ocean [19].

As previously mentioned, ridges are assumed to be generated by the ejection of material from a crack, due to the progressing squeezing of the two side of the rift in time. Pappalardo and Coon [67] firstly proposed an analog between ridges on Europa and on Earth. Terrestrial sea ice is assumed to crack after the tensile strength is reached. After that, the forced opening and closure of the fracture generates the ridge. In the work of Pappalardo and Coon [67], a 4-phase sequence analogous to Earth-based processes is set for a general Europa's rift formation:

1. When the non-synchronous stress, together with the diurnal component has reached the ice tensile strength, a crack might form. Liquid water from the underneath ocean arises, filling the gap just formed. The new liquid surface starts to freeze, generating an Arctic-like thin ice layer also termed 'lead'.

2. After some hours, the stress field changes orientation and the crack begins to close. The thin lead layer is forced to be destroyed and new liquid is accumulated near the top of the crack.

3. The crack approaches closure. The new material is squeezed toward the ocean and toward the top of the ice shelf, forming a ridge.

4. During an other diurnal cycle the process starts again, leading to accumulated material on the top of the shelf.

In Pappalardo and Coon [67], this process is assumed to be due by the mutual interaction of diurnal tides and NSR only. Nevertheless, the interaction of TPW, non-zero obliquity and physical libration of the crust may induce further accuracy in the model.

The 4-phase opening-closing cycle directly suggests the presence of a sort of dilatation phenomenon on the surface of Europa, since new lithospheric mass is forced to reach the surface (e.g. the results that the wax experiment of Manga [56] that addresses dilational band analogs). On Earth this happens, for instance, at the bottom of the Atlantic mid-ocean ridges, where continuous material is ejected from the cracks and leads to dilatation of the lithosphere. On Europa, bands and ridges are elements that suggest a strong and evident presence of lithospheric extensional phenomena. Tufts et al. [106] firstly proposed that diurnal tides, superimposed to secular stress deforms a crack within one Europan day in a way that new material is continuously ejected and accumulated on the top of the rifts. The progressive effects of diurnal opening and closing of the crack [67], prolongate this effect in time and the amount of material that arises from the lower part of the crust is forced to move away from the crack, replaced by new emerging mass. Key parameter that governs the extension of lithosphere in the model of Tufts et al. [106] is the dilation parameter γ_D, already presented in Equation 3.1 while talking about the wax experiment of Manga [56]. This a-dimensional parameter consists in the secular rate of dilation during one Europan day (e.g. NSR) on the rate of dilation due to diurnal tidal cycle (i.e. non-zero eccentricity and non-zero obliquity). Small values of γ_D imply a huge accumulation of material on the top of the cracks, hence of the formation of high ridges. On the other hand, large values of γ_D represent evident extensional phenomena which lead to the formation of small and spread-out bands. Extremely large values of γ_D imply no visible effects of crack closure due to diurnal tides, therefore continuous ejection of material is suggested. The model of Tufts et al. [106] allows an accurate description of Class II ridges (as classified in Greenberg et al. [18]), of dilation bands and of strike-slips, which are linked to tidal walking. Moreover, it investigates several *Galileo* images and produces a model that is able to explain extensional phenomena of the Europan lithosphere. Some years after, this model has been positively applied to Earth rifts as well. Hurford and Brunt [32] adopted the model to a crevasse that was generated in the large Antarctic Ross ice shelf in 2005. By changing the dilatation coefficient from ratio of dilatation rates into ratio of dilatation amplitudes, the process was better explained. Already in Tufts et al. [106], the researchers claimed that further corroborations of the model with terrestrial rifts was needed, in order to extend the range of validity of the model. The crack propagated in 2005 from an existing notch nearby the calving line. In Figure 3.4a an aerial picture of the crevasse has been reported. The locations labelled NN and NS in the picture are surveying stations that allowed the detection of GPS signals. Using GPS measurements, it has been possible to extract via inverse problem the velocities of the ice shelves that were separated by the rift. According to
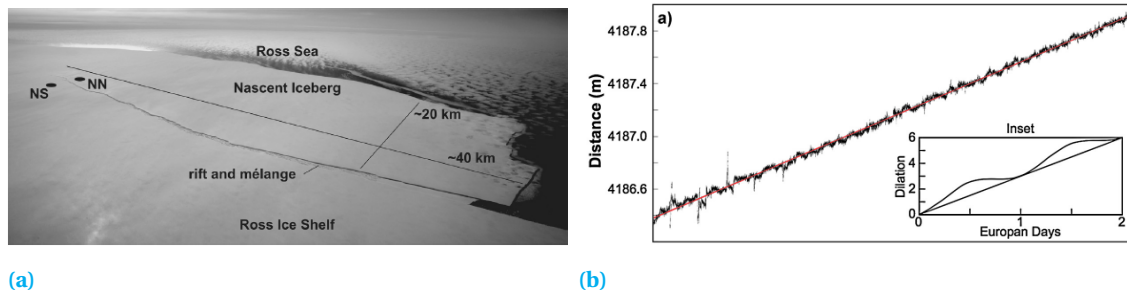
Figure 3.4: (a) Aerial photograph of the rift formed in 2005 in the Ross Ice Shelf, Antarctica. The rift was generated by the propagation of a fracture from the calving front. NS and NN are surveyed station, from which GPS measurements have been taken. The image is coming from the work of Hurford and Brunt [32]. (b) Measurements of rift dilatation in the Ross Ice Shelf in Antarctica [32]. The trend of the data interpolation fits with the model proposed by Tufts et al. [106] for explaining dilatational phenomena for the Europan crust, represented by the secondary image on the right corner. This is the prediction for the trend of the normalised dilatation parameter γ_D (Equation 3.1), as function of time.

the theoretical predictions, the effects of oceanic tides on the two flanks of the ice sheet fit with the dilatation process presented in Tufts et al. [106], that was produced to explain the dilatation phenomena on the surface of Europa. Elaboration of data coming from GPS allowed the discovery of both secular widening and diurnal tidal motion in the area of the Ross Ice Shelf, similarly to what happens on Europa. Figure 3.4b represents the results that the GPS measurements produced for the addressed rift. The changing distance between the two sides of the fault is shown as function of time. In the same picture it is also possible to observe the prediction for the normalised dilatation parameter as function of time, coming from Tufts et al. [106]. The two graphs present a small misfit that allows the Europan dilatation model to be positively applied to terrestrial formations. The positive results that the model of Tufts et al. [106] produced on terrestrial formation, have been a major corroborator for the explanation of extensional phenomena on Europa as imposition of secular components to diurnal tidal deforming effects.

Additionally to the positive terrestrial analogs pointed out by Hurford and Brunt [32], the work of Prockter et al. [78] compared Europan dilatation processes to terrestrial mid-ocean ridges, in particular to the ones at the so-called Rejkyanes Ridge, close to Iceland. Several characteristics of terrestrial mid-ocean ridges and Europan formations are close, but the forces that are driving the processes are considered to be quite different. On Earth, it is clear how the extensional process is directly linked to the subduction of plates. In other words, a terrestrial tectonic plate that is assumed to resemble lithospheric dilatation on one side, directly implies subduction of other sides of plates. This process might cause episodes of volcanism. Indeed, the subduction of the lithosphere drags sediments in lower and warmer layers of the Earth, which may cause the reaching of the melting point, and thus the generation of volcanism [54]. It is the case of the Ring of Fire, surrounding the Pacific Ocean. On Europa, presence of subduction has been proposed by recent studies of Kattenhorn and Prockter [46]. Among others, the evidences are related to the abrupt interruption of some lineament pattern that should be only given by subduction of tabular zones. The strongest source that drive extensional phenomena is again the tidal forcing and the not perfect closure of cracks [106].

Concluding, the process of dilatation directly suggests that an increased amount of material is reversed on the surface of the moon. Dilatational bands are assumed to be the key elements that resurface the Europan surface [78]. The only effects of subduction, might not be enough to determine where the new material is forced to move. On Europa, some compressional ridges have been detected. The work of Prockter and Pappalardo [77] and Schulson [94] found on Europa geological features that can be assumed to be generated by compressional stress. These have the aspect of folds and wedge-cracks. According to other points of view, it has been suggested that the accommodation of material coming from underneath the crust, can be related to the generation of chaotic regions [18] Nevertheless, the amount of compressional formations is definitely the minority of the Europan features. The lack of compressional features and the large presence of extensional ones have been already addressed when talking about the predominant effects of extensional dynamics due to thickening of the ice shell [63].

3.2. STRIKE-SLIPS

Ridges are geological formations that form when the tensile strength in the direction perpendicular to the future lineament is reached by an area of the structure subjected to deformation, hence a crack can be literally opened and eventually, propagated. Generally speaking, it has been shown that diurnal tide can open and close a fracture by inducing the material from the lower warmer layers of Europa to arise and flow on the surface. This process requires a varying stress that is oriented perpendicular to the fracture, in order to be perfectly understood. Nevertheless, with further and more accurate observations the presence of shear stress, even for ridges, might be revealed.

First evidence of a strike-slips has been detected with *Voyager II* images. The spacecraft captured one of the largest lineament in the southern hemisphere of Europa. The feature has been termed after Astypalaea, who, in the Greek mythology, is the name of the wife of Europa. Astypalaea Linea fractures the surface for around 810 km and crosses the southern hemisphere from 85° S to 60° S, approximately (180°-210°W of longitude). The first work that presented Astypalaea as a strike-slip has been Tufts [103].

Compared to terrestrial formations Astypalaea Linea has been identified several time in the literature concerning Europa to be an analog for the large San Andreas fault in California [105]. In these kind of geological features key role is played by shear stress, which is continuously produced by the rubbing between the two oscillating walls of the fracture. A positive mechanism that can explain the formation of strike-slip is referenced as tidal walking, firstly proposed by Tufts et al. [104] and [27]. The idea behind this process is that the diurnal tide redistribute and reorient the stress along the fracture, leading to progressive opening and closure, together with lateral displacement generated by shear stress. Lateral displacement is introduced by oscillation in the stress field from left to right and viceversa. This phenomenon resembles a walking person that puts his left foot forward, push the ground back to go forward, and do the same with the right foot afterward. From here the term tidal walking. A visual representation of tidal walking for the Astypalea Linea is represented in Figure 3.5. The white lines represents tension and black compression. As it can be seen, the stress reorient itself along the crack producing oscillating lateral displacement. For instance, at apojove (Figure 3.5a) the stress is almost perpendicular to the feature while at one quarter of the orbital period (Figure 3.5b), the stress rotated of around 45°, producing right lateral displacement. While the moon completes its orbit around Jupiter, left lateral displacement occurs before reaching the same initial configuration at apojove. Tufts et al. [105] proposed that the superimposition of NSR to non-eccentricity allows an explanation for the possible initiation of Astyplaea and that the further cycles of diurnal tides continuously shapes the aspect of the feature in form of a strike-slip. The subsequent cycles of walking might have led to the generation of lateral displacement and dilation bands that can been observed along the fracture. Diurnal tides are indeed able to explain the mechanism of tidal walking alone, without the contribution of secular components.

A direct consequence of shear stress is the generation of heat, from basic thermodynamic laws. Among others, the work of Nimmo et al. [64] produced a thermal model for the production of heat due to shear stress in strike-slips. The temperature anomaly for a strike-slip has been found to be of 66 K for an ice thickness of 2 km. As consequence, the relatively warmer material might be forced to arise from the crevasse and be accumulated on the top of the rift. That might produce ice melting and possible compression zones around the fracture. Double ridges on Europa (e.g. Class II in Greenberg et al. [18]) can be assumed to fit this thermal model (Fig. 3.1E).

A first attempt of producing an extensive catalog for the observed strike-slips have been proposed in the work of Hoppa et al. [30], who generated a survey of several images taken from the first 15 *Galileo* flybys of Europa. The results revealed 117 strike-slips formations on the surface. According to the survey 95% of the strike-slips in the southern hemisphere are right-lateral. In the area surrounding the equator, an almost equal mix of right and left-lateral is present while in the northern hemisphere the majority of strike-slips is left-lateral. A possible deduction that comes from these observations is that on Europa right-lateral strike-slips are favoured to form in the southern hemisphere while left-lateral strike-slips are preferred in the northern hemisphere. The tidal walking theory fits with this general deduction and with the description of the strike-slips presented in the work. Additionally, Hoppa et al. [30] associated the large majority of strike-slips to ridge formations; 64% of the surveyed strike-slips can be categorised as Class I ridges, 31% can resemble other types of ridges (Class II and Class III) while only 5% of the 117 formations are not showing accumulated material on the top of the crack. Therefore, tidal walking can be enriched with the possibility to accumulate material coming from underneath the shell and a way for accommodating the extra-lithosphere that is generated by extensional phenomena (e.g. Nimmo [63]). A further update to the survey proposed by Hoppa et al. [30] is the one produced by the work of Sarid et al. [90]. The researchers investigated the aspect of several other
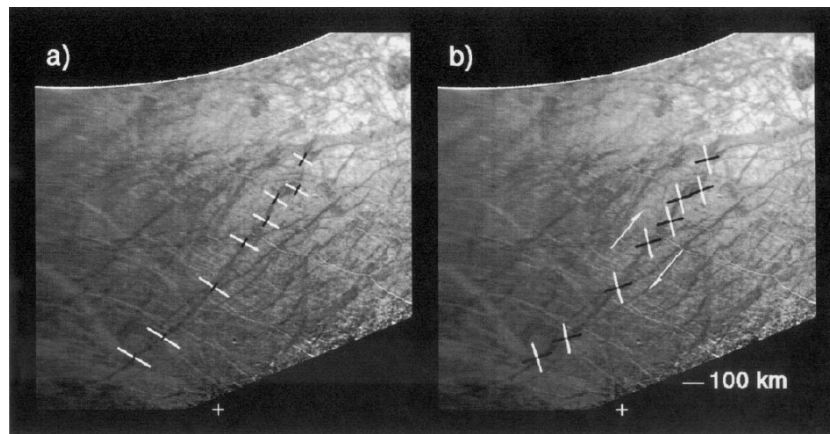
Figure 3.5: Tidal walking process, as proposed in Tufts et al. [104] and Hoppa et al. [27]. (a) Orientation of stress at apojove for Astypalaea Linea. (b) Diurnal stress at 1/4 orbit after apojove. Tension is represented by white lines, compression black. Parts (a) and (b) can also represent stresses at perijove and 1/4 orbit after perijove, respectively, by reversing the signs (i.e., tension black and compression white) [27]. White arrows represents the shear stress, in this case termed left-lateral. The plus (+) symbol, at the bottom of the figures, represents the position of the south pole. The oscillating reorientation of the stress along the feature would produce alternating left and right lateral displacement.

formations that resemble strike-slips, which can be explained by the application of tidal walking. The success of this survey is a further corroboration of the presence of an effective shift in the lateral displacement.

Hoppa et al. [30] and Sarid et al. [90] did not find a preferred lateral displacements for the lineaments in the equatorial region. The favoured right-lateral displacement in the southern hemisphere and the left-lateral displacement in the northern hemisphere predictably yield to a mixed orientation in the areas of the equatorial belt, where chaotic zones are predominant and difficult to model. Spaun et al. [97] produced an analysis for the equatorial region. The presence of pits, domes and lenticulae[4] is generally explained by the presence of diapirism. The work of Spaun et al. [97] surveyed the behaviour of lineaments in two relatively small areas of approximated geographical coordinates of 5°N, 330°W, and 15°N, 270°W respectively. In these areas, the lineaments show a large shear component and the orientation is, for the majority of North-East, North-West directions. These specific orientations of the crack directions can be explained with the strong effects of stresses due to NSR, which can be superimposed to the diurnal deformation. The values for the amount of NSR is calculated to be around 30°-90°. NSR stresses that act in the directions North-South and East-West [18] can explain the inclination of 45° of the majority of lineaments in the equatorial area. As for the lineaments in the polar areas subjected to TPW in Sarid et al. [90], the contribution of secular components is important to understand the dynamical behaviour of strike-slip formations even in the equatorial regions. The work of Rhoden et al. [83] extended the study of the effects that polar wander, non-zero obliquity and physical libration have on cycloids (section 3.3), to strike-slip formations. Even if a single value for the obliquity of Europa has definitely not been assumed, dealing with the findings of Baland et al. [3]), the theoretical predictions of Rhoden et al. [83] fit with the observed behaviour of several strike-slips. The preferred model in the work is that Europa has a 1° of obliquity and the polar wander occurs in longitudinal direction. The influence of physical libration induced an improvement of accuracy in the predictions of faults locations but could not produce a correct direction for the features. Uncertainties in NSR and TPW parameters have been already addressed in section 2.2.

In section 3.1, two ways of accommodating extensional lithosphere have been presented, namely compressive folds [77] and generation of chaotic regions [18]. Nevertheless, the convergence regions deduced by the strike-slips analysis of Sarid et al. [90] did not fit the two accommodating mechanisms. The researchers suggested the presence of some compressional bands, that work under a principle that is opposite to the dilation bands. A possible compressional band can be a strike-slip, Agenor Linea (190°-250°W, 40°S), which cannot be explain by a the definition of a dilational band. Sarid et al. [90] and several other studies failed in reconstructing the closure of this lineament and the effective presence of compression for Agenor Linea suggests that the material surrounding the fracture might have been much further apart than the period of *Galileo* observations. It has been already pointed out that the lacking of compressional features on Europa

---

[4]Lenticulae are defined as circular-elliptic patterns, morphologically produced [69, 70].

is still argument of discussion and doubts. Furthermore, in order to better fit the theory to the observations, Sarid et al. [90] claimed the presence of polar migration (TPW) and, as consequence, that the former north pole, has shifted of around 30° into the present state during a time period that is less than a few million years.

Finally, Preblich et al. [76] simulated the behaviour of the tidal walking phenomenon by the usage of Finite Element Methods (FEM). A viscoelastic model for the material was given to a structure that is floating above a liquid water layer. A stress field that reaches amplitudes and orientations able to fracture the ice layer is applied. The thickness of the ice can vary from 1 to 10 km. For a layer that is 1 km, the simulations result in a fracture that penetrates through all the vertical direction, hence until the reaching of the underneath ocean. On the other hand, the 10 km thickness is assumed to simulate the partial penetration of the fracture. In particular, this last case showed a propagation of the crack until the warm buoyant region of the ice shell interfaces the cold part of the ice. As it has been shown already by the survey of Hoppa et al. [30], the fact that the fracture reaches the bottom of the ice shell, is particularly important because if that happens, the material (even organic) that floats in the ocean can find a way to the surface, generating for example ridges and secondary canals. The current research will try to give more constraints on the eventual possibility of the full fracture of the ice layer.

Concluding, strike-slips are interesting pattern to study, given the remarkable comparisons with terrestrial formations. All of them are assumed to be generated by shear stress due to diurnal tides in a already existing fracture of the brittle surface. The direction and the orientation for the majority of the lineaments in the areas close to the poles can be explained by diurnal tides superimposed to TPW, while for the areas surrounding the equator NSR presumably governs the initiation of shear stress. The majority of strike-slips are associated to accumulation of material from underneath the crust, thus to Class I ridge formation. Accommodation of material can fit with the tidal walking theory. Large strike-slips as Astypalaea Linea are a perfect target for the numerical simulations proposed in the current research, since it has several similarities with strike-slips already existing on Earth, i.e. the large San Andreas fault in California and a numerical model that simulates the tidal walking process has been already proposed.

3.3. CYCLOIDS

The last category of features that will be addressed in this chapter are called cycloids. In the literature, it is also possible to find the Latin term flexus (plural flexi), which is the official IAU denomination. In this section and in the rest of the work, the two terms will be used indistinctly.

Even by giving a rapid look to the global map of Europa, it is possible to observe several lineaments that posses an arcuate shape, each formed by segments of around 100 km on average [29]. These patterns are called cycloids. Example are Cilicia, Sidon and Delphi flexi in the southern hemisphere around 60°S, 170°-180°W. In particular, it is relatively easier to observe these kind of features at high latitudes in absolute values, hence close to the poles. The reason for that will be explained later in this section.

The first attempt of generating a model for the arcuate patterns observed on Europa is contained in the work of Hoppa et al. [29]. This model is mainly based on geometrically matching the theoretical predictions of large cycloids due to tidal stress in the southern hemisphere of the moon, with images of *Galileo*. The simple application of the diurnal tide, expressed in Greenberg et al. [18], can explain the generation and the propagation of the crack, in a way that resembles a flexus. According to the rheological parameters assumed by Hoppa et al. [29], the tensile strength for the Europan ice is reached at 25 kPa. The fracture starts to propagate until a point where the tensile strength is not reached anymore. There, the crack stops to propagate. After a period that can be compared to the day on Europa (≈ 85 hr), the point where the cracked stopped to propagate might undergo to a stress condition that is close to 15 kPa which is the tensile strength for a 'weak' ice that was already initiated. That would lead to a new initiation and propagation of the fracture through the ice shell, namely a reactivation of the precedent crack, with geometrical characteristics which will be different from the precedent. The geometrical pattern that links the two fractures that have been propagated in the two different tidal cycles is called cusp. A cycloid can be formed after several diurnal cycles. A relatively thin layer of ice (less than 100 km) that covers a global ocean, is necessarily required in order to validate the model. By using ice penetrating radar techniques, it has been possible to corroborate the fact that some cracks would penetrate throughout the entire brittle crust, in order to explain the proposed fracturing models [52].

After having obtained new images and new data from *Galileo*, the model of Hoppa et al. [29] has been continuously enriched and substantially improved throughout the years. The model proposed by Marshall and Kattenhorn [57] added new insight in the process of crack initiation, which for Hoppa et al. [29] was only due to tensile strength reached in direction normal to the crack. The relatively new model added the intro-
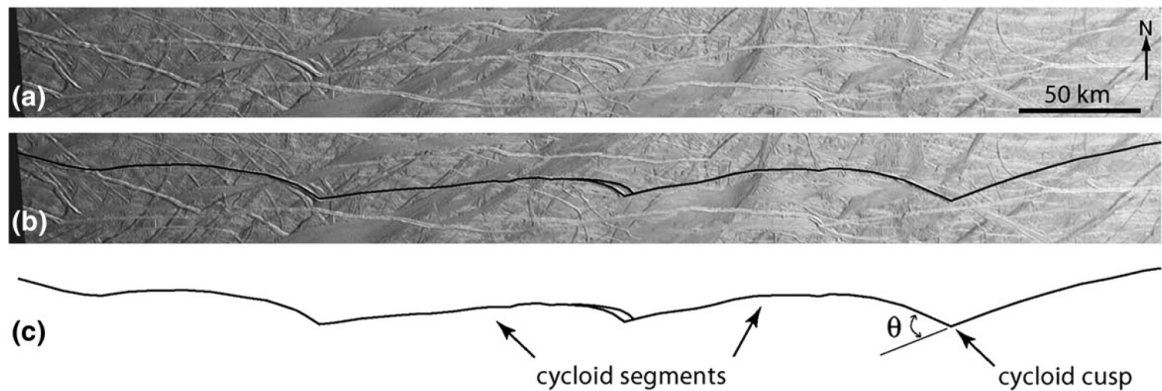
Figure 3.6: Picture taken from Kattenhorn and Marshall [45](a) Image taken from *Galileo* flyby E17 on the southern hemisphere of Europa, capturing a cycloid. (b) The cycloid shape is traced on the image. (c) The cycloidal segments are joined with cusps, tailcrack are evident and described by the cusp angle θ.

duction of shear stress in the analysis and hence of the tidal walking theory, addressed in the previous section for strike-slips formations. Furthermore, the inclusion of the effects of tailcracks have produced remarkable outcomes in the later studies. Tailcracks are formed by shear stress at the end of one fracture in a brittle material. Due to the weakened area that is surrounding the crack, it is relatively easier to initiate new secondary fractures. Additionally, Marshall and Kattenhorn [57] positively introduced the effects of shear stress in cycloidal formations. In particular, the generation of tailcracks has been modelled via linear elastic fracture mechanics (LEFM) just some years later by the same authors [45]. In this work, extensional tailcracks are formed in combination with compressional anticracks and both can be observed in *Galileo* images. Figure 3.6, taken from [45] shows a cycloidal crack observed by *Galileo* in the southern hemisphere of the moon (a). In order to visualise the shape of the crevasse, the trace of the cycloid is plotted in black along the existing shape (b). The formation of multiple cycloidal segments can be seen in Figure 3.6 (c), where the cusp angle θ is indicated. This publication further elaborated the similarities that cycloids have with strike-slips by usage of LEFM techniques, which are able to precisely characterise the magnitude of the tailcrack and anticrack angles . LEFM and FEM analysis have succeeded in several simulations of terrestrial icy fractures. In particular, LEFM will be the key numerical tool used in the current research.

The models that have been presented so far, are characterised by the common fact that they can explain cycloids only by taking into consideration diurnal tides. In chapter 2, it has been pointed out that on Europa diurnal tides are acting in combination with secular contributions, namely NSR and TPW, among others. The first model that introduced NSR in the explanation of cycloids is the one proposed in Hurford et al. [33]. Furthermore, the model achieved an improvement in the simulation of large cycloids by including the possibility of variating rheological parameters during the propagation of the cycloid chains. These two opportunities were not accounted in the previous models. Nevertheless, the results of these simulations confirmed the findings of Hoppa et al. [29] and Marshall and Kattenhorn [57], namely that the effects of NSR improve the matching only of a few flexi. Indeed, in a more recent publication of the same authors [35], the focus has been concentrated in the introduction of other sources of diurnal deformation, such as the non-zero obliquity, instead of secular components. Additionally, as already addressed in section 2.2 while talking about diurnal tides, Rhoden et al. [82] introduced the effects of physical libration, in order to further improve the models for cycloids. A discussion has been already issued in the current literature review, concerning the actual value of Europa's obliquity, that finds several contrasting opinions in the literature, mainly dealing with the publications of Rhoden et al. [82] and Baland et al. [3].

More in details, Hurford et al. [33] and Hurford et al. [35] produced interesting findings in the speed of propagation of a cycloids. Observing cycloidal shapes, values for the propagation speed of 4.8 km/h, initiation stress of 68 kPa and propagation stress of 38 kPa are generally accurate characterising values, on average. The value for the non-zero obliquity is assumed to be 0.1°, similarly to what proposed by the work of Bills [6], an order of magnitude less than the 1° of Rhoden et al. [82] and almost double of the 0.055° of Baland et al. [3]. Propagation of cycloids in both eastward and westward direction, assuming rheological parameters that fit the large cycloids in the Argadnel Regio, are close to the sub-jovian point (200°-230°W at the equator). These features are fit when choosing a argument of perigee that ranges between 180° and 315°. The simulations

allowed the generation of a relatively more arcuate pattern in regions close to the poles. This is the reason why cycloids are better observed at high latitudes. Nevertheless, this does not mean that only polar regions produce cycloids.

The work of Groenleer and Kattenhorn [22] focused more on the effects of tailcracks, which are assumed to be the large factor that generate cusps and hence arcuate cycloids. The models of Groenleer and Kattenhorn [22], as well as the addressed work of Kattenhorn and Marshall [45], used LEFM tools in order to simulate the large flexi in the southern hemisphere. Additionally, a contribution of 600° of NSR better fits the geometry of the patterns. By studying the geometrical aspect of cusps, the researchers improved the models for the cycloids that present a large arcuate shape. Nonetheless, the introduction of tailcracks and NSR is not able to explain the flexi that can be seen in the Argadnel Regio [35]. The already presented work of Rhoden et al. [82], introduced the contribution of physical libration to the initiation of cycloids.

Concluding, cycloids are interesting features to investigate. It is definitely still unknown which are the stressing sources that mostly contributes to the initiation and the propagation of these arcuate patterns. Several studies proposed that the only effects of diurnal tides (non-zero eccentricity, non-zero obliquity and physical librations) are enough to explain the presence of flexi in the region around the equator and close to the sub-jovian point (i.e. Argadnel Regio). On the other hand, the large and arcuate patterns that can be seen close to the poles (e.g. Delphi, Sidon and Cilicia flexi) are more likely to be generated by the propagation of secondary cracks, namely extensional tailcracks. The contribution of secular components such as NSR are still under research and only some authors proposed the necessity of a certain amount of NSR to explain the arcuate pattern of flexi. For sake of the proposed research, the usage of LEFM will result as an useful tool in defining rift's depths, as it will be addressed in the following chapter. Parameters such as the obliquity value will be tuned in order to produce a sensitive analysis. Same considerations can be done with the assumption of physical characteristics of the ice.

II

METHODOLOGY

4

TIDAL POTENTIAL THEORY

The current chapter aims to describe the concept of tides, both from a qualitative and a quantitative point of view. Tides are the effects of a differential gravitational attraction, hence the concept of potential plays a key role in the analysis. As it has been mentioned already, tides can be distinguished into two different groups, namely time dependant and time independent components. If a moon orbits around the host planet in a circular and synchronous motion, the tidal bulge is arising on the line that virtually connects the two centres of the bodies. This is also called as primary tidal components and it maintains its fixed position, excluding natural oscillations that occurs around the equilibrium status (phenomenon known as physical libration). Additionally to the fixed tidal component, the variation of orbital parameters, such as the eccentricity, introduces forced migration of the tidal bulge that would imply stress redistribution, as it is explained later on. These ulterior components are depending on the orbital position of Europa around Jupiter, hence on time. The rest of the chapter deals with fixed and migrating tidal components in order to present tides in a more formal approach.

Section 4.1 starts with the identification of the gravitational law which will be used to obtain the Gauss theorem. This is one of the most important theoretical tools in the investigation of gravitational potentials. In particular, the Gauss theorem in vacuum takes the form of a Laplace equation, whose possible solutions can represent the gravitational field of the Earth in its complexity. These concepts are described in section 4.2. Finally, section 4.3 provides a complete mathematical description of tides and is applying the results to the case of the Jovian moon Europa. This chapter starts with the mathematical background needed for understanding the tidal potential theory, which is the key tool for calculating the stress on the surface of Europa.

As mentioned, the concept of potential provides very useful mathematical tools when one needs to analyze a vectorial field. Generally speaking, the potential is a scalar translation of a specific vectorial property. For instance, the gravitational attraction between two massive bodies is a force directed toward the centers of mass of the two, according to Newton's laws. In three dimension, such as when considering an object attracted by the Earth, the gravitational force can be represented by a vectorial field around the globe. Since gravitational force is a central force, mathematically it also possible to state that this force is nothing more than a gradient of a scalar field, which is the gravitational potential [59]. In symbols this concept is expressed as:

$$\mathbf{v} = \nabla U \qquad (4.1)$$

where U is the so called potential. An other property that would define a field as conservative is that the curl of the field itself to be null [9]. Anyhow, for the sake of the current purposes, the identification of conservative field as gradient of a potential is enough. The reader is encouraged to refer to calculus textbooks for further insights. The gravitational attraction of a mass is a conservative force, hence the gravitational potential can be found. A property of a conservative field is that the work between 2 points is always non dependent of the path taken[1]. This can lead to the identification of the potential energy, which is nothing more than the

---

[1]This condition can also be taken as a requirement for a force to be conservative.

potential, changed in sign. The difference between potential is often confusing and it merely depends on assumptions.

Isaac Newton firstly proposed that two massive bodies are attracting each other by a force that is proportional to their masses. Equation 4.2 represents the universal gravitational law for two point masses. Henceforth, these will be called bodies or points without distinction. In the formula, the force of body 2 on body 1 F_{21} is expressed. G is the universal gravitational constant, measuring $6.6740831 \times 10^{-11}$ m^{3}kg^{-1}s^{-2} in alignment with the indications of the Committee on Data for Science and Technology. Additionally, m_1 and m_2 are the masses of the two bodies. $\mathbf{r}_{21}$ is the vector pointing from body 2 to body 1. Its module is r_{21}. The remain of the mathematical analysis of this section is based on [12].

$$\mathbf{F}_{21} = -\frac{Gm_1 m_2}{r_{21}^3}\mathbf{r}_{21} \tag{4.2}$$

Gravitational forces as every other force in nature follows the additive property meaning that if two or more points are acting on an other one, their contribution can be added and the resulting force is following standard parallelogram rules.

Tides are just the differential action of two attractors to a single point in the space. If this point is located to the surface of a moon, and the attractors are the host planet and the moon itself, the tidal force is the differential pull of the host planet at the surface subtracted to the one at the center of the moon [54]. After the description of potential in terms of spherical harmonics, the current chapter focusses on the mathematical presentation of tides.

4.1. GAUSS THEOREM

For sake of simplicity, one of the two mass of Equation 4.2 will be called the attractor. The second one will be called test mass. The gravitational attraction acting on the test mass can be found dividing the gravitational force itself by the mass of the test body. Result is an acceleration, measured in m/s^2. Therefore, it is possible to measure a vectorial field around the mass which is not affected by eventual test masses. Equation 4.3 represents the gravitational field of a an attractor with mass m. Again $\mathbf{r}$ is the vector from the attractor with module r.

$$\mathbf{g}(\mathbf{r}) = -\frac{Gm}{r^3}\mathbf{r} \tag{4.3}$$

It is also possible to find the gravitational attraction of a 3D body with an other shape, just by evaluating the specific value for its mass. In other words, m must be integrated over the volume of the body in the following form:

$$dm(\mathbf{r}) = \rho(\mathbf{r})dx dy dz \tag{4.4}$$

where the coordinate reference system is a pure Cartesian x, y and z right-hand system.

As consequence, it is possible to calculate the gravitational attraction of an arbitrary shape by the solving the integral:

$$\mathbf{g}(\mathbf{r}) = -G\iiint_V \rho(\mathbf{r}')\frac{\mathbf{r} - \mathbf{r}'}{|\mathbf{r} - \mathbf{r}'|^3}dV \quad \text{where} \quad dV = dx dy dz \tag{4.5}$$

In the equation, $\mathbf{r}$ is the vector that represents the position of the attractor, while $\mathbf{r}'$ is the position of the test mass, with respect to the center of the reference frame.

A further step in the description of the potential is the introduction of the concept of flux. Qualitatively, the flux is defined as the 'amount' of stream line of a certain vectorial field that pass through a fictitious surface. Mathematically, an arbitrary vectorial field $\mathbf{v}$ produces a flux through a surface S defined as:

$$\Theta = \iint_S \mathbf{v} \cdot \mathbf{n}\, dS \tag{4.6}$$

where the scalar product is between the vectorial field $\mathbf{v}$ and the normal to the surface S, indicated by the unitary vector $\mathbf{n}$. The idea of the flux is particularly useful in fluid mechanics, where one can visualise the stream of lines as a fluid current, for instance. According to the orientation of the surface (hence to its normal

vector), the flux can be maximum, when the surface is perpendicular to the stream lines or null, when the surface is parallel to the vectorial field. This behaviour is mathematically determined by the dot product. In other fields of physics, such as in electromagnetism or gravity, the idea of flux is much more abstract, but the analogs with liquid stream lines always holds as comparison.

A further step in the analysis of the flux is the usage of the divergence theorem. This is particularly useful when one wants to calculate the flux through a closed surface. The theorem states that the closed surface integral (which can be expressed by the symbol $\oiint$) of the vectorial field through the surface itself is equal to the volume integral of the divergence of the same vector for the space confined by the surface [9]. In mathematical terms:

$$\oiint_S \mathbf{v} \cdot \mathbf{n} \, dS = \iiint_V \nabla \cdot \mathbf{v} \, dV \tag{4.7}$$

It is relatively easy to explain the divergence theorem with the fluid mechanics analog once again. In this case, the flux through a close surface can be produced by the presence of some kind of positive or negative source in the interior of the surface itself. In the liquid case, these can be represented by a fountain or a well. In other words, some kind of source has to exist in the confined volume. Otherwise, if the closed surface is placed through a liquid current the net flux would be zero, since the amount of liquid that enter, is the same that exit. This does not happen if there's some sort of leak, mathematically explained by the divergence operator. The theorem keeps track of what happens inside a confined volume.

The application of the flux and the divergence theorem to the gravitational field is the key operation for the implementation of the potential theory that can give enormous understanding for mass transport processes on Earth or on other planets. The flux of the gravitational field of a point mass can be expressed by the following equation:

$$\Theta = \iint_S \mathbf{g} \cdot \mathbf{n} \, dS \tag{4.8}$$

The result has the same properties of the flux expressed by Equation 4.6. The gravitational vectorial field $\mathbf{g}$ for a point mass is shown in Equation 4.3. Therefore, it is possible to insert Equation 4.3 into Equation 4.8. This also means that the closed surface has to envelope the point mass, otherwise the net flux would be null.

$$\Theta = \oiint_S \mathbf{g(r)} \cdot \mathbf{n} \, dS = \oiint_S -\frac{Gm}{r^3} \mathbf{r} \cdot \mathbf{n} \, dS = -\frac{Gm}{r^2} \oiint_S \frac{\mathbf{r}}{|\mathbf{r}|} \cdot \mathbf{n} \, dS \tag{4.9}$$

where the factors that are not related to the calculation can be taken outside the integral. For simplicity, a sphere can be assumed as closed surface with the point mass at the very center. Therefore, it is possible to see that the radial vector $\mathbf{r}$ and the normal to the sphere $\mathbf{n}$ are always parallel, leading to a dot product that is always unitary. Thus, the flux can be expressed:

$$\Theta = -\frac{Gm}{r^2} \oiint_S dS = -4\pi Gm \tag{4.10}$$

where the integral is reduced to the evaluation of the area of the sphere, measuring $4\pi r^2$. It is possible to prove that in every closed surface the scalar product between a radial vector and the normal to the surface (terms inside the integral) is always 1. So, the results of Equation 4.10 are valid for every geometrical configuration.

Equation 4.10 itself represents already very interesting results. This is called integral formulation of the Gauss theorem. The flux of a point-mass gravitational field through a closed surface that englobe the point itself is only related to the measure of its mass. Additionally, it is possible to prove that for every 3D massive body (whose gravitational attraction is expressed by Equation 4.5) the results are the same of Equation 4.10 where m would be the mass of that body. This is also valid if one considers 2 or more massive objects instead of one. The only constraint is that the surface has to envelope the entire masses; thus the term m would be the sum of the masses.

Next step would be the application of the divergence theorem, expressed in Equation 4.7. The flux Θ can be calculated with the solving of the volume integral for the divergence of the gravitational attraction. The results can be summarised in the following equation:

$$\Theta = \iiint_V \nabla \cdot \mathbf{g} \, dV = -4\pi Gm \tag{4.11}$$

In the equation, it is possible to re-write the mass term as function of the density as shown in Equation 4.4. Indeed, the evaluation of the total mass of a generic 3D body is nothing more than the volume integral of the density itself.

$$m = \iiint\limits_{x,y,z} \rho \, dx \, dy \, dz = \iiint\limits_{V} \rho \, dV \tag{4.12}$$

Substituting Equation 4.12 into 4.11, it is possible to write the following:

$$\iiint\limits_{V} (\nabla \cdot \mathbf{g}) \, dV = \iiint\limits_{V} (-4\pi G \rho) \, dV \tag{4.13}$$

which give as differential formulation:

$$\nabla \cdot \mathbf{g} = -4\pi G \rho \tag{4.14}$$

The result is called differential formulation of the Gauss theorem. Operationally, Equation 4.14 has the same meaning of Equation 4.10 because the only mathematical operation is the identity given by the divergence theorem[2]. The theorem links the direct gravitational attraction to the composition of the attractor. If the Gauss theorem is applied in vacuum (ρ=0), Equation 4.14 simplifies into:

$$\nabla \cdot \mathbf{g} = 0 \tag{4.15}$$

The identification of a null divergence makes the vectorial field to be solenoidal, which characterises incompressible fields in fluid mechanics, for example Bramanti et al. [9]. Furthermore, if the vectorial field is also conservative, it is possible to express it as a gradient of a certain potential (Equation 4.1) [9]. It has been already stated that the gravitational attraction is a conservative field, hence the concept of gravitational potential can be used. The gravitational potential is called Φ and it can be related to the gravitational attraction as follows:

$$\mathbf{g} = \nabla \Phi \tag{4.16}$$

A valid function of Φ that satisfies Equation 4.16 is the following, that will be used in the rest of the chapter as definition of gravitational potential:

$$\Phi = G \frac{m}{r} \tag{4.17}$$

Substituting the definition of gravitational potential of Equation 4.16 into the differential formulation of the Gauss theorem links the gravitational potential to the density of the attractor. This operation simplifies the case because the problem can be solved in a scalar dimension instead of a vectorial.

$$\nabla \cdot \nabla \Phi = -4\pi G \rho \quad \text{hence} \quad \nabla^2 \Phi = -4\pi G \rho \tag{4.18}$$

where the mathematical operator ∇^2 is called Laplacian and Equation 4.18 is called Poisson equation. If one wants to apply the same cosideration to the vacuum case, the equation simplifies into:

$$\nabla^2 \Phi = 0 \tag{4.19}$$

which is known as Laplace equation. Functions that are among solutions of the Laplace equation are called harmonic functions. The Laplace equation describes lots of natural phenomena such as heat transfer or the conformation of the gravitational field around a planet, which is the case that will be investigated in the next section.

4.2. SPHERICAL HARMONICS

The solution of a partial differential equation (PDE) is a function that substituted into the PDE itself, generates the identity. Theoretically speaking, given a simple PDE, the number of solutions is infinite [89]. If one wants to find a specific solution for a specific case, some constraints have to be set. These are called boundary or initial conditions. There are specific ways of solving a PDE. It is possible to implement numerical algorithms that can produce solutions by minimising the residuals from the true solution. On the other hand, some

---

[2]In many texts, the usage of Gauss theorem or divergence theorem has the exact same meaning, intending the indentity of Equation 4.7.
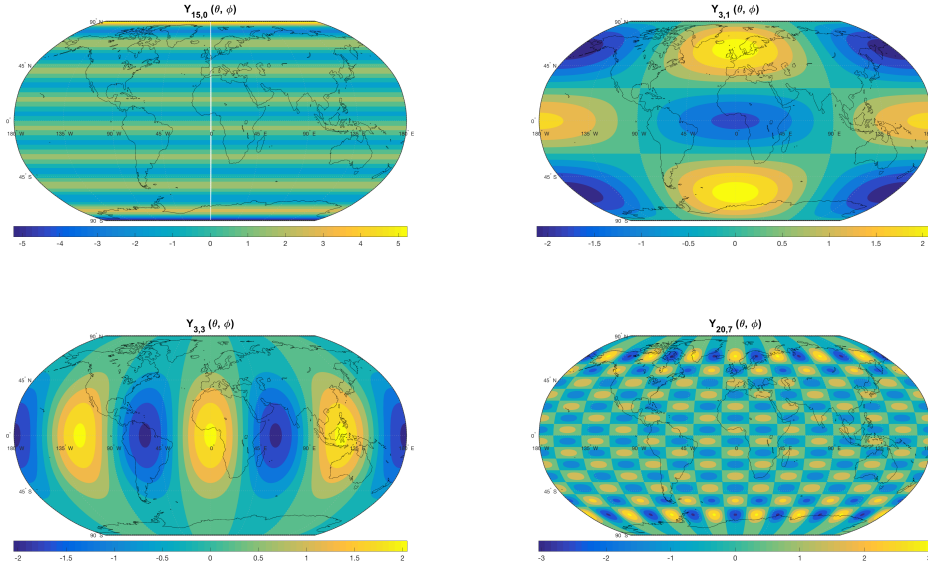
Figure 4.1: Representation of various degrees and orders for the non-normalised surface spherical harmonics $Y_{l,m}$, where l is the degree and m the order. The scalar function is plotted over the surface of the Earth. When the order m is null, the harmonics are called zonal and it is possible to notice no dependency with the longitude. If the order is $m = \pm l$, the functions are called sectorial and the symmetry with the equator is evident. All other spherical harmonics are called tesseral.

analytical techniques can be proposed, although for the large majority of PDEs a correct analytical solution is difficult or impossible to find [89].

One of the most common analytical technique is the so-called separation of variables. The general idea behind this technique is the decomposition of a PDE's potential solution into different factors, each one function of a specific variable in the game. After that, the function is substituted into the actual PDE in order to find whether or not it is a solution. For example, if a specific PDE's domain is set in time and space, a valuable separation of variable would be factorise the candidate function in a term that is dependent of time and one that is dependent of space. The separation of variables technique is a purely empirical method which produced elegant and relatively simple solutions to a discrete amount of PDEs. Nevertheless, for complex equations it is often convenient to adopt numerical integrators.

The Laplace equation (Equation 4.19) is a PDE and also a very common representation of several phenomena of physics and science. Solutions of the equations are called harmonics function and equation can be translated in finding functions whose Laplacian operator is null. If the right member of Equation 4.19 is not zero, then its name is Poisson equation. The Laplace equation of Equation 4.19 describes the gravitational potential for every point outside the radius of the Earth.

It is also possible to state that a function can be represented by an expansion of other (usually more simple) function. Details of the problem of a function representation are given in Appendix A. Examples are the generalised Fourier expansion (Equation A.11) or the usage of an arbitrary set of orthogonal functions (e.g. the Legendre polynomials of Equation A.4). It is possible to represent the gravitational potential as a series of expansion as well. The only constraint is that it should be a series of harmonic functions, given that their linear combination should satisfy the Laplace equation. One might decide to divide the representing function in terms of different factors, each one dependent of a different parameter, as the variation of variables technique provides. When dealing with spherical bodies, it is particularly useful to express the equation in the spherical coordinates, comprehending longitude φ, colatitude θ and distance from the centre of the attracting body r. Particularly useful types of orthogonal functions that satisfy the Laplace equation are called solid spherical harmonics which is described by the following relation:

$$H_{lm}(r,\theta,\varphi) = \left(\frac{R}{r}\right)^{l+1} P_{l,|m|}(\cos\theta) \begin{cases} \cos m\varphi & \text{if } m \geq 0 \\ \sin|m|\varphi & \text{if } m < 0 \end{cases} \tag{4.20}$$

where the term l and m are the degree and the order of the harmonics. The term R is the radius of the Earth. The function is formed by three different functions depending on different parameters. The first depends on the distance from the center of the Earth, the second one depends on the latitudes while the last one on the longitudes. This is an emblematic example The term $P_{lm}(\cos\theta)$ is a generalisation of the Legendre polynomials and it is called associated Legendre function of degree l and order m. The explicit formulation for the factor $P_{lm}(\cos\theta)$ can be found in Moritz [59] and it can be written as:

$$P_{lm}(x) = 2^{-l}(1-x^2)^{m/2} \sum_{k=0}^{\texttt{floor}[\frac{l-m}{2}]} (-1)^k \frac{(2l-2k)!}{k!(l-k)!(l-m-2k)!} x^{l-m-2k} \tag{4.21}$$

where the term $\texttt{floor}[A]$ is the largest integer lower than the term A. Equation 4.21 is practically hard to solve and for the majority of the cases, the terms P_{lm} are calculated via recursive methods [25]. When setting $m = 0$, the equation that calculates the associated Legendre functions become the definition Legendre polynomials (addressed in Appendix A). It is possible to state that the associate Legendre functions are a generalisation of the Legendre polynomials.

If one extracts from the solid spherical harmonics the factor that is dependent with the distance from the center of the Earth, what remains is only function of the specific location given by colatitude and longitude. These part of the solid spherical harmonics are called surface spherical harmonics and it is defined as the term Y_{lm}, as follows:

$$Y_{lm}(\theta,\varphi) = P_{l,|m|}(\cos\theta) \begin{cases} \cos m\varphi & \text{if } m \geq 0 \\ \sin|m|\varphi & \text{if } m < 0 \end{cases} \tag{4.22}$$

The surface spherical harmonics can also be obtained by restricting the solid spherical harmonics to the surface of the Earth, meaning setting $r = R$ in Equation 4.20. The dependance of Equation 4.20 and 4.22 with the degree l is the same that the Fourier series has with the number of harmonics. An higher degree means a faster variation of the spherical harmonic between two different points. On the other hand, the order m gives indication about the spatial distribution [12]. More in specific, depending on the order of the harmonic, it is possible to define zonal, sectorial and tesseral harmonics. Zonal harmonics are identified by a null order. These functions are constant along a certain latitude, hence there is no dependency with the longitude. Sectorial harmonics' degrees and orders satisfy the relationship $l = \pm m$ and their representation over a sphere is symmetric with the equator. All the other kinds of spherical harmonics are called tesseral. The representation of four different types of spherical harmonics, plotted over a map of the spherical Earth is shown in Figure 4.1, where zonal, sectorial and tesseral harmonics can be visualised. Spherical harmonics allows the representation of functions that would be very difficult to define otherwise.

By convention, it is possible to scale the mentioned coefficient with an arbitrary real constant [12]. As a matter of fact, one useful operation that is usually applied to the spherical harmonics is the so called 4π normalisation. The L^2 norm of the surface spherical harmonics is defined as:

$$||Y_{lm}|| = \sqrt{\iint_w Y_{lm}^2(\theta,\varphi)\mathrm{d}w} \tag{4.23}$$

where $\mathrm{d}w = \sin\theta\mathrm{d}\theta\mathrm{d}\varphi$ is the area of a surface element. The spherical harmonics that are divided by their 4π norm are also called as normalised spherical harmonics and labelled as $\overline{Y}_{lm}$. Of course, the same procedure can be applied to solid spherical harmonics and to the associate Legendre function [12].

Appendix A presents the basics of how to represent a function in terms of a series of other function. This is particularly useful to describe complex non-linear relationships between parameters of a function. In this sense, it is possible to approximate the gravitational potential Φ, function of radius r, co-latitude θ and longitude φ as a series of solid spherical harmonics. This is possible because spherical harmonics are a possible solution of the Laplace equation, therefore the potential can be written as a expansion of them. In the specific

$$\Phi(r,\theta,\varphi) = \sum_{l,m=0}^{\infty} \overline{C}_{lm}^{(\Phi)} \left(\frac{R}{r}\right)^{l+1} \overline{Y}_{lm}(\theta,\varphi) = \sum_{l,m=0}^{\infty} \overline{C}_{lm}^{(\Phi)} \overline{H}_{lm}(r,\theta,\varphi) \tag{4.24}$$

where the coefficients $\overline{C}_{lm}$ are the Fourier coefficient of the series and also known as Stokes coefficient for the gravitational potential Φ and calculated as:

$$\overline{C}_{lm}^{(\Phi)} = \iint_w \Phi(r,\theta,\varphi)\overline{Y}(\theta,\varphi)\mathrm{d}w \tag{4.25}$$

where again w is the area of the infinitesimal surface. Equation 4.24 represents the most common way of writing the gravitational potential. As it has been previously mentioned, also the tidal potential can be represented as a linear combination of gravitational potential calculated at different locations. hence the formulation of the tidal potential in terms of spherical harmonics is possible. The concept of tides is presented in the next section.

4.3. TIDES

On Earth, tides are intimately linked to the oscillating pattern of the sea level in the coastal areas. Anyone who has been to maritime areas, has experienced rise and fall of the sea surface at least twice a day. Depending on the location on Earth, the amplitude of the sea level oscillations can vary between a few centimetres to several meters. Notorious example is the coast of Normandy which experience very large tidal oscillation. Certain places in North France, such as the castle on Mount St. Michel, cannot be reached on foot when the tide is high. Oceanic tides are the most evident results of the gravitational disturbance of the Sun and the Moon on Earth. In reality, also the solid Earth is affected by tides that deform its structure but these results are more difficult to observe. The reason is that liquid matter responds faster than solid matter to such perturbations. Despite the fact that both continents and oceans are affected by the variating gravitational attraction that falls under the name of tides, only ocean are responding to these perturbations in a timely way. Tides are also the longest waves in oceanography and can be easily and precisely predicted [93]. Tides mixes and redistribute chemicals components in the ocean, producing fertile conditions to an extremely large number of organisms. On Europa, where tides are orders of magnitude higher than the one on Earth, the effects are though to be even more relevant in the global understanding of the moon dynamic. Indeed, the most relevant gravitational source that acts on Europa is the massive Jupiter, which is at the distance Earth-Moon but it is 20000 times more massive [16]. As consequence, tides on Europa are easier to study and larger to visualise, with respect to the ones on Earth.

The gravitational attraction of multiple massive bodies creates differential forces that deform the surface and the interiors of all the bodies. On Earth, the bodies that are influencing the most the gravitational potential are the Moon and the Sun. On Europa, only Jupiter induce relevant variations but a more complete analysis would include also the effects of the other Galilean moons. The rest of the current section is describing the mathematical analysis for the understanding of tides by using the described tidal potential theory. The basics vectorial formulation for the tide generating force is expressed in section 4.3.1, including the application of the spherical harmonics. The current approach is the same of Jara-Orue and Vermeersen [42] and its results provide an analytical formulation for the stress acting on the surface of Europa by the usage of normal mode theory. These results are summarised in section 4.3.2.

4.3.1. TIDE GENERATING POTENTIAL

The following section is based on the Kaula approach [47] and summarised in Schrama [93]. As it has been mentioned before, tides are the result of the differential gravitational attraction between two or more body. Figure 4.2 represents the two dimensions geometry of the problem of tide generating potential between two celestial objects. Assuming that two bodies are orbiting each other in two dimensions, the primary object called P and the moon M. The forces are acting on a point of the surface of P named location S. The gravitational attraction of the moon of the surface of the primary body can be called as $\mathbf{f}_{PM}$ and $\mathbf{f}_{SM}$, with the directions shown in Figure 4.2, the former being the reaction of the moon action on the centre of the body P and the latter being the actual effect of the moon on the surface. The differential gravitational attraction can be expressed by a simple vectorial summation as:

$$\Delta \mathbf{f} = \mathbf{f}_{SM} - \mathbf{f}_{PM} \tag{4.26}$$

Recalling the first details for the potential theory, the gravitational force, being conservative, can be rewritten as the derivative of the scalar function called potential (Equation 4.16). Stated that, it is possible to rewrite Equation 4.26 in terms of gravitational potential as follows:

$$\Phi^T = \Phi^{SM} - \Phi^{PM} \tag{4.27}$$

where the term Φ^T is called tidal potential. Since the tidal potential is a difference between two gravitational potential, it assumes the form of a gravitational potential itself (Equation 4.17). As consequence, the term
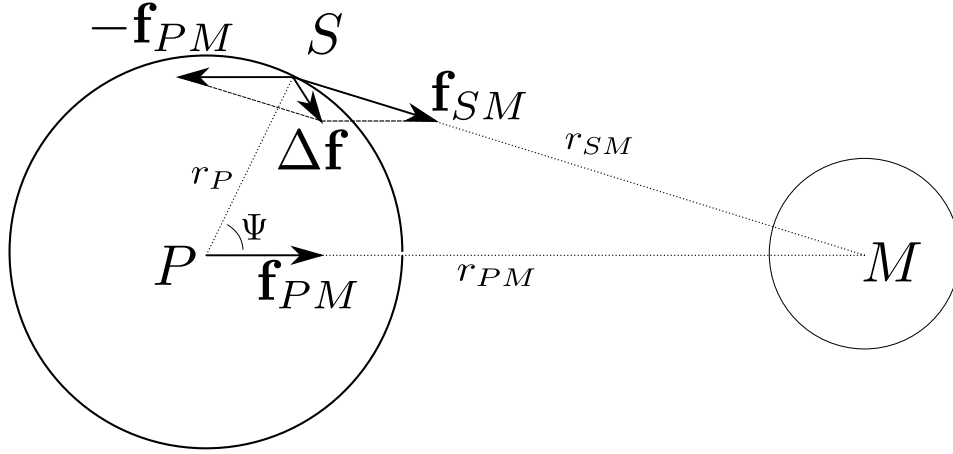
Figure 4.2: Two dimensions geometry used to describe the tidal generating potential problem. *P* is the primary body, *M* is the moon and *S* is a point on the surface of the planet *P*. The various terms labeled as **f** are the gravitational attraction calculated between the different segments of lengths *r*.

Φ_{SM} can be written as:

$$\Phi^{SM} = Gm_M \frac{1}{r_{SM}} \tag{4.28}$$

where m_M is the mass of the moon *M* and r_{SM} is the distance between the surface point *S* and the centre of the moon *M*. Applying the same process to the term Φ^{PM} implies that it is possible to write:

$$\Phi^{PM} = Gm_M \left(\frac{1}{r_{PM}} - \frac{r_P \cos \Psi}{r_{PM}^2} \right) \tag{4.29}$$

Including Equation 4.28 and 4.29 into 4.27, produces the following result:

$$\Phi^T = Gm_M \left[\frac{1}{r_{SM}} - \left(\frac{1}{r_{PM}} - \frac{r_P \cos \Psi}{r_{PM}^2} \right) \right] \tag{4.30}$$

which is the analytical formulation of the tidal potential at the point *S* for the geometry presented in Figure 4.2, where Ψ is the angle formed by the two segments *PM* and *PS*.

As previously mentioned, if we considered that the two bodies are placed in vacuum, the Laplace equation (Equation 4.19) holds for the gravitational potential. Therefore, possible valid solutions that satisfy the Laplace PDE are the spherical harmonics. Since the tidal potential is a linear combination of gravitational potentials, calculated at different locations (Equation 4.27), it can be expressed in forms of spherical harmonics (Equation 4.24), expansions that is known to satisfy the Laplace equation [41]. After some mathematical manipulations of the equations presented, the tidal potential can be re-written as an infinite series of solid spherical harmonics:

$$\Phi^T = Gm_M \frac{1}{r_{PM}} \sum_{n=0}^{\infty} \left(\frac{r_P}{r_{PM}} \right)^n P_n(\cos \Psi) \tag{4.31}$$

where the term P_n is the symbol for the associate Legendre function of order *n*. It is possible to see the same structure of Equation 4.24, where the dependance with the radial distance from the center of the planet *P* is calculated as r_P and the Ψ is the angular distance from the centre of *P*, replacement of the geographical coordinates θ and φ.

If now the idea is to apply the formulation of the tidal potential for the case of Jupiter and Europa, and the arising tides has to be calculated on the surface of Europa itself, the parameters in the equations need to be changed. In particular, Figure 4.2 changes completely its purpose. Now the point is to calculate the tidal potential on the surface of Europa, hence the point *S* will be attached to the body *E*, staying for Europa. On the other hand, the tide-rising body is now Jupiter, labeled *J*. The equation governing the tidal potential on the surface of the Jovian satellite can be written as:

$$\Phi^T = Gm_J \frac{1}{r_{EJ}} \sum_{n=0}^{\infty} \left(\frac{R}{R_{EJ}} \right)^n P_n(\cos \Psi) \tag{4.32}$$

where m_J is the mass of Jupiter, R is the radius of Europa, and R_{EJ} is the average distance between the centre of Europa and the gas giant. In order to better understand the dependance of the tidal potential with respect to the orbital position of Europa around Jupiter, it is convenient to express the term Φ^T as function of the Europa orbital parameters. Additionally, for a complete description of the problem, a three dimension geometry has to be assumed. The reader is encouraged to refer to Kaula [47] for the complete derivation of the expression for the tidal potential as function of the orbital parameters. In the following of the current chapter, only the most important outcome of the mathematical analysis are presented. As a further simplification, theoretical studies demonstrated that is enough to truncate the series of spherical harmonics to the third degree in order to appreciate the most relevant contribution of the tidal potential.

The tidal potential can be distinguished in two different contributions that are acting at two different timescales. Basic astrodynamics usually works with the concept of mean motion of the orbit [112], calculated as:

$$n^2 = \frac{Gm_J}{a^3} \tag{4.33}$$

which is defined as function of the Jupiter mass and the semi-major axis of Europa with respect to Jupiter, term a.

The tidal potential for the surface of Europa can be considered to be formed by the primary and time-invariant for a circular, tidally locked orbit with a zero-obliquity for the rotation axis. In the case some perturbations for the mentioned parameters, the tidal potential equation needs to be modified:

$$\Phi^T = \Phi_0^T + \Phi_e^T + \Phi_v^T + \Phi_{ns}^T \tag{4.34}$$

where the apexes 0, e, v, ns stay for: primary component, eccentricity-driven, obliquity-driven and non-synchronous rotation-driven tidal potential. These four terms are analysed in details in the next paragraphs and referred to Jara-Orue and Vermeersen [42]. The formulation of the auxiliary functions called associate Legendre function $P_{l,m}(\cos\theta)$ of degree l and order m are reported in Appendix A.

Having stated the definition of mean motion, the time-invariant potential, which would be the only contribution acting if the orbit were tidally locked and circular, can be written as:

$$\Phi_0^T = (nr_E)^2 \left\{ -\frac{1}{2}P_{2,0}(\cos\theta) + \frac{1}{4}P_{2,2}(\cos\theta)\cos 2\varphi \right\} \tag{4.35}$$

where the angles θ and φ are the longitude and the co-latitude of the Europa's geographical map and r_E is the radius of Europa.

The time dependant proportionality with respect to the eccentricity e of the orbit is given by:

$$\Phi_e^T = (nr_E)^2 e \left\{ -\frac{3}{2}P_{2,0}(\cos\theta)\cos nt + \frac{1}{4}P_{2,2}\cos\theta \cdot [3\cos 2\varphi\cos nt + 4\sin 2\varphi\sin nt] \right\} \tag{4.36}$$

Being the term t is the time and in astrodynamics, the factor nt is defined as mean anomaly [112].

A further contribution can be given by a tilt for the rotation axis of the satellite, term v. The contribution of such phenomenon is acting on a short timescale as follows:

$$\Phi_v^T = (nr_E)^2 \left\{ P_{2,1}(\cos\theta)\cos v\sin v\cos\varphi\sin(w+nt) \right\} \tag{4.37}$$

where the term w is the argument of pericentre.

If one considers the effect of a non-synchronous rotation of a period T_{ns}, and orbital frequency Ω_{ns}, this can be taken into account by tidal potential. The last contribution to the term Φ^T is:

$$\Phi_{ns}^T = (nr_E)^2 \left\{ -\frac{1}{2}P_{2,2}(\cos\theta)\sin(2\varphi + \Omega_{ns}t)\sin(\Omega_{ns}t) \right\} \tag{4.38}$$

Equation 4.35 to 4.38 represent the contributions of time-independent tide and eccentricity, obliquity and non-synchronous rotation driven tide, respectively. The summarised formulation is written in Equation 4.34. Tidal potential is now expressed as a function of the orbital parameters of Europa around Jupiter and the time taken from an arbitrary reference period. The next section represents the application of the normal mode theory [87] to the mentioned equations that are describing the tidal potential for Europa. The results are the calculation of the stress induced by the four components on the surface of the satellite. This would also be relevant as opening source for the modelled crevasses.

4.3.2. TIDAL STRESS ON EUROPA

This last section of the chapter aims to present a general overlook to the stress field on Europa. As it has been explained already in the last chapter, the Jovian moons are battered by a continuous deforming action that operates both at secular and diurnal timescales. The most important sources are described in section 2.2 and distinguished between non-zero eccentricity and obliquity, physical libration coupled with non-synchronous rotation and true polar wander. The evidence of these stress sources come from both theoretical and observational studies. Nevertheless, the physical characteristics that describe the different sources are far from being completely determined. The problem is set by the lack of data on the surface of the moon. The only missions that probed the Europa environment were not able to fully characterise the processes that deform the surface. Therefore, the numerical studies on Europa need to simplify and assume many physical properties. The current research did the same. An example is the vertical stratification for the moon which was presented in Table 2.1 and fixed the radii of the several layers assumed to form to moon. As consequence, also the stress field obtained by the manipulation of the tidal potential will be highly sensitive to the parameters used.

As it has been explained from the last chapter about linear elastic fracture mechanics, one key factor in the calculation of the stress intensity factor is the stress, of course. The stress tensor calculated in Jara-Orue and Vermeersen [42] is the baseline for the fracture analysis presented in the next Part of this document. The stress field that is used as deforming source in the current research is the outcome of the normal mode application to the tidal potential as produced by Jara-Orue and Vermeersen [42]. As already mentioned, the numerical work takes the potential presented in the previous sections and, by normal mode theory, produces analytical formulation for the stress tensor. A full presentation of normal theory is beyond the scope of the current research which takes only the analytical formulation of the stress tensor. The reader is encouraged to find references in Sabadini et al. [88] or in Jara-Orue and Vermeersen [42] for a theoretical description of the mathematical tools. For sake of the current project, it is enough to understand that the stress tensor is calculated from the tidal potential via frequency response. The analytical functions that are governing the tidal stress on Europa are reported for sake of completeness in Appendix B.

Figure 4.3 and 4.4 represent the results of the work Jara-Orue and Vermeersen [42]. In particular, the two figures describe the stress field distribution on the moon for different time period. Figure 4.3 shows the dependance of the stress with respect to the orbital position around Jupiter. The physical parameters for the two simulations are a moon eccentricity of 0.0094 and a axial tilt of 0.5°. As it can be seen the tidal bulge (high stress with respect to the background) is moving around the surface of the moon and this is considered to be the cause of the peculiar fractures observed. Already with this diurnal stress, the structure might reach the material threshold fixed at 100 KPa, differently to what found in the literature, e.g. in [18]. The reason stays in the already mentioned high sensitivity to the physical parameters used. Figure 4.4 is the perfect visualisation of this problem. The image shows the dependance with the non-synchronous rotation rate. The meaning of the factor Δ is described by the following Equation 4.39

$$\Delta = \frac{\mu/\eta}{2\Omega_{ns}} = \frac{T_{ns}}{4\pi\tau_M} \tag{4.39}$$

where $\tau_M = \eta/\mu$ is the Maxwell time, ratio of viscosity η and rigidity μ. This specific time is an important parameter to take into account. For the current project τ_M for the lithosphere is around 9000 years and a constant given by the constant values presented in Table 2.1. If the timescale taken into account for the simulation have the same or lower order of magnitude, the regime of the material can be assumed as elastic. If the order of magnitude is higher than the Maxwell time, viscosity starts to be not negligible anymore and material undergoes relaxation and the pure elastic response is not applicable. Since the linear elastic fracture mechanics require an elastic matter, the simulations will use timescale at diurnal scale where the elastic regime is acceptable. Returning to the figure meaning, the variation of the term Δ describe the variation of the non-synchronous frequency and rate (terms Ω_{ns} and T_{ns}, respectively). Being τ_M fixed as assumption, the term Δ is only dependant on the non-synchronous rotation. In the figure, Δ assumes 0.1 (around 1400 years of NSR period), Δ=1 (around 10^4 years of NSR period), Δ=10 (around 10^6 years of NSR period) and Δ=100 (around 10^7 years of NSR). As it can be seen in the figure, the faster the rotation (low values of Δ), the higher the stress reached by the surface. Numerical simulations that investigate material thresholds such as toughness or tensile strength are very sensitive to such high values of stress. In fact, this can lead to a full failure of the structure that implies trivial outcomes. Therefore, a model such as the one of the current project has to assume specific values for the physical parameters in order to avoid the trivial results and obtained valid and interesting outcomes instead.
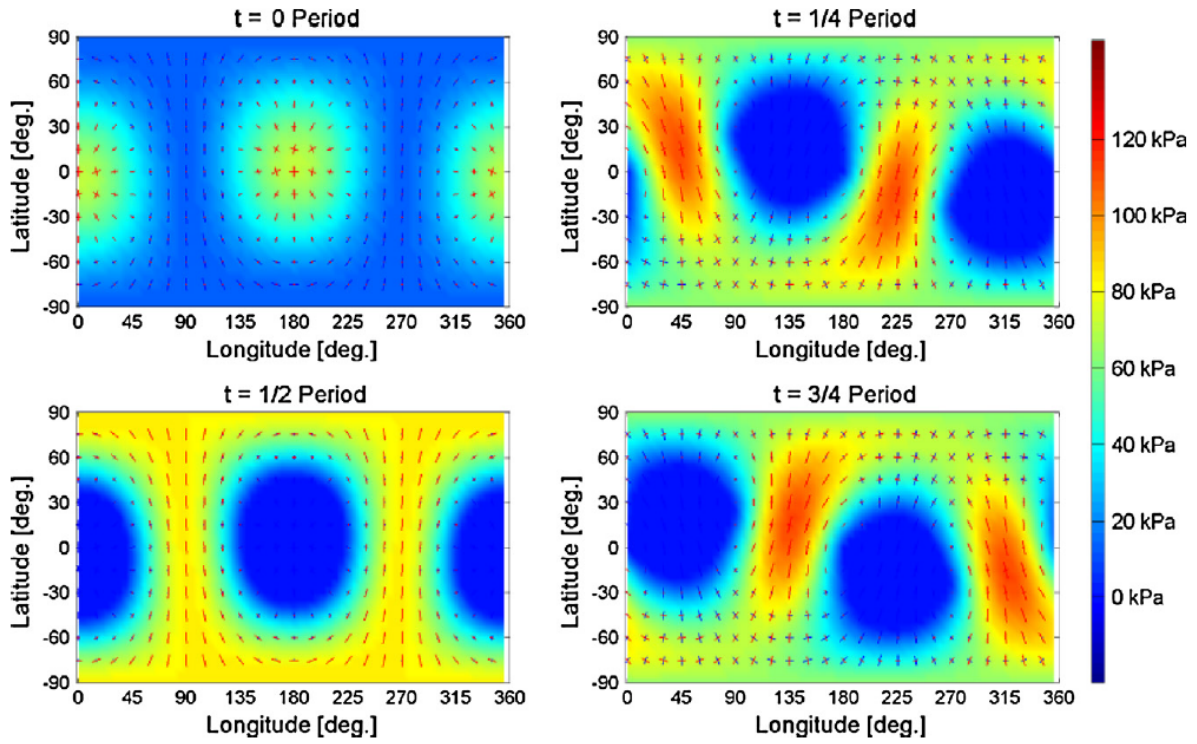
Figure 4.3: Stress map calculated by Jara-Orue and Vermeersen [42], assuming a NSR a-dimenisional parameter of $\Delta = 40$, a diurnal tides due to the combination of non-zero eccentricity of magnitude $e = 0.0094$ and non-zero obliquity of magnitude $\epsilon = 0.5°$.
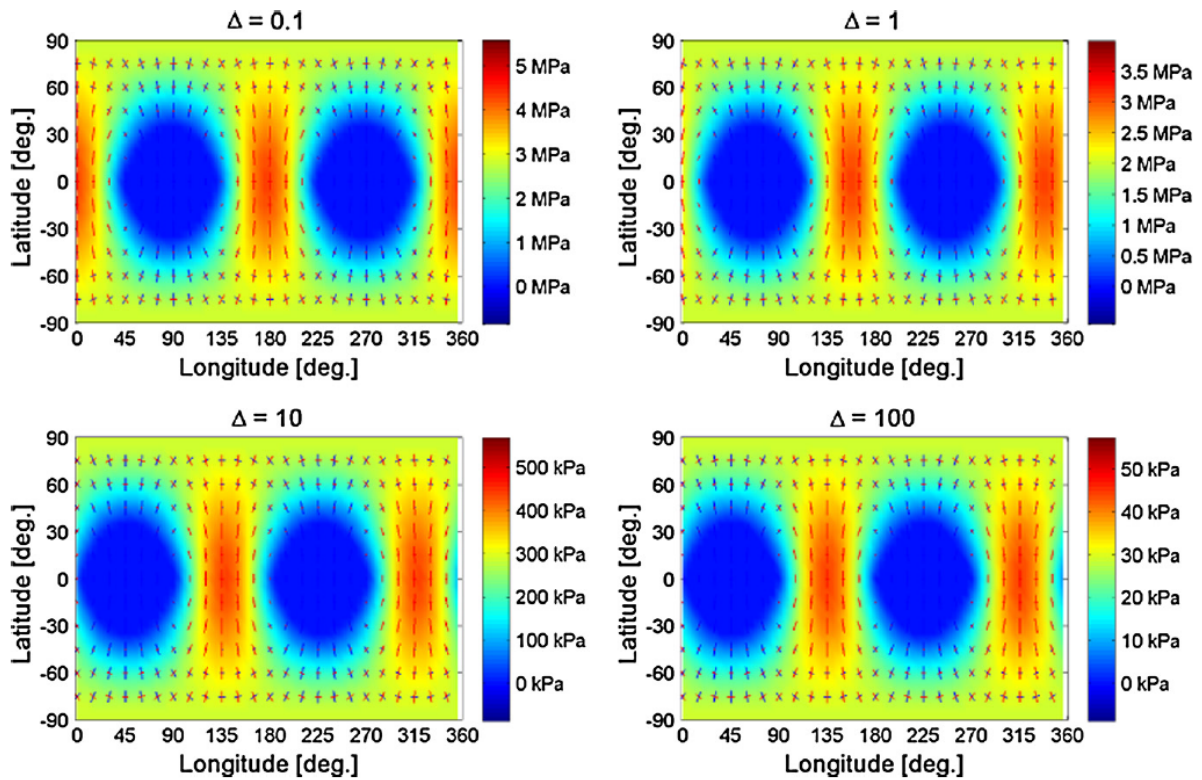
Figure 4.4: Stress map calculated by Jara-Orue and Vermeersen [42], assuming a NSR a-dimenisional parameter Δ that varies from very fast rotation to more secular timescales.

5

LINEAR ELASTIC FRACTURE MECHANICS

This chapter is the most technical part of the current research. It aims to describe the engineering tools derived from the elasticity theory in order to study cracks' propagation and to set up the numerical analysis that presents its results in the next Part. In the specific of the current case, the branch of fracture mechanics that investigates brittle failures of structures is called linear elastic fracture mechanics, also known as LEFM. This analysis has been firstly proposed by the English aerospace engineer Alan Arnold Griffith during World War I with the specific purpose of investigating brittle failures. The theory of Griffith was tested on brittle glass with a background characterised by purely energetic approach. The theory was able to positively describe the propagation of a crack in a purely elastic material. Despite the positive outcomes of the Griffith fracture theory, the approach was only designed for merely fragile materials. When ductile matters were tested, the predicted numerical results for propagation were far from fitting the reality. Hence, the developed theory encountered several doubts and contestations during the modern history of fracture mechanics. During World War II, George Irwin, an American scientist working for the US Naval Research Laboratory, improved the Griffith theory by introducing plasticity to the problem. Irwin and his research group introduced a plastic zone around the tip of the crack allowing a better understanding of crack growth. Irwin was the first one who introduce the concept of stress intensity factor, which is the key numerical element used in the current research. In result of the Irwin improvement of the LEFM, partly ductile materials were also positively described by LEFM. As mentioned, the theoretical assumption of LEFM are induced from the experimental world. During the years, thousand and thousand of different specimen have been tested, in order to provide constraints in a correct representation of the structure geometry.

The most important assumption of the LEFM analysis is the acceptance that a crack exists already. If a structure is cracked, LEFM can study the propagation of the failure, by the investigation of the structure's status around its tip. Therefore, LEFM provides no insights concerning crack initiation. Initiation of a crack is reached when the structure reaches certain material's threshold, called tensile strength. On the other hand, for a LEFM analysis, the crack exists and if the area around its tip reaches certain conditions (different from the tensile strength), this crack will eventually propagate. Initiation and propagation are two completely different aspects of fracture mechanics but it is very easy to mix the terms. The current analysis focusses only on propagation and does not touch initiation processes at all.

A complete technical and mathematical description of the linear elastic fracture mechanics, starting from the Griffith theory, passing by the improving of Irwin and reaching the modern application is presented in section 5.2, which represents the key mathematical aspect of the current research. LEFM bases its calculation on the assumption that the structure under investigation is described by a purely elastic material. Therefore, section 5.1 presents a short summary of elastic theory that gives the basics of every structural analysis. After the modification of Irwin, the LEFM analysis became the most efficient way of investigating brittle failures. Therefore, completely different branches of engineering and science applied LEFM analysis in the most diverse problem, from medical issues to Earth science. In particular, glaciology produced one of the most interesting field of the theory application. Large ice shelves are floating chunk of extremely cold material.

Already in the '80 scientists applied LEFM techniques in order to study calving events and/or iceberg formations. Section 5.3 describes the application of such fracture mechanics tools to terrestrial crevasses in Antarctica and Greenland, which are the works used as baseline of the current research.

The current analysis applies LEFM techniques to the ice shell of the Jovian moon Europa. The literature survey presented the surface of the moon as an extremely cold material that is continuously deformed by tidal effects. The low temperature of the ice shell, together with the calculated stress field are two key aspect that suggested the application of LEFM for Europa. The key result of the research, presented in the next Part, investigates vertical and horizontal propagation for the crevasses observed on the surface of the moon.

5.1. ELASTICITY

In nature, almost every material behaves for a specific time in an elastic way, somehow. The property called elasticity is the ability of a material under stress to return to the original conditions after the deforming sources stops to act. Therefore, a perfect elastic material will support every stress condition, below a certain threshold, and will return to the original state once stopped to be loaded. In reality, a perfect elastic material does not exist and the combination with plasticity, most likely occurs. For the purposes of the current research only perfect elastic matter are studied. Basic books that are presenting elastic theories are Timoshenko and Young [102] and Love [55] and these will be used as baseline for the current section, when not cited otherwise. Additionally, the materials considered here behave as isotropic matter, meaning that these show the same physical properties in the entire structure[1]. It is important to notice that a complete description of elastic theories goes beyond the scope of this chapter, which only aims to extrapolate the necessary background to understand linear elastic fracture mechanics tools.

The presentation of elastic theory begins with the definition of stress state, which can be a very difficult concept to understand. If one consider an elastic body that is loaded with external forces, the body will be subjected to inner forces between its different parts. When considering only one part of the loaded body, it can be stated that it is in equilibrium with the mentioned external forces. Furthermore, the inner forces are distributed in order to produce a reaction between the different parts of the body in order to maintain this equilibrium. These forces are usually measured by the amount of force per unit area, and also called as stress. Mathematically speaking the stress can be written as:

$$\sigma = \frac{\Delta F}{\Delta S} = \frac{dF}{dS} \tag{5.1}$$

where F is the force applied on a surface of area S. Stress is measured in Pascal.

The next step in the presentation of the stress status of a body is the application of Equation 5.1 to three dimensions, which can represent the infinitesimal part of an elastic body. In particular, Figure 5.1 identifies the stress configuration around a virtual body in standard Cartesian coordinates. The stress status can be represented by a second order tensor which is called $\underline{\underline{\Sigma}}$ and contains the decomposition of stresses for the different surfaces of the body.

$$\underline{\underline{\Sigma}} = \begin{bmatrix} \sigma_{xx} & \sigma_{yx} & \sigma_{zx} \\ \sigma_{xy} & \sigma_{yy} & \sigma_{zy} \\ \sigma_{xz} & \sigma_{yz} & \sigma_{zz} \end{bmatrix} \tag{5.2}$$

where the columns can be substituted by three vectors (red vectors in Figure 5.1) that correspond to the Cartesian decomposition of the stress vector. It is possible to consider these three vectors as a further decomposition of a stress configuration that can be represented by a single vector in three dimensions. The stress tensor is symmetrical, meaning that stresses with the same indexes (hence not considering the order) have the same magnitude. Hence, counting the number of independent parameters, from the 9 components of a second order tensor, one can rewrite the stress in vectorial form. This is also called as Voigt formulation of the stress status.

$$\sigma = [\sigma_{xx}, \sigma_{yy}, \sigma_{zz}, \sigma_{xy}, \sigma_{yz}, \sigma_{zx}] \tag{5.3}$$

which is a first order tensor, better manipulated than a second order one.

One of the most important theorem of calculus is the Spectral Theorem that describe the decomposition of a matrix into eigenvalues and eigenvectors [9]. The theorem evokes complex mathematical insights that are related to Hermitian spaces and advance vectorial analysis. A simple deduction of the theorem is that

---

[1]In reality, the materials present non-homogeneous properties for their body and a pure homogeneous body does not exist.
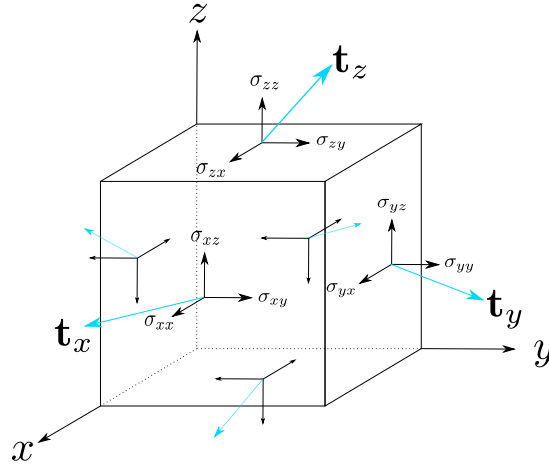
Figure 5.1: Classical representation of the Cauchy stress tensor, where the prism represents an infinitesimal part of an elastic body. The red terms $\mathbf{t}_x$, $\mathbf{t}_y$ and $\mathbf{t}_z$ represent the Cartesian decomposition of the stress vector, while the black terms are its further decomposition into a second order tensor.

a real and symmetrical matrix is similar to a diagonal matrix, through an orthogonal matrix. An orthogonal matrix is a matrix that satisfies the condition expressed below:

$$\underline{\underline{M}}^T \underline{\underline{M}} = \underline{\underline{M}}\, \underline{\underline{M}}^T = \underline{\underline{I}} \tag{5.4}$$

where $\underline{\underline{M}}$ is a square matrix and $\underline{\underline{I}}$ is the identity matrix. Orthogonal matrices' columns are formed by orthogonal vectors, whose definition can be found in basic calculus and linear algebra books, such as Bramanti et al. [9]. The mentioned Spectral Theorem can be applied to the stress status $\underline{\underline{\Sigma}}$, which can be written as:

$$\underline{\underline{\Sigma}} = \underline{\underline{V}}^T \underline{\underline{D}}\, \underline{\underline{V}} \tag{5.5}$$

where the diagonal values of $\underline{\underline{D}}$ are called eigenvalues or principal stresses' magnitude and the columns of $\underline{\underline{V}}$ are called eigenvectors or principal stresses' direction. Eigenvalues and eigenvectors are forming a normal base for the stress status [9]. Eigenvalues are some of the most useful mathematical tools in linear algebra. They are calculated as invariants of a matrix and can indicate an easy representation of a complex matrix.

Beside the stress status, a further important concept in structural mechanics is the deformation. If an elastic body is loaded with external forces, this will tend to deform naturally[2]. Deformations can be largely visible, or completely unnoticeable. Deformation is nothing more than the difference between the position of a body's point at rest and the position of same point under a load. An analogue representation of a body deformation is the concept of strain. As it has been done in Equation 5.1 for the stress, one can write strain as:

$$\epsilon = \frac{\Delta s' - \Delta s}{\Delta s} \tag{5.6}$$

where s is the position of a body's specific location at rest and s' is the deformed position. Strain is a a-dimensional parameter. The numerator of Equation 5.6 is nothing more than the definition of deformation. If one considers a three dimension body, a infinitesimal part of this body can be represented by Figure 5.1. Hence, applying the same approach for the second order tensor representing the stress status, one can also write the second order tensor that represents the body's strain status as follows:

$$\underline{\underline{E}} = \begin{bmatrix} \epsilon_{xx} & \epsilon_{yx} & \epsilon_{zx} \\ \epsilon_{xy} & \epsilon_{yy} & \epsilon_{zy} \\ \epsilon_{xz} & \epsilon_{yz} & \epsilon_{zz} \end{bmatrix} \tag{5.7}$$

---

[2]Temperature variations can also produce deformation of a body, among other sources.

where the columns are vectors that decompose the strain status of a body.

The key of elastic theory is the relationship that can be built up between stress and strain, which is usually called as constitutive equation. As mentioned already, the qualitative description of the elastic behaviour of a material is that, given a certain load, the material will respond with a proportional deformation, until a certain limit that is call strength of the material. Above this level of stress or strain the structure fails and the material breaks. Considering an axial stress, the constitutive equation that governs elastic materials is called Hooke's law and can be expressed as:

$$\sigma = E\epsilon \tag{5.8}$$

where the proportional coefficient E is the Young modulus of the material, usually measured in Pascals. On the other hand, of the loading axis is shear, the Hooke's law is written as:

$$\sigma_{xy} = \mu\epsilon_{xy} \tag{5.9}$$

where the coefficient μ is called modulus of rigidity or more simple rigidity. The two mentioned coefficients E and μ are material's properties and their relationship forms the material's Bulk modulus B, found in re-elaboration of the following equation:

$$E = \frac{9B\mu}{3B + \mu} \tag{5.10}$$

knowing two parameters between Bulk, Young and rigidity moduli allows the calculation of the other by using Equation 5.10.

Equations 5.8 and 5.9 can be re-written for a three dimension body, such as the one depicted in Figure 5.1 as well as for a two dimension problem. A common two dimension analysis where 5 out 9 tensor's components are zero is also called as planar stress, meaning $\sigma_{zx} = \sigma_{xz} = \sigma_{zz} = \sigma_{yz} = \sigma_{zy} = 0$. As consequence, using the Voigt formulation for stress and strain, the planar formulation of the Hooke's law can be written as:

$$\begin{bmatrix} \sigma_{xx} \\ \sigma_{yy} \\ \sigma_{xy} \end{bmatrix} = \frac{E}{1-v^2} \begin{bmatrix} 1 & v & 0 \\ v & 1 & 0 \\ 0 & 0 & 2+2v \end{bmatrix} \begin{bmatrix} \epsilon_{xx} \\ \epsilon_{yy} \\ 2\epsilon_{xy} \end{bmatrix} \tag{5.11}$$

where the term v is called Poisson coefficient, calculated as the ratio between transverse and axial strain, measured via testing material specimens[102]. It is possible to derive the relationship between the Poisson ration and remaining of the material's moduli through an equation that is similar to Equation 5.10, namely:

$$E = 2(1+v)\mu \tag{5.12}$$

Returning to the constitutive equation, this can be re-formulated by the introduced relations between the stress and strain vectors:

$$\sigma = \underline{\underline{K}}\epsilon \tag{5.13}$$

where $\underline{\underline{K}}$ is called stiffness matrix. Given the linearity of the elastic problem, it is possible to invert the stiffness matrix in order to find the strain when the stress is known. The inverse of the stiffness matrix is called compliance matrix $\underline{\underline{C}}$, and the new formulation for the elastic constitutive equation is:

$$\epsilon = \underline{\underline{C}}\sigma \rightarrow \begin{bmatrix} \epsilon_{xx} \\ \epsilon_{yy} \\ 2\epsilon_{xy} \end{bmatrix} = \frac{1}{E} \begin{bmatrix} 1 & -v & 0 \\ -v & 1 & 0 \\ 0 & 0 & \frac{1-v}{2} \end{bmatrix} \begin{bmatrix} \sigma_{xx} \\ \sigma_{yy} \\ \sigma_{xy} \end{bmatrix} \tag{5.14}$$

The relations presented in the current section are the basic for the development of the elastic theory. A material that is elastic will return to the unloaded position when the force is stopping to act. The linearity of the problem, demonstrated by the two proportionality matrices (stiffness and compliance), implies the fact that stress and strain are mathematically the same thing. In other words, the loaded status can be described via stress or via displacement approach but the knowledge of only one of the two status, directly implies the knowledge of the second, given the material properties. Of course, if the load is exceeding the material threshold a crack will be initiated and the structure will eventually fail.
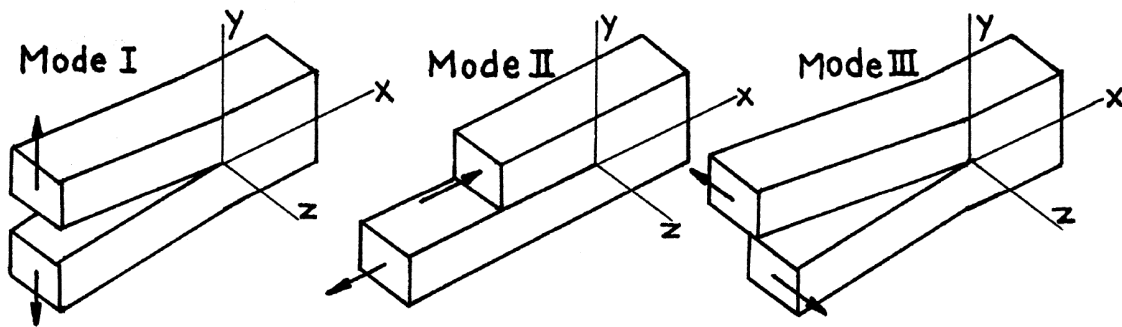
Figure 5.2: Configuration of stress around the tip of an existing crack, image taken from the handbook of Tada [100]

5.2. APPROACHES OF LEFM

In the literature, a large number of books and handbooks have been written in order to present fracture mechanics tools and in the specific, LEFM analysis, since it is based upon interpolation of experimental work. Of course, the works of Griffith and Irwin are the baselines for all the other researches, being the first documents that presents the LEFM techniques. Among others, manuals of fracture mechanics that contains the experimental results of specimen tests are very important for the application of LEFM techniques to other fields of science and engineering. The handbook that is taken as reference in the current research is Tada [100] and the rest of the section is based on it, when not cited otherwise.

The stress distribution around the tip of an existing crack can be divided into three different modes that depends on the type of acting source that is deforming the area. The three modes are shown in Figure 5.2 and represent the different ways of acting on a crack. Mode I is also called opening mode, where the crack's flanks are move away from each other (in the y-direction). Mode II is the edge-sliding mode where the two sides of the crack are sliding over each other perpendicularly to the leading edge of the crack (in x-direction). Finally, in Mode III or tearing mode the surfaces are sliding on each other parallel to the leading edge of the crack itself (in the y-direction). The superimposition of the three Modes is sufficient to represent the majority of the fracture mechanics problems. In the remain of the current chapter, only Mode I is presented, limiting the analysis to a 2D problem. In the elaboration of the research aim, only the opening mode (Mode I) is used in the investigation of crevasses' propagation as well. Essential assumption of the LEFM, is that the structure has to be fractured already. LEFM does not provide any insights in the initiation of crack, instead it can only describe if the fracture can eventually grow.

Two categories of LEFM approaches can be distinguished, although these are essentially investigating the same process. The first LEFM analysis is based on an energy balance approach, trying to find the energy equilibrium for the extension of crack. Historically speaking, this is also the oldest and first attempt that built the basics for the future LEFM improvement. The energy balance approach is often named as Griffith theory, in honour to the aerospace engineer who firstly proposed. A more practical approach is the one which introduce the concept of stress intensity factor, that measures the criticality of the conditions around the tip of an existing crack. This last approach is the one that is used in the development of the current research project. The two approaches are presented in the following section 5.2.2 and 5.2.1, respectively.

5.2.1. THE STRESS INTENSITY FACTOR APPROACH

Using the Irwin [40] approach, based on Westergaard [115], it is possible to represent the planar stress around the tip of the crack that is placed in a infinite large layer that is biaxially loaded by the mechanical stress σ. This works with produces the so-called Westergaard solution. The mathematics behind the simplification of Westergaard is using second order differential equations named Airy functions. A complete mathematical formulation of the Airy functions goes beyond the purposes of the current research and the reader is encouraged to view Hertzberg [24] for details. The result of the Westgaard solution is a set of equation that describe the stress field as function of both the geometry and the load, specifically in the area of space that surrounds the tip of the crack. It is necessary to specify that the Westergaard solution is only valid in the close proximity

of the tip. Considering a pure Mode I fracture geometry, the equations governing the stress around a crack in biaxially loaded infinity large plate are the following:

$$\sigma_x = \frac{\sigma\sqrt{\pi a}}{\sqrt{2\pi r}} \cos\frac{\theta}{2}(1 - \sin\frac{\theta}{2}\sin\frac{3\theta}{2}) \tag{5.15a}$$

$$\sigma_y = \frac{\sigma\sqrt{\pi a}}{\sqrt{2\pi r}} \cos\frac{\theta}{2}(1 + \sin\frac{\theta}{2}\sin\frac{3\theta}{2}) \tag{5.15b}$$

$$\tau_{xy} = \frac{\sigma\sqrt{\pi a}}{\sqrt{2\pi r}} \sin\frac{\theta}{2}\cos\frac{\theta}{2}\cos\frac{3\theta}{2} \tag{5.15c}$$

where the three coordinates are referred to Figure 5.2, for Mode I fractures.

The structure of the three equations is the same. All of them are formed by different factors that are functions of different parameters. First of all, crack's geometry and the deformation background are expressed in the Westergaard solution through the length of the crack l and the stress σ. After that, fixing a polar reference system to the crack's tip allows the identification of the radius r and polar angle θ. A more visual representation of the three equations is given by the following:

$$\sigma_\alpha = \sigma\sqrt{\pi l} \, \frac{1}{\sqrt{2\pi r}} \, f_\alpha(\theta) \tag{5.16}$$

where the index α can be x, y or xy, depending on the acting source. As it can be seen from the equation, there are three main factors that contributes to the stress distribution σ_α. Two of them are related to the position of the place we want to measure the stress. These are the geometrical function depending on the polar angle, meaning the term $f_\alpha(\theta)$ and the singularity term $1/\sqrt{2\pi r}$. The latter factor goes to infinity when $r \to 0$ which is the definition of singularity. On the other hand, the largest is the distance with the tip ($r \to \infty$), the more the stress approaches to the applied load ($\sigma_\alpha \to \sigma$). The work of Irwin [40] introduced the occurrence of plasticity[3] around the tip, in order to avoid the mathematical problem of singularity. The other relevant term of Equation 5.16 is the dependance with the geometry of the crack coupled with the background stress:

$$K_I = \sigma\sqrt{\pi l} \tag{5.17}$$

which is named stress intensity factor calculated for a crack in a infinite plate, biaxially loaded. In the equation, l is the length of the crack. Equation 5.17 is a function that keeps track of the stress condition around the tip. This is the most important equation for a LEFM analysis and as consequence, also for the current research project. The stress intensity factor is measured in Pa m$^{1/2}$ but it is more common to find order of magnitudes of KPa m$^{1/2}$ in the majority of fracture mechanics problems. For a propagation study of a crack, the stress intensity factor is constantly monitored. When this reaches a certain threshold, called material's toughness K_{IC}, the structure fails, and the crack can eventually propagate.

The same approach can be implemented for the other two fracturing modes, but their description is not part of the current work and is avoided. The stress intensity factor was derived by the build-up of the first Griffith theory which is based on energy balance. Next section gives a short presentation of the energy approach and the equivalency of the two approaches, which will suggest the usage of the stress intensity factor.

5.2.2. THE ENERGY BALANCE APPROACH

During World War I, an English aerospace engineer, Alan Arnold Griffith started to specialise in the study of the brittle glass fractures. Key outcome of his experimental researches is that the presence of micro-defects and fractures that weakens the structure, as consequence, the fracture is more prone to propagate in the material. Griffith coupled experimental work with the elaboration of a new fracture theory [21]. In qualitative terms, the work of the loading scenario at the tip of an existing crack can be translated into an amount of energy that is available for the fracture's growth. Considering a pure elastic regime[4], the energy factor is called G and it can also be viewed as the variation of the body's potential energy over the displacement change, hence it is usually called as energy release rate. In symbols, this can be written as:

---

[3]Measured via the yield strength.

[4]The addition of non-linearity to the constitutive equations governing stress and strain are taken into account by a further factor, usually labelled as J factor[100].

$$G = -\frac{\partial U(A, \Delta s)}{\partial A} \tag{5.18}$$

where U is the total strain energy in the fractured body. This factor is function of the crack's area A and the load point displacement Δs. Despite the positive results of the application of the LEFM to studied specimens, the energy balance approach is intrinsically complex to understand and to apply to real cases. So for the majority of the practical cases, it is more convenient and efficient to use the stress intensity approach.

Despite the difference between the two approaches, it is possible to draw a relationship between the factor G and the factor K. Assuming that a crack in an elastic body is extended by an external load and it is pulled closed over a length l [100]. It is possible to write:

$$G = -\frac{\partial U(A, \Delta s)}{\partial A} = \lim_{l \to 0} \frac{2}{l} \int_0^l \left(\frac{\sigma_{yy} v}{2} + \frac{\sigma_{xy}}{2} + \frac{\sigma_{yz}}{2} \right) dx \tag{5.19}$$

where the stresses σ_{yy}, σ_{xy} and σ_{yz} are the stresses that are acting on the tip of a crack and which are the loading factors that gives the name to the three fracture modes. Indeed, u, v and w are the displacements in the three directions of Figure 5.2, related to their scaled version, the strain. By some mathematical manipulations, the term G of Equation 5.19 can be written as:

$$G = \frac{1-v}{2\mu} K_I^2 + \frac{1-v}{2\mu} K_{II}^2 + \frac{1}{2\mu} K_{III}^2 \tag{5.20}$$

where v and μ are the Poisson ratio and the rigidity modulus of the material (linked by Equation 5.12) This equation represents the relationship between the stress intensity factor approach and the energy balance approach. In the rest of the chapter, the application of the stress intensity approach to the study of terrestrial crevasses is presented.

5.3. FRACTURE MECHANICS APPLIED TO TERRESTRIAL CREVASSES

One of the most complex and less understood phenomenon of glaciology is the calving process. Calving is the episode of the breaking of large chunks of ice that are reversed in the sea from terrestrial ice sheet. The floating blocks of ice are usually called icebergs. One of the most famous and recent calving event is the breaking of the Larsen C ice sheet in Antarctica, after months of progressive propagation of a large crack on the surface of the ice shelf itself. The Larsen C fracture is imaged in Figure 5.3 and reversed into the ocean the highest amount of ice recorded in the history of humanity. At the beginning of the calving phenomenon, there always the initiation of large fractures on the ice sheet. In particular, the ice at the extreme locations of an ice sheet is considered to be weakened by multiple potential effects, such as global warming and tidal oscillations of the sea level, among others.

In the rest of the research project, ice is treated as a purely elastic matter in order to allow the possibility of applying the mathematical tools provided by the LEFM, described in the previous section. Nevertheless, in nature, ice behave as elastic material only in specific and controlled conditions in the testing laboratories[5]. When one deals with fractures on glaciers and/or on ice sheets, viscosity starts to play a key role. The viscosity is a parameter that is extremely dependent on the temperature of the material. Viscous and visco-elastic materials are extremely difficult to model given the non-linearity introduced. In fact, viscosity can be added to the constitutive equation of the material by adding a non-linear term in the Hooke's Equation 5.8 as follows:

$$\sigma = E\epsilon + \eta \dot{\epsilon} \tag{5.21}$$

where $\dot{\epsilon}$ is the strain rate. As it has become clear, the constitutive equation is now non-linear with the introduction of a time-dependant factor, the strain rate. Among others, ice is one of the most difficult material to model and the relationship of the viscosity with the temperature is given by the Glen's flow law:

$$\eta = \frac{\zeta}{2\epsilon_e^{\frac{n-1}{n}}} \tag{5.22}$$

where ζ is the hardness of the ice, ϵ_e is one of the stress invariant of the stress tensor[102] and n is the Glen's flow coefficient, usually set as 3. Physics of glaciers' flows and of ice sheets is a complex field of glaciology and

---

[5]Where LEFM techniques can be experimented, for example.

Figure 5.3: Aerial image of the Larsen C crevasse, in Antarctica.

its description goes beyond the scopes of the current document. The non linearity introduced by the viscosity makes the ice one of the most difficult material to model. The reader is referred to Hutter [39] for a complete presentation of the glaciology issues. The current chapter aims to describe the most relevant numerical analysis that have been produced regarding vertical and horizontal propagation of terrestrial crevasses (section 5.3.1 and 5.3.2, respectively). The two sections are fundamentals of the current research project since the models developed are taken as reference the works cited here.

5.3.1. VERTICAL PROPAGATION

Historically speaking, the first attempt of applying LEFM tools to the propagation of terrestrial crevasses is the work of Rist et al. [85]. The paper was the first one to propose the analogue between ice shelves and the specimen that are tested in order to study the behaviour of the fracture. More in specific, an ice shelf can be visualised and modelled as a finite specimen for studying deep crevasses and a semi-infinite layer for more shallow crevasses. A couple of years after the mentioned work, a further improvement to the application of LEFM was presented. Van der Veen [108] and Van der Veen [109] developed a study for surface and bottom crevasses respectively, re-elaborating the work of Rist et al. [85] with a more consistent and schematic approach. The basics of the paper are the fracture mechanics tools presented in section 5.2.1 with the application of the stress intensity factor approach for surface and bottom vertical crevasses. Results presented amounts of stresses and conditions necessary to find a crack that cross the entire layer and would eventually separate the two flanks of the ice sheet. Of course, the motivation of the research is the understanding of the calving phenomenon, which would explain the iceberg formation, among others. The formulation of a calving law has been one of the key aims of glaciologists and it is still an unanswered question. The current research takes as mathematical and numerical baseline the work of Van der Veen, in order to study the vertical propagation of crevasses. The geometry of the model is shown in Figure 5.4, where surface and bottom cracks are presented. A further step in the LEFM mathematics allows to find insights in the horizontal propagation, referencing to Larour et al. [50] and better explained in section 5.3.2.

Surface crevasses can be considered to be deformed by various stress sources. In reality, an infinite number of actors are accounted in a virtual full understanding of the crevasse's behaviour. In the numerical world, it is enough to take into account opening (or closing) stress, overburden ice pressure and water pressure. Tensile or compressive stress can be due to the flowing of the glacier or to tides; these are only example and in reality lots of factors are acting on the flanks of the rift. Overburden (or lithostatic) pressure is the weight of the ice that is above the tip of the crack. The deeper is the crack, the more intense is the closing action of the ice above. Lastly, if water is filling the crevasse, this is counteracting the closing effect due to lithostatic pressure, via water pressure. Only considering these first implications, one can already deduce that water-filled crevasses potentially reach greater lengths. The three conditions are applicable also to bottom crevasses for ice sheets, meaning ice layer in contact with water below.

The geometry of the LEFM application to surface crevasses is shown in Figure 5.4a. The various terms are presented in the following paragraphs. Some key simplifications need to be explained before proceeding
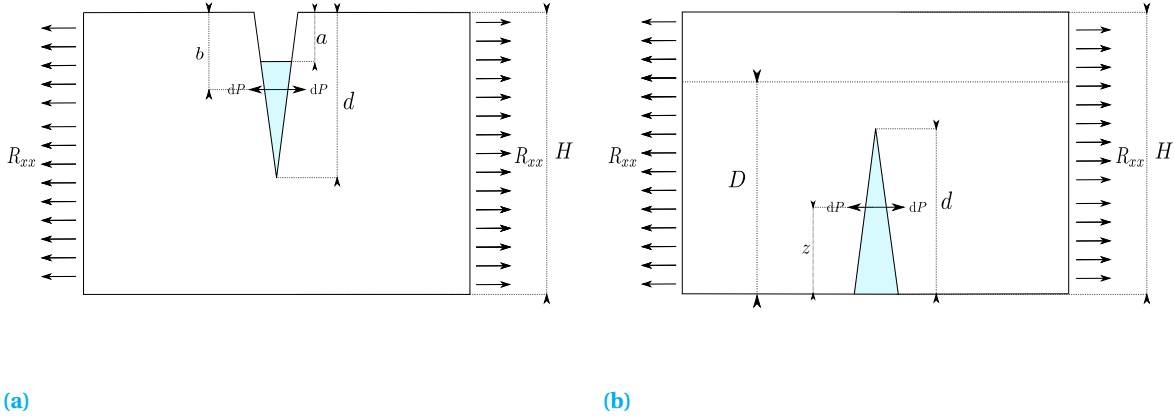
(a)

(b)

Figure 5.4: Geometry of the crevasse vertical propagation problem. Figure readapted from the description of Van der Veen [108]and Van der Veen [109]. For both the figures, d, H and R_{xx} represent the crack length, the ice thickness and the tensile stress, respectively. (a) represent the surface crevasse geometry, where a is the water level, b is s variating parameter that measures the lithostatic pressure (term dP) from the top of the ice sheet. On the other hand, (b) represents the bottom crevasse geometry, where dP is still the overburden pressure and D is the depth of the glacier sole below sea level. For completeness, $H - D$ is the piezometric head and z the variating vertical position, calculated from the bottom of the ice sheet.

with the description of the Van Der Veen model (VDV). First of all, in all the simulations proposed, the tensile (or compressive) normal stress acting on the crevasse's flanks is constant with depth (term R_{xx}). This happens both for surface and bottom crevasses. Secondly, the ice behaves as a purely elastic matter and it has a density that include a depth profile that takes into account the lower densities of the upper snow layers. In the specific:

$$\rho(b) = \rho_i - (\rho_i - \rho_s)e^{-Cb} \tag{5.23}$$

where b is the variating vertical position, ρ_i and ρ_s are the solid ice and the snow density, while C is a constant. Taking into account experimental field works and glaciology handbooks (e.g. Paterson [72]), the values can be assumed to be 917 Kg/m^3 and 350 Kg/m^3 for solid ice and snow density, respectively; and 0.02^{-1} for the constant C. Thirdly, water filling the crevasses is considered to reach a specific level that can be chosen arbitrarily. For bottom crevasses, the assumptions are the same with the only exception that the water is filling the entire crack from below.

Concerning surface crevasses, the stresses acting on the flanks of the fracture are basically three: tensile stress, lithostatic stress and water pressure. The next equations describe the model of VDV for surface crevasses and the symbols found are referenced to Figure 5.4a, when not cited otherwise. Standard tensile (or compressive) stress is:

$$\sigma_{xx} = R_{xx} \tag{5.24}$$

Lithostatic stress, with the introduction of the density-depth profile mentioned in Equation 5.23 is:

$$\sigma_l(b) = -\int_0^b \rho(z)g\mathrm{d}z = \rho_i gb + \frac{\rho_i - \rho_s}{C}g(1 - e^{-Cb}) \tag{5.25}$$

Finally, water-filled crevasses need to take into account water pressure as follows:

$$\sigma_w(b) = \rho_w g(b - a) \tag{5.26}$$

where a is the depth below the surface of the water layer and ρ_w is the constant density of fresh water. Equation 5.24 to 5.26, represent the stress acting on the flank of a surface crevasses. The last two equations are dependent of the vertical position (term b that variates from 0 to the crack length d), while the first one is constant by assumption.

As presented in section 5.2, stress status needs to be coupled with the geometry of the problem in order to calculate the stress intensity factor for the tip of the crack (measured as d in Figure 5.4a). Therefore, for each stress source presented before, a factor K_I can be calculated in order to satisfy Equation 5.17.

The stress intensity factors calculated for Equation 5.24 is:

$$K_I^{(1)} = F(\lambda) R_{xx} \sqrt{\pi d} \tag{5.27}$$

where $\lambda = d/H$ is the ratio between the crack depth and the ice thickness. The function F is a a-dimensional parameter that is only dependent on the crack geometry. This factor, together with the stress condition are the two parameter that combined summarise the stress intensity factor approach. In the specific case of an ice sheet, simplified as a finite plate specimen [100], the function F is shown as the solid curve in Figure 5.5 and it can be written as:

$$F(\lambda) = 1.12 - 0.23\lambda + 10.55\lambda^2 - 21.72\lambda^3 + 30.39\lambda^4 \tag{5.28}$$

The equation is calculated on polynomial curve based on numerical fitting of stress intensity factors for the finite specimen [100]. For relative shallow cracks ($\lambda \to 0$) or for very thick ice layers ($H \to \infty$), the function F assumes a constant value of 1.12, which is the geometrical factor for a semi infinite layer. The semi-infinite layer plane curve is shown in dashed lines in Figure 5.5. The result of the stress intensity factor calculation for a pure tensile (or compressive) stress implies that the main behaviour of $K_I^{(1)}$ is that the deeper the fracture, the higher is the intensity. In other words, the deeper the fracture, the easier is to continue the propagation.

The stress intensity factor in differential form for Equation 5.25 can be calculated with the following equation [100]:

$$dK_I^{(2)} = \frac{2\sigma_l(b)db}{\sqrt{\pi d}} G(\gamma, \lambda) \tag{5.29}$$

where σ_l is expressed in Equation 5.25 and the factor G, function of the ratio between the crack depth and the ice thickness λ together with the variating factor $\gamma = b/d$ has the same geometrical implication of function F in Equation 5.28, but now it is a bit more complex and written as:

$$G(\gamma, \lambda) = \frac{3.52(1-\gamma)}{(1-\lambda)^{3/2}} - \frac{4.35 - 5.28\gamma}{(1-\lambda)^{1/2}} +$$
$$\left[\frac{1.3 - 0.3\gamma^{3/2}}{(1-\lambda^2)^{1/2}} + 0.83 - 1.76\gamma \right] \left[1 - (1-\gamma)\lambda \right] \tag{5.30}$$

which is taken from Tada [100], similarly to function F. The equation is also calculated on polynomial curve based on numerical fitting of stress intensity factors for the finite thickness specimen. The $K_I^{(2)}$ is in differential formulation because of the dependance with the vertical position b. Therefore, the net stress intensity factor can be calculated by integration of Equation 5.29 as follow:

Figure 5.5: Function F shown in Equation 5.28 taken from [108]. The solid curve represents the finite layer model with respect to d/H as the ratio between the crevasse length and the ice thickness. Dashed line correspond to the semi-infinite layer approach ($H \to \infty$).

$$K_I^{(2)} = \int_0^d dK_I^{(2)} = \frac{2\rho_i g}{\sqrt{\pi d}} \int_0^d \left[-b + \frac{\rho_i - \rho_s}{\rho_i C}(1 - e^{-Cb}) \right] G(\gamma, \lambda)db \tag{5.31}$$

Differently to Equation 5.27, Equation 5.31 is an integral function, because of the dependance with the vertical parameter b. The result of the stress intensity factor calculation for the overburden pressure implies that the main behaviour of $K_I^{(2)}$ is that the deeper the fracture, the higher is the intensity of the closing action of the ice layer. The physical explanation is simple: the ice on the top of the crack has a certain weight (or pressure) and this tends to close the crevasse naturally.

Lastly, in the case that water is filling the crevasse, the pressure of the liquid tends to counteract the lithostatic ice pressure and its behaviour is described by the implementation of the stress of Equation 5.26 in form of net stress intensity factor as follows:

$$K_I^{(3)} = \frac{2\rho_w g}{\sqrt{\pi d}} \int_a^d (b - a) G(\gamma, \lambda)db \tag{5.32}$$

(a)   (b)

Figure 5.6: Figure taken from Van der Veen [108], showing the dependance of the stress intensity factor (y-axis in Figure 5.6a and x-axis in Figure 5.6b) with depth of the crevasse (x-axis in Figure 5.6a and y-axis in Figure 5.6b) and the effective presence of water that is filling the fracture. Both the figures are referring to a 500 m thick ice shelf where a bilateral stress of 100 KPa is acting. Figure 5.6a shows the dependance with the water layer (labelled numbers on the right of the curves). The higher the water level (smaller values of a), the higher magnitude of the stress intensity factor. Figure 5.6b represents the stress intensity factor for a water-free crevasse (heavy solid line), and of a water-filled crevasse (without superficial firn layer with the thin solid line and with the layer with the dashed solid line). d_m and d_w are the maximum depth for a water-free crevasse and the minimum depth for a water-filled crevasse, respectively. More details in the text.

where a is the water level calculated from the upper surface and G is the geometrical function shown in Equation 5.30. The aspect of the water pressure-related stress intensity factor is the same of Equation 5.31 because of the dependance with the term b variating from a to d. Water pressure is an important parameter and its only presence can modify the depth of the crevasses in order of magnitudes [72, 85, 108].

The VDV model finds its key equations in the three stress intensity factors presented in the Equation 5.27, 5.31 and 5.32 that characterise an ice crevasse's stress configuration. The last two functions are dependant with the crevasse depth d, differently from the first one which is constant by assumption. These can be summed together in the total net stress intensity factor via the superimposition principle, as previously mentioned:

$$K_I^{\text{net}}(d) = K_I^{(1)} + K_I^{(2)}(d) + K_I^{(3)}(d) \tag{5.33}$$

The stress intensity factor approach of the LEFM states that crack propagation occurs when K_I^{net} reaches a certain threshold, called material toughness K_{IC}. This condition is reached for a specific value of crevasse's depth, that can be called as critical depth, in symbols:

$$K_I^{(1)} + K_I^{(2)}(d) + K_I^{(3)}(d) = K_{IC} \tag{5.34}$$

Solving this equation, given material properties and stress conditions, allows the calculation of d, the penetration depth of the crevasse. This procedure, that elaborate the stress intensity factor around the tip of the crack, is the final purpose of the LEFM analysis applied to terrestrial crevasses. Main outcome of the presented analysis is that the combination of three different stressing sources on the flanks of an existing ice fracture can lead to crack propagation until a point where the critical conditions are not reached anymore and the crack stops to propagate. The results of the VDV model for surface crevasses vertical propagation are shown in Figure 5.6 taken from Van der Veen [108]. In the specific, both 5.6a and 5.6b are showing the net stress intensity factor (Equation 5.33), the former in the vertical axis and the latter in the horizontal axis. Both the graphs have the same parameters for ice thickness ($H = 500$ m) and for a bilateral tensile stress ($R_{xx} = 100$ KPa). Figure 5.6a shows the dependance of the K_I^{net} with respect to crevasse depth (vertical axis)

and to the water parameter a. The closer the water to the surface. the smaller value of a and the higher the stress intensity factor. In the image, the toughness does not appear so the critical depth can not be deduced. On the other hand, Figure 5.6b shows[6], with the heavy solid curve the crevasses in absence of water, with the dashed curve the case of a crevasse of $a = 15$ m with a firn layer, and with the thin solid curve the solution for a constant density profile (firn layer removed). The two vertical dashed lines are upper and lower limits for the ice toughness in a glacier. In the figure, d_m represents the maximum value reached by the crevasse depth while d_w is the minimum depth of a water-filled crevasses. These two values represents the theoretical limits of a crevasse depth in a ice layer of 500 m and under the tensile stress of 100 KPa. As stated in Van der Veen [108] the results obtained for the crevasses depths can be considered as an upper limit for their effective values. The material threshold is an other critical factor that affect the results of the LEFM. Experimental works found that potentially correct values for the glacier ice toughness are in the range of 0.1 to 0.4 MPa m$^{1/2}$, which is the range that plotted with the two vertical dashed lines in Figure 5.6b. In reality, terrestrial crevasses are affected by a large number of different physical phenomenon which modify the actual geometry of the crack such as temperature and/or ablation of the ice. Additionally, a better representation of terrestrial ice is a visco-elastic material but this state would not allow LEFM to be applicable.

The application of LEFM to bottom crevasses follows the same procedure of the surface fracture with the only difference that water is considered to be filling the crevasse entirely. The theoretical background for this last part of the section is referring to Van der Veen [109]. Geometry of the problem is pictured in Figure 5.4b, where R_{xx} and H are still the tensile stress and the ice thickness. Water can reach a level that is represented by the term D. In glaciology, the term $H - D$ is called piezometric head H_p. Considering the water pressure at the bottom of the ice layer, this cannot surpass the weight of the ice sheet itself. In symbols:

$$\sigma_w^{\max} = \overline{\rho} g H \tag{5.35}$$

where the term $\overline{\rho}$ is the depth-averaged ice density, calculated from solving the density-depth profile (Equation 5.23) via integration:

$$\overline{\rho} = \rho_i - \frac{\rho_i - \rho_s}{CH}[1 - e^{-CH}] \tag{5.36}$$

The calculated water pressure $\sigma_w^{\max}$ represents the maximum pressure of the water[7]. The minimum pressure for the water column is found at the highest reachable point, i.e. at level D:

$$\sigma_w^{\min} = \rho_w g D \tag{5.37}$$

Knowledge from basics glaciology relates ice thickness is related to the term D via the following formula, when for a floating ice shelf, maximum and minimum pressures are equal.

$$H = \frac{\rho_w}{\overline{\rho}} D \tag{5.38}$$

Considering that the piezometric head is written as $H - D$, it follows by logical implication of Equation 5.37 and 5.35 that:

$$D \leq H_p \leq \frac{\overline{\rho}}{\rho_w} H \tag{5.39}$$

which is an important equation in the development of the rest of the glaciology problem.

For surface crevasses, a complete analysis of the three different characteristics affecting the stress intensity factor, i.e. tensile stress, water and lithostatic pressure. For bottom crevasses the process is the same so it is possible to summarise the steps, finding a stress equation that is, again, depth-dependant:

$$\sigma_n(z) = -\rho_i g(H - z) + \frac{\rho_i - \rho_s}{C} g[1 - e^{-C(H-z)}] + \rho_w g(H_p - z) + R_{xx} \tag{5.40}$$

where z is now the vertical dimension calculated from the bottom of the ice layer as it can be seen in Figure 5.4b. For a single crevasse, the stress intensity factor acting on the tip of the fracture can be calculated by the following function, similarly to what happens for surface crevasses:

$$K_I^{\text{net}} = \int_0^d \frac{2\sigma_n(z)}{\sqrt{\pi d}} G(\gamma, \lambda) \mathrm{d}z \tag{5.41}$$

---

[6]Which has the axis rotated on 90° counter-clock wise with respect to Figure 5.6a.

[7]No oceanic phenomenon are considered and the water is assumed to be in equilibrium with the ice above. Currents, eddies and other actor can change this this value substantially.

where the function G is written in Equation 5.30 and σ_n is the normal stress acting on the flanks of the crevasse as stated in Equation 5.40.

The results of the LEFM applied to bottom crevasses have the same aspect of the ones for the surface crevasses. Still, the stress intensity factor needs to reach a critical threshold in order to propagate the fracture. Similarly to what happens in Equation 5.34, the net value of K_I assumes the value of the material toughness K_{IC}:

$$K_I^{\text{net}}(d) = K_{IC} \tag{5.42}$$

As previously mentioned, the stress intensity factor depends on the crack length d and one can find this value from the critical condition by iteration of the threshold Equation 5.42. LEFM is a pretty straightforward numerical analysis to implement and, given the full description of the background conditions (ice thickness, material properties, and stress status), it is possible to find lots of interesting results such as the crack length. Figure 5.7 represents the results for the calculation of the stress intensity factor as function of the crevasse depth. As it was seen for surface crevasses, the curve (in heavy solid black line) can be compared with the material toughness (minimum and maximum allowed values in thin solid line) in order to detect the critical height of the crevasse above the lower surface of the ice sheet. Considering a minimum toughness of 0.1 MPa m$^{1/2}$, the crevasse height is of 90 m, while with a value of 0.4 MPa m$^{1/2}$, the height is lowered to a maximum of 55 m. Surface and bottom crevasses can be considered to be present at the same time in an ice sheet.

A last consideration that is needed to be mentioned is the problem of numerical stability. It is possible to appreciate the issue with reference to Figure 5.7 but the implications are the same also for surface crevasses. As already stated, the critical length of the crack can be found by iteration of Equation 5.42. Among the different types of solutions that the equation can produce, a double valid solution might also emerge. Mathematically speaking, these solutions are both valid and can be easily visualised in Figure 5.7, considering the intersection between the vertical line representing the maximum limit of 0.4 MPa m$^{1/2}$ for the toughness and the heavy solid curve representing the stress intensity factor. Two solutions are shown to be present, the first one with a lower magnitude than the second one. These points projected onto the vertical axis, shows the critical length of the crevasse. In a complete LEFM analysis, only the solution with a positive derivative of the K_I factor with respect to d needs to be taken into account. The reason is that, when dealing with the first solution (with the negative derivative), this presents a condition of instability. Indeed, if the crack length presents a value that is somehow lower than the critical limit, the stress intensity factor assumes values that are lower than the threshold and the crack will naturally tend to close. On the other hand, if the length is a larger than the critical value, the stress intensity factor, being higher than the threshold K_{IC}, will induce the crack length to grow till the material limit again. This is represented by the second solution, after which the toughness threshold is not reached anymore. This solution is stable; values that presents small differences with the critical limit would produce stress intensity factors that are induce the length to return in the equilibrium position. In the figure, the stable and unstable solutions are indicated as $\overline{d}_{\text{ST}}$ and $\overline{d}_{\text{UN}}$; the discussion addressed so far can be visualised by looking at the mentioned variations around the two equilibrium points.
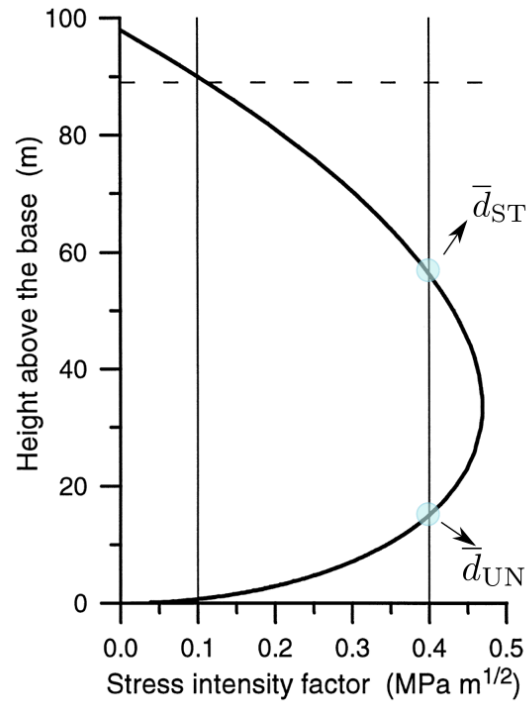
Figure 5.7: Figure re-adapted from Van der Veen [109], showing the dependance of the stress intensity factor (x-axis) with the height of the crevasse (y-axis). The figures refers to a 500 m thick ice shelf where a bilateral stress of 60 KPa is acting. The two thin vertical lines corresponds to the minimum (0.1 MPa m$^{1/2}$) and the maximum value (0.1 MPa m$^{1/2}$) for the ice toughness on a glacier.

5.3.2. Horizontal Propagation

So far, the focus of the chapter was pointed to the vertical propagation of crevasses and, historically speaking, the VDV model is one of the most successful numerical analysis that investigates depths of terrestrial crevasses. The outcomes of the simulations allow the determination of the vertical depth of such fractures in ice at its brittle regime.

Beside the vertical propagation of VDV, further works applied the LEFM in order to study horizontal propagations of crevasses. It is the case of Larour et al. [51], which investigates the behaviour of a rift formed on the Ronne Ice Shelf, near the Hemmen Ice Rise in Antarctica. Radar and optical images taken during the years 1992 to 1997 clearly showed the presence of multiple surface crevasses in the area, with the probable presence of bottom fractures as well. Interferometric radar images allowed the scientists to detect a horizontal creep flow on the ice sheet. Coupling digital observations with the numerical tools offered by LEFM, succeeded in the determination of important dynamical parameters that governs the horizontal propagation of these crevasses. If a planar geometry is considered to model the area around the crack, an other geometrical formulation of the stress intensity factor needs to be evoked [100]. In particular, by rotating the vertical geometry of Figure 5.4a to horizontal direction, the propagation of the eventual crack is intended to be in the direction parallel to the surface of the ice sheet. The LEFM analysis applied to find the displacement movement can produce outcomes that are relevant to study propagation rates, beside the simple crack length growth. If one derive in time the displacement found in the LEFM analysis [100] the results are the following:

$$\delta = \frac{4\sigma l}{E} V(d) \rightarrow \frac{\partial}{\partial t}\left[\delta = \frac{4\sigma l}{E} V(l)\right] \tag{5.43}$$

where the term l is the crack's length, E is the young modulus of the ice, and V is the a-dimensional parameter that governs the geometry of an horizontal plate. Results of the derivative can be summarised as:

$$\frac{\partial l}{\partial t} = f\left(\sigma, \frac{\partial \sigma}{\partial t}, l, \frac{\partial \delta}{\partial t}\right) \tag{5.44}$$

which can be described as the variation of crack length in time (also known as propagation rate) as function of stress, stress rate, crack length and displacement rate. These last parameters that are governing the propagation rates are all known and measured by satellite observations. More in particular, the displacement used in the model is nothing more than the opening width of the crevasse. Of course, this kind of analysis is possible if observational data are available, as happens for the numerous crevasses on terrestrial ice sheets. The current research aims to apply the same concept of Larour et al. [51] but for crevasses on Europa. In this sense, the lack of observations for the icy surface of the moon are limiting the results of the numerical studies and bring problems in the implementation of a correct model. The solution adopted in this project deals with the simplification of the opening width and the displacement rate with the introduction of the strain rate, calculated from the stress equation via the constitutive equation. More details in the following part of the document.

A further work that investigated the horizontal propagation of crevasses on the Ronne Ice shelf is Hulbe et al. [31] that applied a numerical model that is based on LEFM but intrinsically using different mathematical tools than the one of Larour et al. [51]. After the calculation of the stress intensity factor around the tip of the existing ice cracks, the research applied a displacement continuity boundary element method that is able to compute stresses in complex mesh-geometries in order to proceed with the identification of a potential crevasse propagation, together with its direction. Terrestrial crevasses have been observed to arrest their propagation at specific locations called suture zone. These areas are intersections between different and adjacent ice flows. The results of the work Hulbe et al. [31] suggested that these crevasses are unlikely to be stopped in those locations, in the case of absence of suture zones.

Concluding, some numerical works have been already applied to horizontal propagation of terrestrial crevasses. In particular, LEFM theory has the potentiality of simulating longitudinal propagation of crevasses by rotating the geometry of the VDV approach. The current research applies the approach of Larour et al. [51] in order to find relations for the horizontal propagation of the features observed on the icy surface of the moon Europa.

III

LINEAR ELASTIC FRACTURE MECHANICS TO EUROPA

6

RIFT PROPAGATION MODEL

So far, the main focus of Part I presented the key findings that were found in the literature survey about the Jovian moon Europa. The satellite's current view is seen as a global icy shell that covers a liquid water ocean. Speculations about the potential habitability of this global water layer have kept the focus of the scientific community toward the tiny Europa. Habitable conditions, mainly deduced by the maintained liquid state of the H_2O layer, are due to large tidal dissipation that is thought to occur in the interior of Europa. Indeed, heat dissipation is supposed to be constantly generating energy used to keep the liquid state and avoid the global freezing. Beside being the extreme shield protecting the water ocean from the deadly radiation of Jupiter, the outer ice shell of the moon represents of the most curious surfaces observed in the Solar System. Tides are the key deforming sources that are acting on the different layers of Europa.

Beside waves and heat that are assumed to be tidal actions on the Europa ocean, stress due to tides continuously deforms also the upper layer of the moon. The extremely cold temperature and the brittle regime lead the ice shell to reach deformations that ranges on orders of magnitude way higher than what happen on terrestrial ice. This, combined with the fragile properties of the ice, induce the crust to eventually initiate and propagate fractures. Result is the wide number of lineament features observed on the surface by the several mission that reached the Jovian environment. Stress sources are acting on Europa at both short and long timescales. The former are composed by tidal influence of non-zero eccentricity and non-zero obliquity together with the generation of physical libration of the crust. Secular terms are non-synchronous rotation and true polar wander. Fractures on Europa have different shapes, depending on the location on the moon and on the different characteristics of the stress acting along it. Lots of models have been applied in order to study the initiation and the propagation behaviour of the fractures observed on the surface of the moon. Nevertheless, the lack of observational data has not allowed a full knowledge even of very basics properties of these fractures, namely depth or age, for example.

The current research tries to answer to one of the most intriguing question for the propagation of the cracks observed on Europa by using mathematical tools provided by the coupling of fracture mechanics and tidal potential theory in a numerical model. Part II presented the mathematical tools that are needed in the developing of this research purpose. In the specific, a description of tides that uses the tools of the potential theory allowed the identification of analytical functions for the stress field on the surface of the moon as function of the various orbital parameters assumed for the orbit of the satellite around Jupiter. The technique used to translate potentials in terms of stress tensor is the normal mode theory, not presented in the current document. After a stress field is provided, fracture mechanics tools such as the LEFM can investigate cracks on theoretically pure elastic materials. The Europa surface's extremely low temperature allows the assumption of an elastic material as first order approximation. Being the LEFM a technique firstly used in the World War, more recent studies applied its key features also to the investigation of terrestrial crevasses, among others.

Taken this important finding from the literature on Europa and from terrestrial glaciology, it is possible to build a numerical model that investigates the crevasses' propagation on the icy surface of the moon as well. The current chapter aims to present the model in its technical details. Section 6.1 describes the numerical

Parameter	Symbol	Value	Reference
Bulk Modulus	B	9.3 GPa	Wahr et al. [111]
Rigidity	μ	3.487 GPa	Wahr et al. [111]
Poisson ratio	ν	0.33	Jara-Orue [41]
Young Modulus	E	9.29 GPa	Equation 5.10

Table 6.1: Rheological parameters of the ice crust of Europa, including references of the values.

model's set-up. It starts from basic properties of the structure and the material to end by finding characteristics for vertical and horizontal crevasses' propagation. Additionally, the most important assumptions of the model are here listed. The idea is to give already the general potentiality of the numerical routines, together with its inner limitations. Four different sub-sections are here included, namely one describing the input files needed, two showing vertical and horizontal propagation routines and one briefly presenting the outcomes, but these are fully presented in chapter 7. On the other hand, section 6.2 shows the procedure of validation of the numerical code. It is important to mention already the problem encountered when dealing with validation of the code. The behaviour and the parameters that rule crevasses on Earth is still unknown for the majority of the properties. The location where crevasses are observed, are remote, hardly-accessible and extremely dangerous places for potential field works. Additionally, ice is known to be a very hard material to model, given the large amount of parameters that affects its properties. Therefore, even the most basic parameters (such as the depth of a crevasse) are hard to measure and to constrain via numerical models. If for Earth the data for crevasses are rare but still are present in the literature, information on Europa fracture are limited to a hundred of spacecraft's images, not even of an high quality. The strategy adopted to avoid the problem of having a non-validated model, is to use the built model to find depths of a crevasses' set that were measured in Iceland. This work is the only one of the kind, because of the mentioned problem of accessibility and dangerousness of the eventual field-work.

At the end of this chapter, all the tools for running the codes are provided and the document proceeds with the analysis of the outcomes of the numerical simulations. The outcomes of the simulations are presented in the next chapter where details for vertical and horizontal propagation for Europa's crevasses are investigated.

6.1. Numerical Set-Up

The current sections provides the numerical set-up for the calculation interested in vertical and horizontal propagation of crevasses. Being the aim of the current research an improvement to the existing models that study the depths and the propagation rate for the crevasses, the layout of the numerical routines can be distinguished into horizontal and vertical propagation, respectively. Before starting the presentation of the technical details of the model, the most important assumptions have to be made clear in order to foresee already the potentiality of the model and its necessary limitation. The following bullet list includes assumptions whose field of validity ranges between the arguments that have been discussed in the past two Parts of the documents.

- The tidal stress on the surface of the moon is considered constant along the entire thickness of the ice layer and as results of normal mode theory applied to tidal potential.

Potential theory allowed the identification of the tidal potential as function of the orbital parameters of Europa around Jupiter. In the specific, the normal mode theory allows the manipulation of the tidal potential in order to derive the stress that is acting on the Jovian satellite. The work that is used as reference is Jara-Orue and Vermeersen [42] which takes into account non-zero eccentricity, non-zero obliquity and non-synchronous rotation for a 5 layer Maxwell model for the interior of the moon as described in Table 2.1. When not specified in other ways, the thickness of the ice is considered to be of 5 km. The two first stress sources, namely eccentricity-driven and obliquity-driven background fields are defined by a value of 0.0094 and an axial tilt of 0.5°, respectively. The two sources are deforming Europa on a short, diurnal timescale whose magnitude has the same order of the orbital period (around 85 hours). Secular stress source is the non-synchronous rotation with a period set as 10^7 years. These numbers are taken from the literature survey of Europa and used also in Jara-Orue and Vermeersen [42]. For more details about the stressing sources on Europa, the reader is encouraged to refer to chapter 2, with a focus on section 2.2. The work of Jara-Orue and

Vermeersen [42] applied the results of normal mode theory to a viscoelastic stratified moon and produced analytical formulations for elastic and viscous stress tensor that can be calculated for every point of the moon. In the current research, only elastic stress can be used as acting source on the crevasses, if one wants to apply LEFM. The analytical functions are reported in Appendix B.

- Europa 's outer layer is considered to be a constant thickness solid ice crust that is behaving as a pure elastic material.

This is considered to be the first and most important assumption for the model developed in the current research. Europa icy crust is assumed to be a finite thick layer in contact with the lower global ocean. The ice is purely elastic and its constitutive equation is the Hooke's law (Equation 5.8). In reality, it is more likely that ice is also flowing on Europa but the introduction of visco-elasticity would not allow the linear elastic fracture mechanics to be applicable. The key physical properties that have been assumed for the Europan outer layer are listed in Table 6.1. It is important to notice that the parameters mentioned in the table are considered constant throughout the entire thickness of the ice. The limitation of a pure elastic plate is the key for the application of the LEFM to crevasse propagation.

- The linear elastic fracture mechanic investigation aim to find the stress intensity factor for various locations of the moon, by assuming a single edge notch specimen on a finite plate geometry

This simplification is maybe the most limiting one, while talking about the effective validity of the model. LEFM is a theoretical technique that is based on experimental work done on materials cracked in the laboratory. Obviously, the dimensions of the specimens are far from the scales of crevasses on Europa. Some features are observed to stretched along half on the moon's surface reaching total lengths of thousands of kilometers. Laboratory specimens maximum dimensions are meters. Therefore, it is necessary to take the effective validity of the results very cautionary. Although LEFM is been applied and validated with terrestrial crevasses, the VDV model provides just a first order approximation of icy crevasses. If data are partially available for Earth, for Europa even the more basic information is discussed. So it is necessary to critically understand that at such at large space scale no complete validation can be found. Additionally, the extremely large values of the length and the fact that some Europan crevasses are crossing almost the entire surface of the moon would imply a geometry that is definitely not plane, as the one assumed for terrestrial crevasses in Van der Veen [108] and Van der Veen [109], where the curvature of the Earth could be depreciate. For a complete analysis, planetary curvature should be taken into account. So doing, the problem would be translated into the LEFM analysis of a crack in a shell. In the literature on fracture mechanics, some analysis of fractured shell are present (e.g. Tada [100]). Unfortunately, the nature of the tidal forces expressed in Jara-Orue and Vermeersen [42], used as acting stress on the crevasses, is not suitable for vertical propagation. Concluding, the finite thick plate is applied to both the cases for sake of uniformity in the development of the work. Future work might include the curved geometry into the numerical model. In the current research, only a single edge notch specimen on a finite plate geometry is considered. Details on LEFM applied to such type of cracks has been already described in chapter 5, and more in specific in section 5.2. Figure 5.4 represents the geometry that is used for the vertical propagation.

The rest of the section describes the numerical passages that are needed to evaluate depth of the crevasses and horizontal propagation rate from the tidal stress of Jara-Orue and Vermeersen [42]. The key executable that is the basic of every routine that deals with the propagation of a crack is the evaluation and the monitoring of the stress intensity factor around the tip of the fracture. This is presented in section 6.1.1 and is based on the comparison of the K_I factor with respect to the toughness of the ice. This process is an iterative calculation that aims to find the crack length whose stress intensity factor is equal to the material toughness. Given its iterative nature, it is also called as LEFM loop. This routine is the basics of both vertical and horizontal propagation. If for the former the length represents the final product and the arrest of the simulations, for the latter this is the first step of the numerical analysis, which continues with the calculation of the propagation rate via time derivation. Vertical propagation is based on the VDV model presented in section 5.3.1 while the horizontal propagation on section 5.3.2, as it will become clear from the rest of the chapter. Of course, the executables need to receive input parameters that describes the general representation of Europa and the stress tensor that is the deforming background of the LEFM loop. Additionally, the parameters that governs the LEFM loops have to be included, in order to translate the model firstly developed for the Earth to Europa's crevasses, whose geometry is slightly different. This part is presented in sections 6.1.2 and 6.1.3. Finally, a short presentation of the outcomes of the simulations is reported in section 6.1.4. This just serves to show
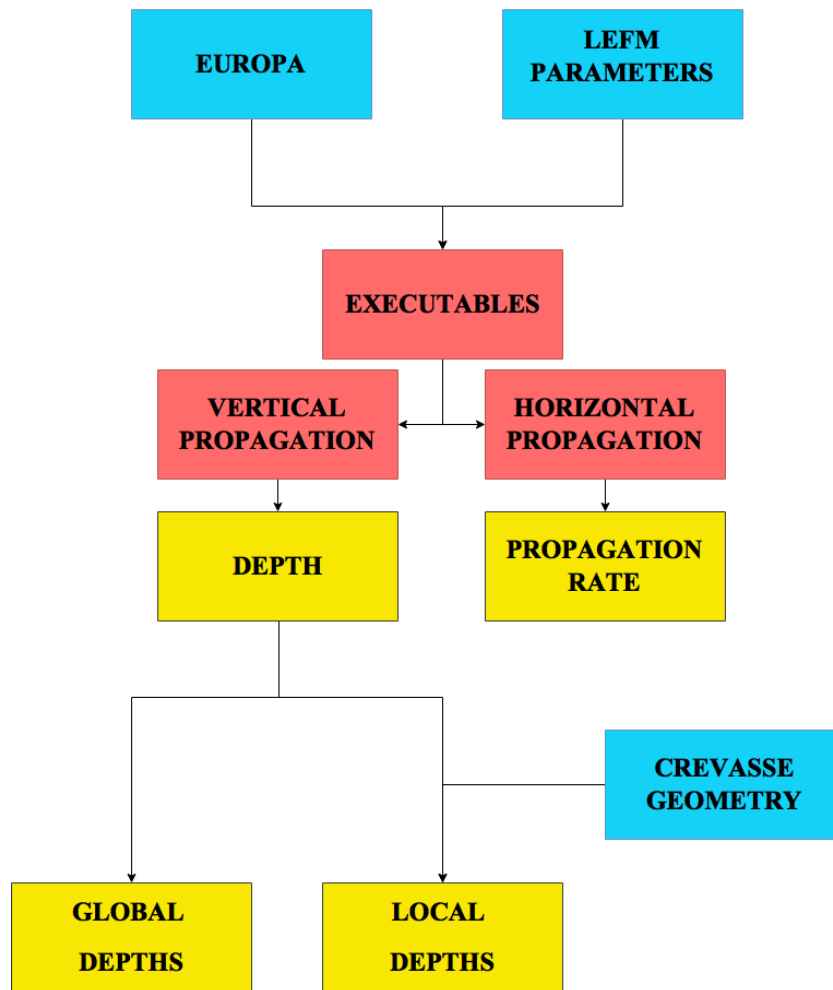
Figure 6.1: Representation of the numerical procedure of the research project, distinguishing between input files (in blue), executables (in red), and outcomes (in yellow). In particular, the input files consist in the Europa description, the parameters used for a LEFM loop and the geometry of the particular feature, if this is requested. The two categories of output files are vertical depths and horizontal propagation rates. The two executables are coded in order to find the two outcomes with different types of routines.

how the results would look like, instead of showing the exact numerical results of the simulations. A complete critical presentation of the results of the current research project are presented in chapter 7.

The scheme of the numerical routine is pretty straightforward, beginning with a set of input files that represents the planet conditions and the most relevant physical parameters, passing through the executables routines in order to produce relevant results. The actual diagram that represents the flux of the numerical model is shown in Figure 6.1. In the scheme, the executables are marked with the red boxes and differentiated, the two different types of outcomes are marked with the yellow boxes. The input files are represented by the blue boxes. Important is to notice that the geometrical aspect of specific crevasses is added only when the simulations needs to calculate the actual depth of specific fractures. The geometry is needed in order to to calculate the rotation matrix that would allow the reorientation of the stress tensor in terms of the actual opening stress normal to the crevasse. For the calculation of global depths, the geometry is not needed.

6.1.1. INPUT FILES

The current section discusses the input files that are describing the background of the simulations. In particular, these include the parameters that can be tuned in order to also produce sensitivity analysis, beside dealing with the effective answer to the research question. For sake of simplicity, the input files needed for running the numerical routines can be divided into three different categories. The three blocks of input files can be seen with the blue boxes of Figure 6.1. Referring to the scheme, two out of the three input files are

needed at the very beginning of the simulations. These are the physical description for Europa and the LEFM parameters. The third input is the geometry of an existing crevasse. More in specific, the discretised crevasse can be shaped along the map of the moon through the usage of Geographic Information System, also called as GIS softwares. This kind of input file is needed only when dealing with the local approach of the vertical dimension as it is mentioned later on. The software used in the current research is the open source software QGIS[1]. Among the possibility of the GIS program, the ability of discretising and manipulating geographical maps is given. In particular, the approach adopted in the research is the discretisation and the digitalisation of a list of target features observed on the surface of Europa in nodes and segments. So doing, the LEFM routines can be applied point-wise to the nodes found. Basic reference map is Figure 3.2. The next part of the section aims to describe the three input files in details.

The first two input files are the physical parameters that describe the Europa environment and the ones that govern the LEFM simulations. Dealing with the first of the two, the physical factors are needed for the calculation of the stress tensor as derived from Jara-Orue and Vermeersen [42]. Again, the analytical formulation of the stress tensor is included in Appendix B. The orbital parameters and the key elements that are describing the physical background environment of Europa are reported in Table 6.2, which summarises values that have been already discussed in chapter 2 and in the rest of the sections of the current document. This table is an essential part of the simulation and can be seen as the blue box called Europa in Figure 6.1. The rest of the parameters about the vertical stratification of the moon are listed in Table 2.1. Nevertheless, the parameters listed in this last table are not used in the calculation of the LEFM analysis but are only needed in the derivation of the stress tensor from the tidal potential, instead [42]. Additionally, some key factors are still needed in order to produce a full and valid LEFM simulation for Europan crevasses. The LEFM loop is better explained in section 6.1.2 and based on the VDV model presented in section 5.2. The geometry for a LEFM applied to an ice crevasse (for both surface and bottom fractures) is shown in Figure 5.4. In the specific, a constant thickness ice layer is subjected to a tensile stress of magnitude R_{xx}, among other stressing sources. The ice's density is represented by a depth-profile (Equation 5.23) where the values that are governing the ice are listed in Table 6.3. The general values that are governing the density profile have been taken from Van der Veen [108] and Van der Veen [109], given the similar characteristics of the elastic ice that is investigated in the terrestrial model. Tables 6.2 and 6.3 represent the key parameters that are needed to perform the numerical routines explained in sections 6.1.2 and 6.1.3, in order to produce a fracture propagation analysis.

Concerning the last input file, this is needed only when the actual local depth of the crevasse is required. the description of the single crevasse's geometry is one of the key aspect of the simulations. Purpose is to describe the shape of the lineament feature that is observed on the surface of the moon. The map that is taken as reference is Figure 3.2 which represents the most recent digitalisation of images from *Voyager*, *Galileo* and *New Horizon*, elaborated by IAU. As it can be seen from the map, the white lines are the lineament features are labelled with their name and these can be discretised via GIS and taken as targets for the current simulations. The process of discretising the lineaments of Europa can also be called shaping, term that derives from the type of file that is produced after the process, shape file, for instance. The two terms will be used arbitrarily in the rest of the document. Discretising a feature proceeds with the differentiation in nodes and segments,

---

[1]http://qgis.org/en/site/, last viewed on October, 29th 2017.

Europa Physics	**Symbol**	**Value**	**Reference**
Radius of Europa	R	1562 km	Lissauer and De Pater [54]
Superficial gravity	g	1.315 m/s^2	Lissauer and De Pater [54]
Semi-Major Axis	a	671080 km	Lissauer and De Pater [54]
Eccentricity	e	0.0094	Jara-Orue [41]
Obliquity	υ	0.5°	Jara-Orue [41]
Argument of pericenter	w	345°	Lissauer and De Pater [54]
NSR period	T_{ns}	10^7 years	Jara-Orue [41]
Mass of Europa	M_E	4.7998×10^{22} kg	Jara-Orue [41]

Table 6.2: Table that summarises the key parameters that govern the model representing Europa. The majority of the values are discussed in chapter 2.
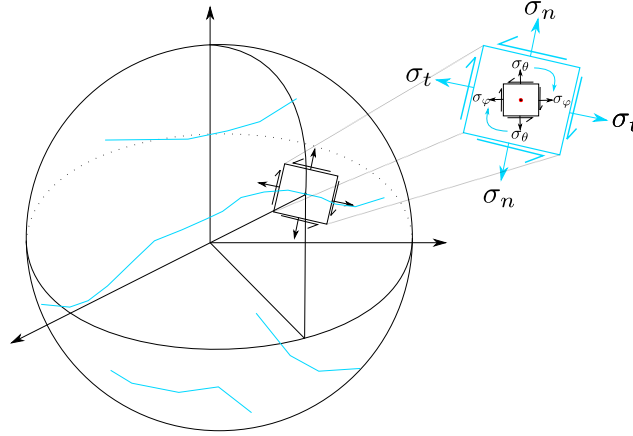
Figure 6.2: Visualisation of the stress tensor rotation applied to the geometry of a crevasse on Europa. The blue dashed lines represents lineaments on the surface. The black small tensor on the right represents the analytical formulation of the stress tensor in longitudinal σ_φ and co-latitudinal direction σ_θ. On the other hand, the red tensor is rotated with respect to the geometry of the crack.

which can be found along the continuous aspect of a feature. Figure 6.2 represents the problem of rotating the stress tensor with respect to the single crevasse. With the blue dashed line, the lineament feature is represented. Jara-Orue and Vermeersen [42] found the stress tensor as function of longitude φ and co-latitude θ. As first part of the numerical simulations, while dealing with the global view of the results, the stress tensor is diagonalised in order to find its eigenvalues, whose most tensile is used as opening source for the point in question. Therefore, it is enough to adopt the stress tensor as it is, in co-latitudinal and longitudinal direction, and then proceed with the finding of the eigenvalues, before applying the LEFM. On the other hand, when the routines are applied to a specific crevasse, in order to find the actual normal stress acting on the tip of the existing fracture a rotation matrix needs to be added to the simulation.

Considering the definitions provided in chapter 5 and in particular with Equation 5.7, the stress tensor in co-latitudinal and longitudinal direction can be written as:

$$\underline{\underline{\Sigma}} = \begin{bmatrix} \sigma_\theta & \sigma_{\theta\varphi} \\ \sigma_{\varphi\theta} & \sigma_\varphi \end{bmatrix} \tag{6.1}$$

where the dependance of the various stress components with respect to time and position can be found in Appendix A. The rotated stress tensor with respect to the observed crevasse, which distinguishes between normal stress σ_n, lateral stress σ_t and shear stress τ, can be written as:

$$\underline{\underline{\Sigma}}_R = \begin{bmatrix} \sigma_n & \tau \\ \tau & \sigma_t \end{bmatrix} \tag{6.2}$$

Parameter	Symbol	Value	Reference
Ice Thickness	H	5 km	Billings and Kattenhorn [5]
Ice density	ρ_i	917 kg/m^3	Van der Veen [108]
Surface Ice density	ρ_s	850 kg/m^3	Van der Veen [108]
Water density	ρ_w	1000 kg/m^3	Lissauer and De Pater [54]
Density profile constant	C	0.02	Van der Veen [108]
Ice touchness	K_{IC}	100 KPa m$^{1/2}$	Van der Veen [108]

Table 6.3: Table that summarises the key parameters that govern the LEFM routines.
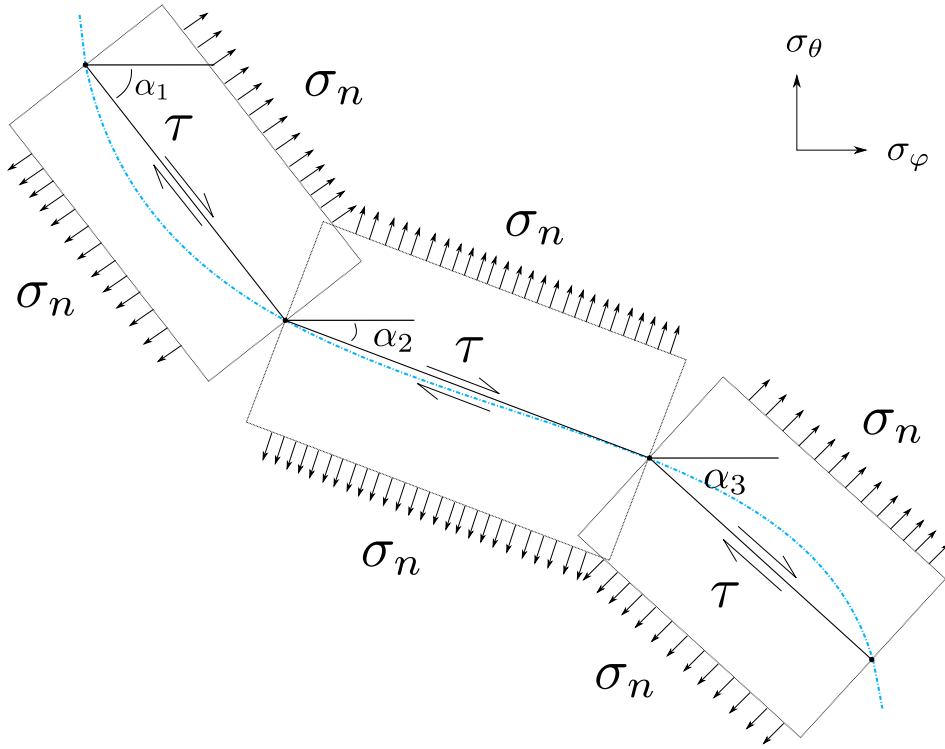
Figure 6.3: Representation of the crevasse discretisation in nodes and segments (black solid lines) of the crevasse (blue dashed lines). The rotation angle α is shown, together with the original and rotated stresses σ_θ, σ_ϕ, σ_n, and τ. Rotation of the stress tensor is written in Equation 6.3.

It is possible to introduce the operation of matrix rotation, function of the rotation angle α, as follows:

$$\begin{bmatrix} \sigma_n & \tau \\ \tau & \sigma_t \end{bmatrix} = \begin{bmatrix} \cos\alpha & -\sin\alpha \\ \sin\alpha & \cos\alpha \end{bmatrix} \begin{bmatrix} \sigma_\theta & \sigma_{\theta\varphi} \\ \sigma_{\varphi\theta} & \sigma_\varphi \end{bmatrix} \begin{bmatrix} \cos\alpha & -\sin\alpha \\ \sin\alpha & \cos\alpha \end{bmatrix}^T \tag{6.3}$$

which can be summarised by the following equation, that includes the so-called rotation matrix $\underline{\underline{R}}$, function of the already mentioned rotation angle α[102]:

$$\underline{\underline{\Sigma}}_R = \underline{\underline{R}}\,\underline{\underline{\Sigma}}\,\underline{\underline{R}}^T \tag{6.4}$$

The operation of rotating a stress tensor allows the identification of the stress status with respect to a different reference system. In the actual case, the initial reference system is given by the generic geographical directions, co-latitude and longitude (as the tensor provided by Jara-Orue and Vermeersen [42]). With the rotation, the actual geometry of the features starts to assume a relevant role. A LEFM application to such geometry allows the calculation of the actual depth of the crack, instead of a generic role given by the evaluation of the most tensile principal stress.

It is important to understand the role of the angle α. This is represented in Figure 6.3 where the actual discretisation of the existing crevasse is addressed. The blue dashed line represents the actual continuous shape of the crevasse, as seen from the map of the moon (i.e. the white lines of the global map of Figure 3.2). The black solids line, linked by the black dots are the segments and the nodes used to discretise the crevasse. The original reference system is stated at the upper right corned of the image and represents co-latitudinal θ and longitudinal φ directions. The angles α are shown at the intersections between the continuous and discretised crevasses, namely at the nodes. The stress that is described as the original reference system is rotated with respect to the actual orientation of the segment, and the rotated tensor is applied to the most western of the two nodes that represent the extremes of the segment. The terms σ_θ, σ_ϕ, σ_n, and τ are the ones written in Equation 6.3. The rotated stress is considered to be constant along the entire segment, as the first part of the current document mentioned already.

The lineament features observed on Europa reaches total dimensions of thousand of kilometers. At such spatial scale, the ratio between the total length of the fracture and the radius of the moon approaches to the
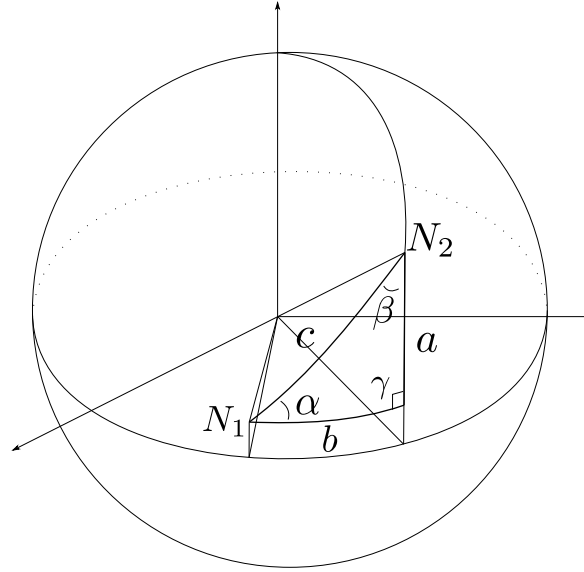
Figure 6.4: Identification of angles (in capital letters) and sides (in small letters) for the geometry of a spherical triangle. In particular, the current triangle has a right angle for γ. Nodes 1 and 2 represent the extreme limits

unity. This means that a spherical geometry needs to be evoked in order to represents the correct values of angles and segments. The problem of spherical geometry can be translated into the analysis of spherical triangles. In the specifics of the current case, the latitude and the longitude of the nodes that represent the extremes of the segments in Figure 6.3 are known, since they are found with the usage of GIS softwares, as already mentioned. A good reference when dealing with spherical geometry is Wertz [114] and the rest of the analysis is based on it. Assuming a sphere of radius equal to 1 and a spherical triangle; the sides are named a, b and c, while its angles are α, β and γ. It is possible to visualise the geometry of angles and sides in Figure 6.4 and the segment of the discretised crevasse can be seen as the lineament connecting N_1 and N_2. If one considers the angle γ as 90° for simplicity, it is possible to write the side angles a and b as the difference between latitudes and longitudes of the two nodes. With an eye on the Europa problem, the idea is to relate the length of the crack and the rotation angle to the values of latitude and longitude that are known. In the specific, the rotation angle that represents the rotation from the longitude and latitude components can be assumed to be α in Figure 6.4, while the angular length of the discretised segment of the crack is c. Terms a and b can be written as function of co-latitude θ_N and longitude φ_N of the nodes N_1 and N_2 as follows:

$$a = |\theta_{N_1} - \theta_{N_2}| \tag{6.5a}$$

$$b = |\varphi_{N_1} - \varphi N_2| \tag{6.5b}$$

Knowing that $\gamma = 90°$, it is possible to find α, β and c with the following routine [114]:

$$c = \text{acos2}[\cos a \cos b, \text{Hemi}(C)] \tag{6.6a}$$

$$\alpha = \text{acos2}\left[\frac{\cos a - \cos b \cos c}{\sin b \sin c}, \text{Hemi}(a)\right] \tag{6.6b}$$

$$\beta = \text{acos2}\left[\frac{\cos b - \cos a \cos c}{\sin a \sin c}, \text{Hemi}(b)\right] \tag{6.6c}$$

where the function acos2 is defined as:

$$\text{acos2}[\phi, \text{Hemi}(\phi)] = \text{Hemi}(\phi)\text{acos}\phi \tag{6.7}$$

where:

$$0° \leq \text{acos}(\phi) < 180° \tag{6.8}$$

and the hemisphere function Hemi is defined as:

$$\text{Hemi}(\phi) = +1 \text{ if } 0° \leq (\phi) < 180° \tag{6.9a}$$

$$\text{Hemi}(\phi) = -1 \text{ if } 180° \leq (\phi) < 360° \tag{6.9b}$$

For the Equations 6.5 to 6.9, the angles assumes values that stay in the range 0° to 360°[114]. The current analysis allowed the calculations of the angular distance between two points on a unity-radius sphere. If the radius is changed, this implies that the actual dimension of the segment can be measured as:

$$l = Rc \tag{6.10}$$

where the term R is the radius of the sphere and l is the length of the spherical segment. This value is useful when dealing with the calculation of the crevasse length, key element in the calculation of the stress intensity factor of the crevasse. Additionally, the shown routine is able to find the estimation of the angle α which is the rotation angle introduced with Figure 6.3, dealing with the re-orientation of the stress tensor.

The current section aimed to describe in details the input files that are needed in the elaboration of the routines. Namely, Europa physical characteristics and the LEFM basic parameters are listed in Tables 6.2 and 6.3, respectively. The presentation and the explanation of the several parameters introduced in the current list are taken from the qualitative analysis of chapter 2, together with the presentation of the VDV model of section 5.2. It is now possible to describe the observed crevasses in terms of nodes and segments (Figure 6.3) and the calculation of angles and sides allowed the identification of segment's lengths and rotation angles. These elements are very useful when dealing with the rotation of the stress tensor and with the identification of the crack's length, as it becomes clear in the next two sections, presenting the two key executables produced by the current research.

6.1.2. EXECUTABLE 1: VERTICAL PROPAGATION

This part of the chapter focusses on the description of the kew executables that have been developed for the current research. In Figure 6.1, these are represented with the red boxes and can be distinguished between vertical and horizontal propagation, depending on the type of outcome these eventually produce. The results of the vertical propagation routine is the vertical depth of the crevasse which can be calculated in a global or in a local point of view. On the other hand, horizontal propagation allows the calculation of horizontal propagation rates for the crevasse. The difference between local and global view consists in the introduction of the rotation matrix $\underline{\underline{R}}$, function of the rotation axis α. The description of this process is given in the last section and it can be visualised in Figure 6.3, where the geographical tensor on the upper right corner is rotated to the local geometry of the fracture.

In the analysis of the two routine that produces different insights in the propagation of Europa crevasse, there is one loop that is common for both. This is the actual LEFM loop that continuously calculates and monitors the stress intensity factor as function of the stress and the length of the crack. The model finds the exact length of the crack whose stress intensity factor at that moment is equal to the toughness of the ice. The description of the LEFM methods are included in section 5.2, where the stress intensity factor approach is introduced, and in section 5.3 where it is applied to terrestrial crevasse in the so-called VDV model of Van der Veen [108] and Van der Veen [109]. The current routine is based on the VDV approach which is used to determine propagation details on Europa.

Dealing with surface crevasses, it is possible to calculate the critical depth for a specific point of the moon at a specific time with the evaluation of the various components of the stress intensity factor. The routine processes values for the K factor as function of the actual depth of the crevasses d_i. Accounting a crevasses that exists and it is very shallow (1 meter by assumption), the routine finds the stress intensity factor for every possible critical depths from 1 to the actual thickness of the ice layer H (meaning a fully fractured ice sheet). The algorithm is presented in Algorithm 1, where the result is the critical depth $\overline{d}_i$ whose stress intensity factor is equal to the material toughness K_{ic} for the specific time-space combination. The routine is built on the VDV model of [108], which is explained in details in section 5.3. As mentioned before, surface crevasses on Europa are thought to be water-free fractures, hence the term $K_I^{(3)}$ is not considered in the simulations (Equation 5.32). In the algorithm the geometrical and a-dimensional functions for a finite thick specimen are included. These are the functions F and G taken from Tada [100] and written in Equation 5.28 and 5.30, respectively. F and G have as varying parameters the terms $\lambda = d/H$ and $\gamma = b/d$.

On the other hand, for a bottom crevasse, the guidelines for the algorithm are reported in Van der Veen [109] and presented in section 5.3. Given the thickness of the ice H, it is possible to calculate the stress inten-

For a specific location on the moon, at a specific orbital position of Europa around Jupiter

while $\sigma > 0$ **do**

> the surface crack's tip is under tensile stress;
>
> **for** $i = 1 : H$ **do**
>
> > evaluation of equilibrium length d;
> >
> > $K_i^{(1)} = \sigma \sqrt{\pi d_i} F(d_i)$;
> >
> > $K_i^{(2)} = \frac{2\rho_i g}{\sqrt{\pi d_i}} \int_0^{d_i} \left[-b + \frac{\rho_i - \rho_s}{\rho_i C} (1 - e^{-Cb}) \right] G(\gamma_i, \lambda_i) \mathrm{d}b$;
> >
> > $K_i^{\mathrm{net}} = K_i^{(1)} + K_i^{(2)}$;
>
> **end**
>
> find critical value $\overline{d}_i$;
>
> $K_i^{\mathrm{net}}(\overline{d}_i) = K_{ic} \rightarrow \overline{d}_i$

end

Algorithm 1: LEFM loop for surface water-free crevasses, from the VDV model of [108].

sity factor for the potential bottom crevasse heights h, instead of depth d. The difference in the terminology between depth and height does not change the fact that they both refer to the fracture length. Accounting a net opening tensile stress σ, lithostatic pressure and water pressure, it is possible to find the K factor as function of h. Assuming that a global water ocean is found underneath the ice crust, the assumption of water filling the crevasse is valid. For a description of the vertical stratification of Europa, the reader is referred to chapter 2. Algorithm 2 represents the numerical routine that is build in order to find heights whose stress intensity factor is equal to the material toughness for the location under investigation and at the specific time. Functions F and G are the same of the ones in Algorithm 2 but defined as dependent of $\lambda = h/H$ and $\gamma = z/h$, differently to the surface crevasse routine.

For a specific location on the moon, at a specific orbital position of Europa around Jupiter

while $\sigma > 0$ **do**

> the bottom crack's tip is under tensile stress;
>
> **for** $i = 1 : H$ **do**
>
> > evaluation of equilibrium length h;
> >
> > $\sigma_n(h_i) = -\rho_i g(H - h_i) + \frac{\rho_i - \rho_s}{C} g[1 - e^{-C(H-h_i)}] + \rho_w g(H_p - h_i) + \sigma$;
> >
> > $K_i^{\mathrm{net}} = \int_0^{d_i} \frac{2\sigma_n(z)}{\sqrt{\pi d_i}} G(\gamma_i, \lambda_i) \mathrm{d}z$;
>
> **end**
>
> find critical value $\overline{h}_i$;
>
> $K_i^{\mathrm{net}}(\overline{h}_i) = K_{ic} \rightarrow \overline{h}_i$

end

Algorithm 2: LEFM loop for bottom water-filled crevasses, from the VDV model of [109].

In the Algorithms 1 and 2, the tensile stress σ can assume two different type of value. While dealing with the global view, this is the most tensile principal stress found by the identification of the eigenvalues of the stress tensor. On the other hand, the local view requires that stress tensor to be rotated and to be express in terms of normal, lateral and shear stress. Here the term σ assumes the value of σ_n.

Although the two explained algorithms allow the identification of critical depths and heights, the calculated equilibrium solution is not always a stable solution. Indeed, it is important to recall the discussion already initiated at the very end of section 5.3.1, in the last chapter. As already mentioned in the work of Van der Veen [108], there are two kind of potential solutions in the vertical propagation model. The difference between the two is whether or not the solution is stable. As it can be seen in Figure 5.6b, the nature of the stress intensity factor curve allows the possibility of finding a lower and an higher value for the crevasse's length. In the specific case, critical lengths that have negative derivative of the stress intensity factor with

if $K_{i+1}^{net} > K_{ic}$ *and* $K_{i-1}^{net} < K_{ic}$ **then**

  non-stable solution;

  $K_i^{net} = K_{i+1}^{net}$;

else if $K_{i+1}^{net} < K_{ic}$ *and* $K_{i-1}^{net} < K_{ic}$ *and* $K_i^{net} < K_{ic}$ **then**

  no intersection between stress intensity factor and toughness ;

  $K_i^{net} = K_{i+1}^{net}$;

else

  critical value $\overline{h}_i$ was found;

  $K_i^{net}(\overline{h}_i) = K_{ic} \rightarrow \overline{h}_i$;

end

Algorithm 3: Stability check loop for the solution found with the LEFM loops.

respect to the length itself are assumed to be unstable. The critical length that generate a positive derivative is considered to be stable, instead. The qualitative reason is that at the equilibrium length with a negative derivative, a small perturbation from the solutions would lead the stress intensity factor to reach either the closure[2] or the other higher solution. In other words, lengths that are a bit smaller than the equilibrium would imply a stress intensity factor that is lower than the toughness and hence closure of the crevasse. On the other hand, lengths that are a bit larger than the equilibrium point implies the K factor to be larger than the toughness and the crack to propagate until the threshold of the material is not reached anymore. This happens at the second (higher solution) where the derivative is now positive. A new routine is needed in order to determine only stable solution. The routine is presented in Algorithm 3 and it consists of three different conditions that are representation of three different situations where the numerical solution needs a double check. The first condition represents the actual unstable solution and it is determined by finding the values of the stress intensity factors for the two length, one step larger and smaller than the actual solution. If the former is higher and the latter lower than the toughness, the solution is unstable[3], as mentioned before. The second condition occurs when there is no intersection between toughness and stress intensity factor. Finally, if the two conditions are not satisfied, the solution is acceptable and the numerical routine stops.

6.1.3. Executable 2: Horizontal Propagation

In section 6.1.2, the description has been entirely focussed on the vertical propagation routine, which leads to the calculation of the vertical depth of the crevasses on Europa. Even if two different types of routine have been included (termed as global view and local view), the background idea is the same. In Figure 6.1 the two are naturally summarised by the red box called vertical propagation. This last part of the section aims to describe the second executable, which evaluates the horizontal propagation rate for existing crevasses. The geometry adopted is the same of the local view of vertical propagation, meaning that the rotation tensor is introduced in order to find the actual stress that is acting normal to the tip of the crack, for reference Figures 6.2 and 6.3. Differently to what happens for vertical propagation, this time the LEFM approach adopted by VDV is not valid anymore because the depth of the crevasse is not targeted in this case. The description of the model is now the one of a centred crack test specimen [100]. Additionally, for sake of the current aim, i.e. the evaluation of propagation rate, the displacement approach of the LEFM is more suitable to the actual case. The finding of the displacement is an alternative to the stress intensity factor, but the idea behind is again the evaluation of the possibility of the material status to reach the critical toughness and of the crack to eventually grow. Nevertheless, in the current project the approach is the same of Larour et al. [50] which coupled the usage of the stress intensity factor with the evaluation of the displacement. The methodology is presented in section 5.3.2. The geometry of the new specimen is shown in Figure 6.5a, where the terms of the

---

[2]In reality, the extreme lower value for the crevasse is not zero, but assumes a value of meter. LEFM does not tell anything about fracture initiation, only propagation can be analysed. Therefore, the crack has to exist in order to apply LEFM routines. Nevertheless, a negative value for the stress acting on the tip, would allow a zero value for the length, by assumption.

[3]The explained control is an alternative to the evaluation of the derivative of the stress intensity factor with respect to the crack's length.

next equations can be appreciated. The displacement can be calculated as:

$$\delta = \frac{4l\sigma_n}{E} V(l) \tag{6.11}$$

where l is the length of the crack[4], σ_n the normal stress and E the Young modulus. V is the geometrical function that describes the centred crack specimen, differently from the function F (Equation 5.28) used for the single notched test specimen. The function V can be written as:

$$V(l) = -0.071 - 0.535\left(\frac{l}{L}\right) + 0.169\left(\frac{l}{L}\right)^2 - 0.09\left(\frac{l}{L}\right)^3 + 0.02\left(\frac{l}{L}\right)^4 - 1.071\frac{L}{l}\log\left(1 - \frac{l}{L}\right) \tag{6.12}$$

where the term L is the thickness of the test specimen. The validity of this equation is hold for every value of l/L so, it is possible to use the equation also for an extremely large value of L, being the current case. The terms l and L can be seen in Figure 6.5a. The stress intensity factor formulation needs to take into account the assumption of the centred crack test specimen instead of the single notched test specimen. This can be done with the introduction of a new a-dimensional geometrical function F_2 [100], that can be written as:

$$F_s(l) = 1 + 0.128\left(\frac{l}{L}\right) - 0.288\left(\frac{l}{L}\right)^2 + 1.525\left(\frac{l}{L}\right)^3 \tag{6.13}$$

which is valid for ratios l/L lower than 0.7. The numerical simulations need to take this into account: since the term L is arbitrary for the case of Europa, it can be calculated as $L = l/0.7$, by assumption.

After the displacement function is expressed, the key mathematical operation that is needed for finding propagation rate is a time-derivative of δ itself. In symbols this can be written as:

$$\frac{\partial \delta}{\partial t} = \frac{\partial}{\partial t}\left[\frac{4l\sigma_n}{E} V(l)\right] \tag{6.14}$$

so by the application of standard calculus manipulations to the right member, the equation can be written as:

$$\frac{\partial \delta}{\partial t} = \frac{4}{E}\left\{\sigma_n V(l)\frac{\partial l}{\partial t} + l V(l)\frac{\partial \sigma_n}{\partial t} + l\sigma_n\frac{\partial V(l)}{\partial t}\right\} \tag{6.15}$$

where the different terms in the right member needs to be described in details. If the term l represents the crack's length, its derivative in time is the actual propagation rate, which is the target of the current simulations. It is known already that the stress tensor is function of time (Appendix B), so its derivative in time is straightforward and can be written as $\dot{\sigma}_n$. A different discussion is needed for the rest of the terms. A common mathematical manipulations in engineering problems is the variation of variables which can be applied to the derivative in time of the a-dimensional function V in order to find again the propagation rate:

$$\frac{\partial V(l)}{\partial t} = \frac{\partial V}{\partial l}\frac{\partial l}{\partial t} \tag{6.16}$$

This operation is particularly useful because now the only derivation that is needed is of Equation 6.12 with respect to the term l.

Larour et al. [50] applied the same idea for the investigation of crack's horizontal propagation rates near the Hemmen Ice Rise in the Ronne Ice Shelf, Antarctica. In the study, LEFM was able to model the order of magnitude for the annual propagation rates of the crevasses. The key element of the research is that the opening width δ and the opening rates $\partial \delta/\partial t$ were available data. In fact, the work used interferometric synthetic aperture radar (inSAR) data in order to fix this two key parameters in Equation 6.11 and 6.14, respectively. Since the current research applied the simulation to Europa, data for opening rates are limited to the (few) pictures that are available for the surface, while for the opening rates no observations are available, although some models have been produced. Therefore, a strategy to avoid the lack of observations needs to be implemented. The opening width δ can be calculated by LEFM with Equation 6.11. The opening rate can be found, by introducing the strain rate $\dot{\epsilon}$:

$$\frac{\partial \delta}{\partial t} = \delta\dot{\epsilon} \tag{6.17}$$

---

[4]Note the substitution in the terminology: from depth d with crack's length l.

(a)   **(b)**
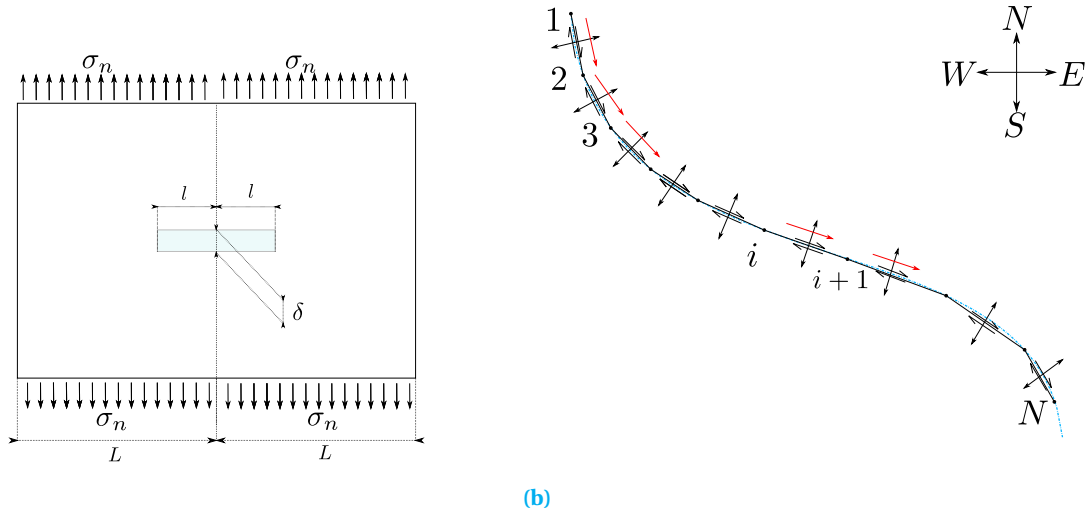
Figure 6.5: The two pictures represent the geometry adopted for the horizontal propagation problem. Figure 6.5a shows the centred crack test specimen, where l is the half-crack length and L the specimen lateral thickness. δ is the crack's opening width while σ_n is still the opening stress. The figure replaces the geometry of Figure 5.4, introduced for vertical propagation. On the other hand, Figure 6.5b represents the discretisation that has been already introduced in section 6.1.1. The number of nodes goes from $i = 1$ to $i = N$, and the horizontal propagation is always assumed to be in east-ward direction. Red arrows represents segments whose stress intensity factor reaches the material threshold. More details in the text.

The strain rate can be found by the derivation of Equation 5.14. By considering an homogeneous, isotropic material, the compliance matrix $\underline{\underline{C}}$ is constant hence:

$$\epsilon = \underline{\underline{C}}\sigma \rightarrow \dot{\epsilon} = \underline{\underline{C}}\dot{\sigma} \tag{6.18}$$

The compliance matrix can be found in Equation 5.14, while the derivative of the stress can be calculated from Jara-Orue and Vermeersen [42].

The discussion that has been proposed allows the possibility of re-writing Equation 6.15 as function of the propagation rate, termed as v:

$$\delta\dot{\epsilon} = \frac{4}{E}\left\{\sigma_n V(l)v + lV(l)\dot{\sigma}_n + lv\sigma_n\frac{\partial V}{\partial l}\right\} \tag{6.19}$$

where, rearranging the two members in a more compact form, the propagation rate at a specific time t can be written as:

$$v(t) = \left[\frac{E}{4}\delta\dot{\epsilon} - lV\dot{\sigma}_n\right]\left[\sigma_n l\frac{\partial V}{\partial l} + \sigma_n V\right]^{-1} \tag{6.20}$$

The variables that are governing the behaviour of v for a specific location of the crevasse, at a specific time are better visualised in:

$$v(t) = f(\sigma_n, \dot{\sigma}_n, l) \tag{6.21}$$

because of the dependance between stress rate and strain rate of Equation 6.18. The term $\partial V/\partial l$ can be calculated from the derivation of Equation 6.12 with respect to the parameter l.

Equation 6.21 can be applied to every single node that discretise the aspect of the Europan crevasses. If the time variable ranges from a reference position, set at the PeriJove, it is possible to evaluate the propagation rate of the full crevasse in time. The discretisation geometry of the problem is shown in Figure 6.5b which is a re-adaptation of Figure 6.3, introduced for the vertical propagation. The evaluation of the horizontal propagation of the nodes follows the current scheme. The base consideration is that the crevasse shape is known a priori (by satellite images of Europa), namely the total length of the crack and its orientation is fixed. Assuming that a small crack is present (segment between node 1 and 2 in Figure 6.5b) at a specific time (PeriJove by assumption), it is possible to evaluate, via the LEFM loop of Algorithm 1, whether or not the material threshold is reached and whether or not the crack grows. The introduction of Equation 6.13 is essential to

For a specific crevasse on the moon, at a PeriJove t_0

for $i = 2 : N$ **do**

    find $\underline{\underline{R}}(\alpha_i)$;

    find l_i;

    find $\dot{\epsilon} = \underline{\underline{C}}\dot{\sigma}$;

    while *check = off* **do**

        for $j = i - 1 : -1 : 1$ **do**

            $l_i = l_i + l_{j-1}$;

        end

        $L_i = l_i / 0.7$;

        $K_i = \sigma_i \sqrt{\pi l_i} F_2(l_i)$;

        $\delta_i = \frac{4 l_i \sigma_i}{E} V(l_i)$;

        $\frac{\partial \delta_i}{\partial t} = \underline{\underline{C}}\dot{\epsilon}\delta_i$;

        $v_i = f(\sigma_i, \dot{\sigma}_i, l_i, \frac{\partial \delta_i}{\partial t})$;

        if $K_i > K_{ic}$ *and* $v_i > 0$ **then**

            check = on;

        else if $t_i - t_0 > 10 T_E$ **then**

            partial formation;

            check=on;

        else

            $t_i = t_i + \Delta t$;

        end

    end

end

Algorithm 4: Numerical routine that summarises the passages needed to find horizontal propagation rates for crevasses on Europa. Nodes $1 : N$ are shown in Figure 6.5b.

describe the new geometry. If the toughness for node 2 is not reached[5], the crack is in a stand-by mode and the time passes, Europa moves around Jupiter and the tidal stress changes, until a moment (if present) when the conditions are favourable to let the fracture propagate. When this happens, the propagation rate v can be calculated and at this speed, the fracture advances at node 3 in Figure 6.5b. Of course, knowing the rate and the length of the new segment, it is possible to calculate the time needed to reach the next node. Therefore, the simulation can move forward and at node 3, time has passed and the crack length has changed, because a new segment has been added. The model applies this concept to the entire crevasse, in order to see whether or not it is possible to reach the last node N or not. Moving at further points in the crevasses rises the problem of what happens behind. As it is now clear the crack length l is a fundamental element in the calculation of the stress intensity factor and of the displacement rate, especially for cracks measuring thousands of kilometers. Therefore, it is important to keep track of the length at every node. It is possible that some parts of the crevasses are subjected to a compressive stress that can lead to a closure of the crack itself. As consequence the routine analyses the stress status to every nodes west to the investigated point in order to see how far the crack remains open. At the end of the simulation, the total time for the full (or partial) completion of the crevasse is found, together with the analysis of the propagation rates.

    The numerical scheme can be seen in mathematical formulation in Algorithm 4. The routine surveyed each node of the discretised fracture in order to determine when and how propagation can occur. Additionally, for every node, also the stress status of the segments left behind are necessary, since these an eventual compressive status means a zero depth, by assumption. A particular discussion needs to be addressed when

---

[5]As mentioned before, only east-ward propagation is considered.

dealing with the calculation of the crack length l. Since the majority of the surveyed crevasses shows dimensions that reaches thousands of kilometers, the curvature of the moon starts to play a relevant role in the model. Therefore, spherical geometry needs to be evoked. A good reference book for geometry of orbits is Wertz [114]. The aim of the problem is to find the length of a segment on sphere, given the latitude, the longitude of the two nodes that represent the extremes of the segment itself. The problem of finding the rotation angle α and the crack length has been already addressed in section 6.1.1.

6.1.4. OUTCOMES

The last part of the current section aims to briefly describe the outcomes of the current numerical model. So far, a pretty straightforward scheme is assumed to be the baseline of the of the calculations. Two different types of executables have the purposes of translating input parameters to relevant results. Summarising, the input files describe the physical aspect of Europa and its ice layer, meaning orbital parameters coupled with rheological and material properties. These values are listed in Tables 6.2 and 6.3. The numerical executables are distinguished between vertical and horizontal propagation. As it can be evinced from the name, vertical propagation aims to find vertical critical depths and heights for surface and bottom crevasses, respectively. The so-called global view takes as opening source the most tensile principal stress calculated from the stress tensor of Jara-Orue and Vermeersen [42]. This is applied globally to every point that represent the surface of the moon, in order to determine whether or not critical areas emerge. On the other hand, the so-called local view applied the LEFM routine to a specific feature of the moon. This is possible with the rotation of the stress tensor with respect to the lineament's geometry (Figure 6.3). The numerical model can also apply LEFM in order to find insights in the horizontal propagation rate of the crevasses' development. The geometry is the same adopted in the local view of the vertical approach with some differentiation in the LEFM equations.

As it can be derived from the previous discussions, the two different executables produce outcomes that are distinguished between vertical and horizontal propagation. In more specific, the global view of the vertical approach allows the identification of areas that can be considered as critical, meaning that are showing depths that on average are higher than zero. The most tensile principal stress is a good representation of the stress status of the actual location at a specific time of the Europa rotation around Jupiter. Additionally, the local approach implies a better and more focussed analysis of specific crevasses on the moon, by finding the actual opening source on the crevasses' flanks themselves. Finally, the horizontal propagation allows the calculation of the horizontal propagation rate of the actual cracks. In the numerical scheme of Figure 6.1 the outputs of the simulations are represented with the yellow boxes at the bottom of the diagram. A complete understanding of how fast the crevasses are formed would be a key aspect to take into account when talking about future exploration missions and the actual detectability of this fracture development. The results of the simulations are described and critically discussed in chapter 7.

6.2. VALIDATION

The last part of the current chapter presents the validation procedure that has been implemented in order to check the correct behaviour of the LEFM routine presented in section 6.1.2. The lack of observation for crevasses on Europa has been mentioned already. The highest quality sources of data are around 150 images of the surface, captured by *Voyager*, *Galileo* and *New Horizon*, plus inclusion of some radar data from *Galileo* itself. The general problem is the same of every numerical model produced for Europa. Without data, it is hard to validate the model. Nevertheless, the current research applies a model that has been designed and used to study terrestrial crevasses. The Europa conditions are added into the routine in form of input information. The strategy adopted to validate the routine is to use data coming from terrestrial crevasses in order to validate the LEFM routine.

As previously discussed, terrestrial crevasses are observed in some of the most remote and dangerous places in the world. The high instability of the crevasse area and the hard accessibility of the locations are factors that limits the experimental fieldworks to study their behaviour. Although crevasses on glacier are some of the most important features that are characterising glaciers's behaviour, a few is known and studied concerning their properties. As already mentioned, they can be used as indicators of the glacier's flow (e.g. Hulbe et al. [31]) and their arrest point (suture zones) can indicate two different parts of the glaciers itself Larour et al. [50]. Additionally, fractures of the ice are considered as interesting phenomenon to study because of the difficulties of elaborating a calving law.

The only recorded experimental work that aimed to benchmark the results of crevasses' models is the
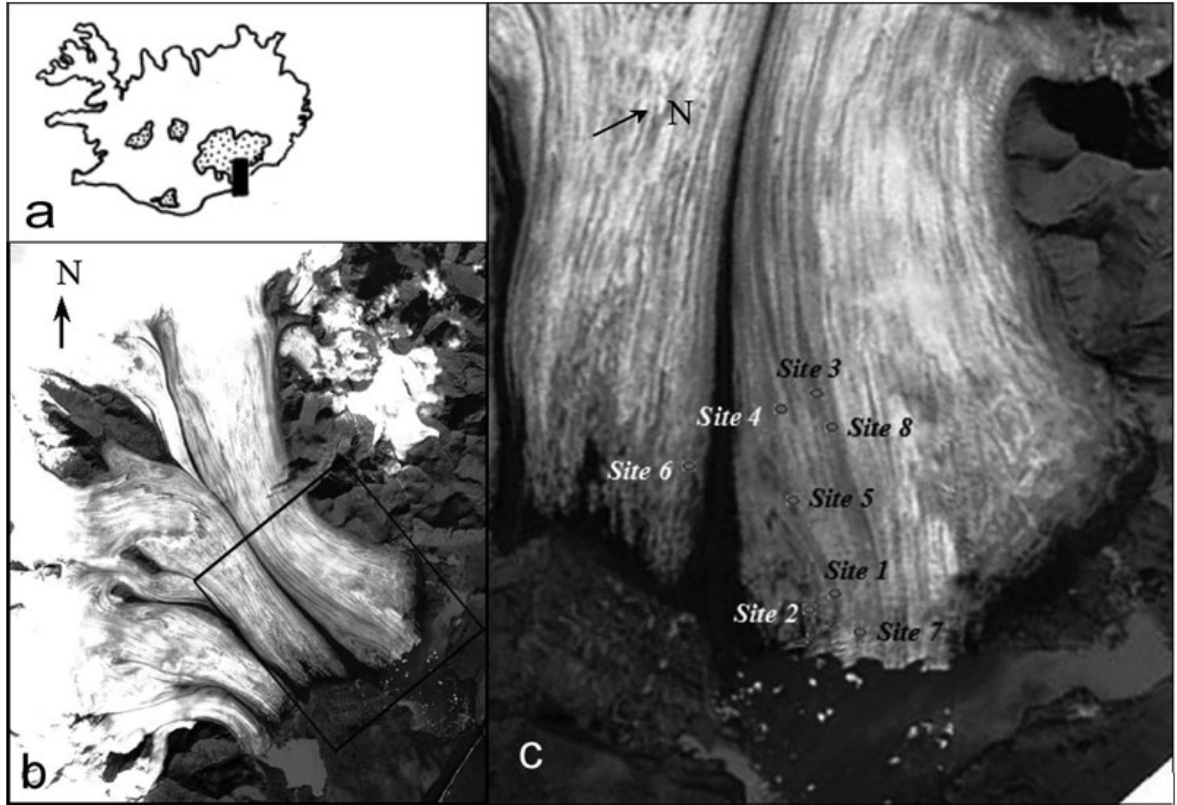
Figure 6.6: Location of the fieldwork of Mottram and Benn [60]. (a) shows the position of the Breidamerkurjokul in the map of Iceland. This glacier is the extreme southern part of the larger Vatnajokull ice cap. The marked areas in the pictures are the large ice caps of the island. (b) shows the area of interest of the glacier itself and (c) represents the 9 different experimental sites. In particular, sites 1 to 6 were studied in 2004 while sites 7 and 8 in 2004.

one of Mottram and Benn [60] which investigates the Breidamerkurjokul glacier in the South of Iceland. The image that shows the location of the different field sites is reported in Figure 6.6a to c. The surveyed glacier is flowing from the large Vatnajokull ice cap and was chosen from its relatively easy access from the land. The glacier is flowing into a lake that is separated from the ocean by a small line of land, where the Icelandic highway is passing. Additionally, this is one of the most studied glacier on Earth, hence bed topography and ice thickness were known. Purposes of the experimental fieldwork were divided into two different campaigns in 2004 and in 2005. At each site, the depth of the crevasse was measured via a simple plumb-line system. Additionally, across crevasses were determined by repeat measurement of the positions of pairs of stakes within each network, using a Leica 1200 laser theodolite [60]. The strain rate could be calculated via a logarithmic formula [26] as follow:

$$\dot{\epsilon} = \frac{1}{\Delta t} \ln \frac{L_2}{L_1} \tag{6.22}$$

where the two terms L_2 and L_1 indicate the two different separation from the stakes at the two different times. The time interval is Δt.

Knowing the strain rate, allows the calculation of the stress between the two flanks of the crevasse by using the Glenn law of Equation 5.22 that governs the viscous model of the ice. This can be re-written in order to find the dependance of the stress with respect to the strain rate:

$$\dot{\epsilon}_e = \left(\frac{\sigma_e}{A}\right)^n \tag{6.23}$$

where σ_e and $\dot{\epsilon}_e$ represent the equivalent stress and strain rate and A is a temperature dependant parameter that is related to the rigidity factor in Equation 5.22. n is the Glen's law parameter that ranges between 2 to 4 and in this case is selected as 3.

Site N^o	Strain Rate [year]$^{-1}$	Stress [KPa]	Ice Thickness [m]	Measured Depth [m]	Calculated Depth [m]
1	0.48	111.41	193.8	19	19.7
1	0.12	70.84	193.8	13.7	11.6
2	0.03	44.82	145.23	3	6.4
2	0.12	70.79	145.23	10	11.7
3	0.33	97.91	404.82	3.5	16.7
3	0.11	68.03	404.82	1.95	11.1
3	0.06	54.85	404.82	2.5	8.5
4	0.13	72.16	395.89	1.2	11.8
4	0.13	72.27	395.89	3.5	11.9
4	0.05	51.37	395.89	4	7.8
5	0.02	41.46	258.84	3	5.7
5	0.43	107.56	258.84	9.8	18.6
5	0.15	75.47	258.84	0.3	12.5
5	0.11	67.33	258.84	3.5	10.9
5	0.55	116.38	258.84	11.5	20.4
5	0.29	94.51	258.84	2	16.1
6	0.02	39.18	298.87	3.3	5.3
6	0.04	47.07	298.87	1.2	6.9
7	0.10	65.80	363.33	12.6	10.6
7	0.19	81.86	363.33	12.8	13.7
7	1.77	171.85	363.33	6.6	30.9
7	0.19	81.51	363.33	9.1	13.6
8	0.51	113.60	109.32	4.8	21.9
8	0.06	56.62	109.32	4.5	9
8	0.24	88.75	109.32	7.6	15.9
8	0.29	93.97	109.32	4.9	17.1
8	0.18	79.90	109.32	5.4	13.9
8	0.01	28.87	109.32	4.9	2.7

Table 6.4: Tabulated summary of the experimental work of Mottram and Benn [60] and the calculated depths found via the LEFM routine elaborated in the current research (Last column). Sites 1 to 6 surveyed in 2005, while sites 7 and 8 in 2004. Experimental sites' location is shown in the aerial image of the glacier in Figure 6.6.

With the evaluation of strain rates and crevasses' depths, models such as the VDV can be validated. In the work of Mottram and Benn [60] the depth results of the VDV model applied to crevasses with stress calculated from the strain rate, described well the observed measurements. Nevertheless, the discrepancies between measured and modelled depths are still large for some sites. According to the authors, the crevasses observed were hard to survey and many times the plumb-line system reached levels where the visibility was limited hence it could not be stated whether or not the weight had touched the actual bottom of the fracture. For the majority of the observations, the crevasse was seen to go deeper than the actual bottom. In fact, additional fractures were present at the bottom and these had flanks separated by few centimeters, hence almost impossible to reach with the plumb line. Furthermore, the 43% of the surveyed stakes presented a negative strain rate which corresponds to a compressive status. Given the scheme of a LEFM loop, a negative stress would not allow a crack to propagate. The solution to this contradiction is that crevasses could be formed in an historical previous stress configuration. A more complete analysis would be to keep track of the strain rate for a longer period of time, although nothing similar to this has never been attempted and recorded.

The current research used the strain rate and the related stress that can be introduced to the LEFM loop presented in Algorithm 1, in order to calculate the modelled critical depths. Table 6.4 shows the data used for the validation of the code. The first column represent the number of the site, ranging from 1 to 8. The first six sites were surveyed in 2005 while the last two in 2004. The location of the sites with respect to the glacier are shown in Figure 6.6(c). The second and the third columns list the strain rate and the stress, calculated by the Glenn flaw law of Equation 6.23, with a coefficient n equal to 3. The fourth column represents the ice thickness, measured with inSAR measurements. The fifth column indicates the depths measured with the plumb-line system. Finally, the last column represents the results of the LEFM loop presented in section 6.1.2 and summarised in Algorithm 1. As it is possible to see from comparison between the last two columns that the LEFM model produces values that are generally a bit higher than the actual measured depths. The general overestimation of the critical depth can be caused by several factors, including systematic errors, for example. Particularly difficult to model is the rheology of the ice and the temperature plays a key role in Equation 6.23.

In order to better visualise the results of the validation process, two figures have been included. The first one is Figure 6.7 which shows the relative errors between measured and calculated depths. The relative error can be written as:

$$e_{\text{rel}} = \frac{d_{\text{mod}} - d_{\text{obs}}}{d_{\text{obs}}} \tag{6.24}$$

where d_{mod} and d_{obs} are the modelled depths (last column in Table 6.4) and the observed depths (fifth column in Table 6.4). The relative error allows the identification of the value offset that is scaled with the actual measurement. As it can be seen in the figure, an e_{rel} of 10^0 means that the two values have the same order of magnitude. Generally speaking the representation of the relative error shows that the LEFM model overestimate the depths, since the majority of the dots have relative values larger than 10^0.

Additionally, the plot of the modelled depths as function of the observed depths has been plotted in Figure 6.8. Here, the blue dots represents the match between the two last columns of Table 6.4. The black dashed line indicates the perfect fit between experimental and numerical approach while the red dashed line is the linear regression of the point. The aim of the current figure is, once again, to indicate that the LEFM depths are overestimations of the actual measured depths. This can be seen from the fact that the red line behaves to the upper part of the graph, divided by the black line.

Concluding, the LEFM loop that is presented in section 6.1.2 is the key numerical tool that is used in the current research. Given a geometry of a crevasse, the thickness of the ice and the background stress it is able to find the correct order of magnitude for the crevasse depth. The normal uncertainties in the rheology of the ice, in the material properties and in the difficulty of correctly measuring the actual length of the fracture lead the model to overestimate the depths, although the general magnitude is roughly matched. For sake of the current research, the LEFM loop can be considered validated and the presentation of the work can proceed to the analysis of the results of the routines when applied to Europa crevasses.
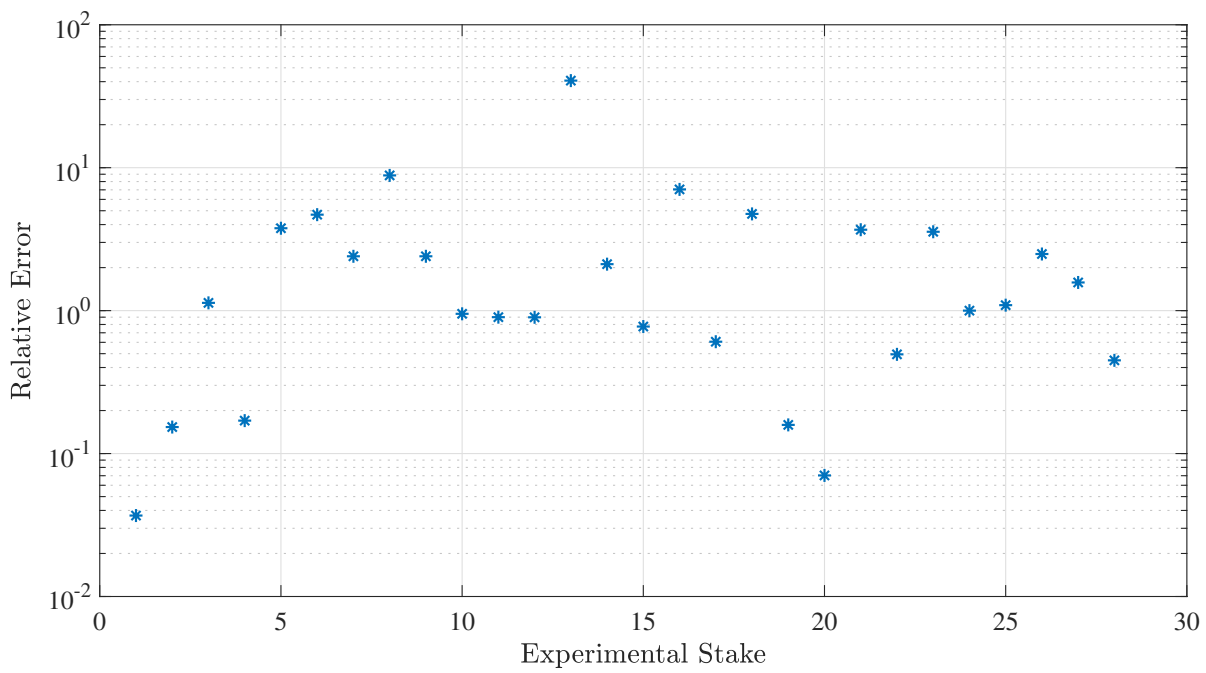
Figure 6.7: Relative error between calculated and measured depths for each experimental site. The value 10^0 for the relative error indicates the same order of magnitude between measured and calculated values.
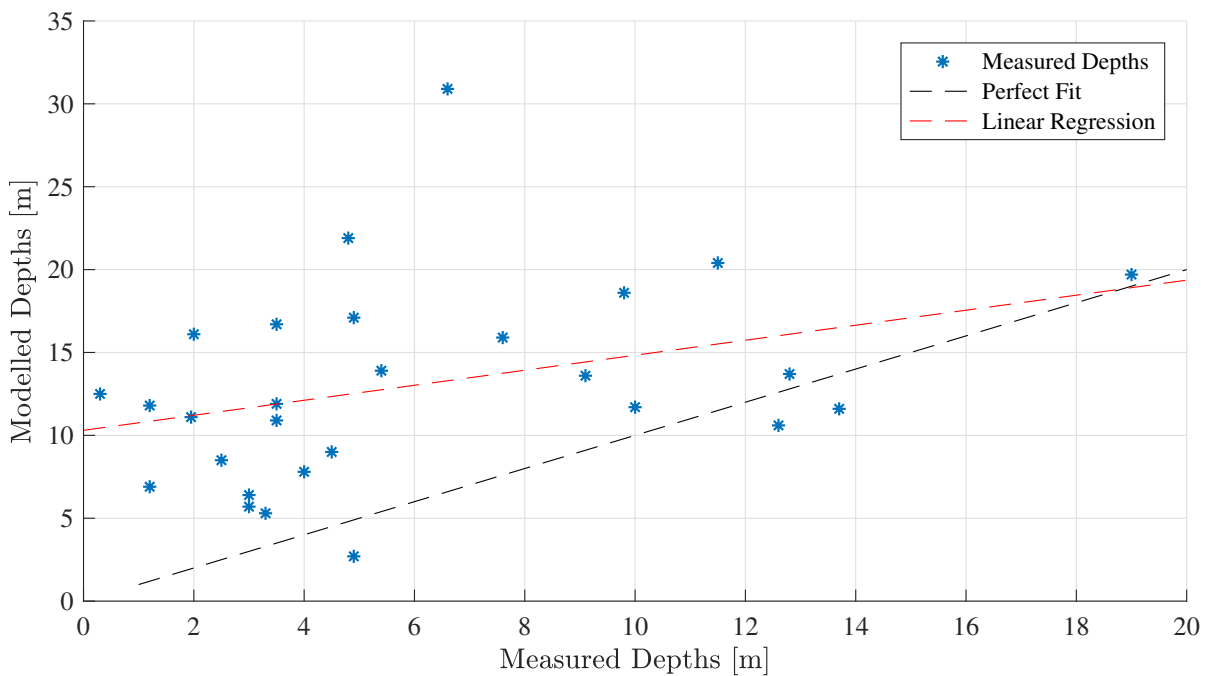
Figure 6.8: Visualisation of modelled and measured depths. Black dashed line represent the perfect fit, while the red line represents the linear regression of the data points.

7

KEY FINDINGS

This chapter represents the final step of the current research and it aims to describe and critically comment the results obtained by the various implemented simulations. Europa's most outer layer is thought to be formed by a global liquid water ocean, covered by a frozen ice crust. This extremely cold and brittle layer of Europa, together with the entire solid body, are assumed to be continuously deformed by tidal effects. These are acting both at diurnal and secular time scales. In the current research, only tidal stress due to non-zero eccentricity, non-zero obliquity and non-synchronous rotation have been included as deforming sources. One of the most efficient ways of representing the tidal stress on Europa is to derive it from the tidal potential via normal mode theory. This mathematical procedure is not included in the current document but the outcomes of the application is taken as key element. This is the analytical formulation of the stress tensor for every point on the surface of the moon. Calculating the tensor and assuming a pure elastic layer for the ice crust, it is possible to apply fracture mechanics tools in order to better understand the behaviour of the lineament crack features observed on the surface of the moon. In particular, the fracture mechanics branch that can be used for a pure elastic material is the LEFM, which was firstly developed from the analysis of racking specimens inside laboratories. Nevertheless, the success of this numerical technique allowed its application to the fractures observed in the large ice sheets on Earth. The current research aims to apply a terrestrial model for understanding vertical propagation of crevasses on ice, to the features observed on Europa.

Part I includes the state of the art for the general description of the Europa environment. Both the components that are forming the tidal stress and the geological implication from the surface observations are addressed in the first part of the document. On the other hand, Part II showed the key mathematical methods that are needed in the completion of the research aim. Tidal potential theory and the calculation of the tidal stress status belongs to this part, as well as a complete and detailed description of LEFM techniques, from its first formulation to the more recent application to Earth science. Chapter 6 included the key technical section of the document, presenting the mathematical and numerical framework of the model that is the most important outcome of the current research. The model, already described in all its parts, can be schematically visualised in Figure 6.1, where the different blocks are represented in different colours. The blue boxes are the input files that are necessary when one wants to describe the physics of the background environment on Europa. Additionally, the parameters and the geometry of the specimen case needs to be added in the routine in order to correctly describe the configuration of the LEFM model. After the entire set of input parameters are set, it is possible to run the LEFM-based routine. These are marked as the red boxes and distinguished between vertical and horizontal propagation. The two different types of routines are investigating two different aspects of crevasse propagation. The first, being the analysis in the vertical dimension, aims to find the critical depths and the critical heights for surface and bottom fractures, respectively. Furthermore, the same routine can be applied to the entire map of the the moon, using the most tensile principal stress as opening source, and to specific lineaments, by rotating the stress tensor the local orientation of the fracture. These two analysis an give two different view of the same problem. If the global approach can distinguish between

areas on the moon that are constantly subjected to a potential propagation, the localised view aims to determine the actual critical depth (or height) reached by a specific crevasse. On the other hand, the horizontal propagation analysis has the main purpose of detecting the horizontal propagation rates. This is possible by using simple time derivations in the formulation of the LEFM routines. In particular, the numerical calculation of vertical depths has been validated with data coming from experimental field works for crevasses in Iceland. Crevasses' depths and strain rate at the flanks of the fractures are used as validating information. The data coming from the field work of Mottram and Benn [60] has been the only recorded attempt of the kind. The dangerousness and the hard accessibility of the locations where crevasses are observed, apparently discouraged campaigns aimed to measure crevasses' depths.

The usage of the most tensile principal stress as opening source identifies the actual stress status of the location. If this analysis is applied to the entire surface of the moon, the purpose is to show whether or not some areas are critically showing a notable value in depth. If any area shows a positive value for the depth, it means that the location is particularly prone to initiate crevasse propagation. On the other hand, a location that is not showing propagation after a short number of orbital cycles, is potentially less favourable to host short term propagating crevasses. Of course, the usage of the principal stress, oriented as the eigenvectors of the stress tensor does not take into account the local geometry of specific cracks which can be oriented in a way that is more suitable to facilitate the propagation. This aspect of the local geometry of existing crevasses is considered in the so called local approach, which aims to describe the crevasse by a discretisation technique. Indeed, the observed crevasse is represented by a set of N nodes and $N-1$ segments. This description of the feature allows the implementation of the LEFM along the crevasse itself, in order to determine whether or not this might show potential areas of the crack which is subjected to higher values of depth than other. On of the first consideration that emerge from the local approach, is when surface crevasses, shaped along an observing rift, can eventually crack the entire layer, reaching the bottom of the crust. This analysis has been implemented already several times in the literature of Europa [52, 113], although nothing has been produced for the depth of the actual crevasses, only the general application of the LEFM for coupled bottom and surface crevasses was investigated. The current research and in particular the current chapter aims to deal with this lack of knowledge and will put the outcomes in the right critical environment in the literature. After a vertical propagation scenario is presented, the further re-elaboration of the geometry and of the LEFM routines allows the analysis the potential horizontal propagation rate for the same crevasses shaped in the local approach.

On a large scale, the implications of vertical and horizontal propagation can generate a strong interest when seen in the contest of future exploration of the moon. NASA's *Europa Clipper* and ESA's *JUICE* are planned to reach the Jovian environment in the late 2020's. The two proposed spacecrafts are planned to orbit the moon several times and the instruments onboard will produce a complete set of observations that can substantially improve the understanding of the surface and of the curious lineaments, among other scopes. Numerical models could help the preliminary identification of areas that are more interesting to survey. For instance, the current global view of the critical depths shows that some areas are more prone to present propagation than other. In this optic, the outcomes of the model can help the selection of the more intriguing target areas. Even more interesting, is the case of the potential *Europa Clipper* lander, proposed by a JPL research group of scientists and engineers [61]. In this case, the target landing area will be specified after some measurements of the orbiter itself, but a general idea of the more valuable landing, is very helpful in the primary design of the missions. The implications of the current research are better presented at the end of the following sections.

As it has been possible to deduce from the previous chapters, the numerical code built for the current project, can generate insights in the vertical and horizontal propagation of Europa crevasses. This chapter aims to describe the most important results that have been found, via the application of LEFM routines. The chapter is divided into two sections that describe vertical and horizontal propagation results, respectively. A large part of the sections is taken by a complete critical discussion. This tries to draw parallels between studies already done and the past literature in order to put the obtained results in the correct critical contest. Vertical propagation in both global and local views is presented in section 7.1, while the results of the horizontal propagation are presented in section 7.2. The numerical simulations are run for a relative short period of time (a few orbital cycles) in order to investigates propagation of crevasses for diurnal cases. The reason can be appreciate when comparing with the timeline of the mentioned future exploration missions such as *Europa Clipper*'s lander that will be able to survive the deadly Jovian environment for 15-20 days maximum. Knowing that the lineaments on Europa are growing at timescales comparable to the lander's lifetime develops very interesting and promising scenarios for the outcomes of the mission. After this sections, the conclusive chapter aims to summarise the most important findings of the project and to set the scheme

(a)   (b)
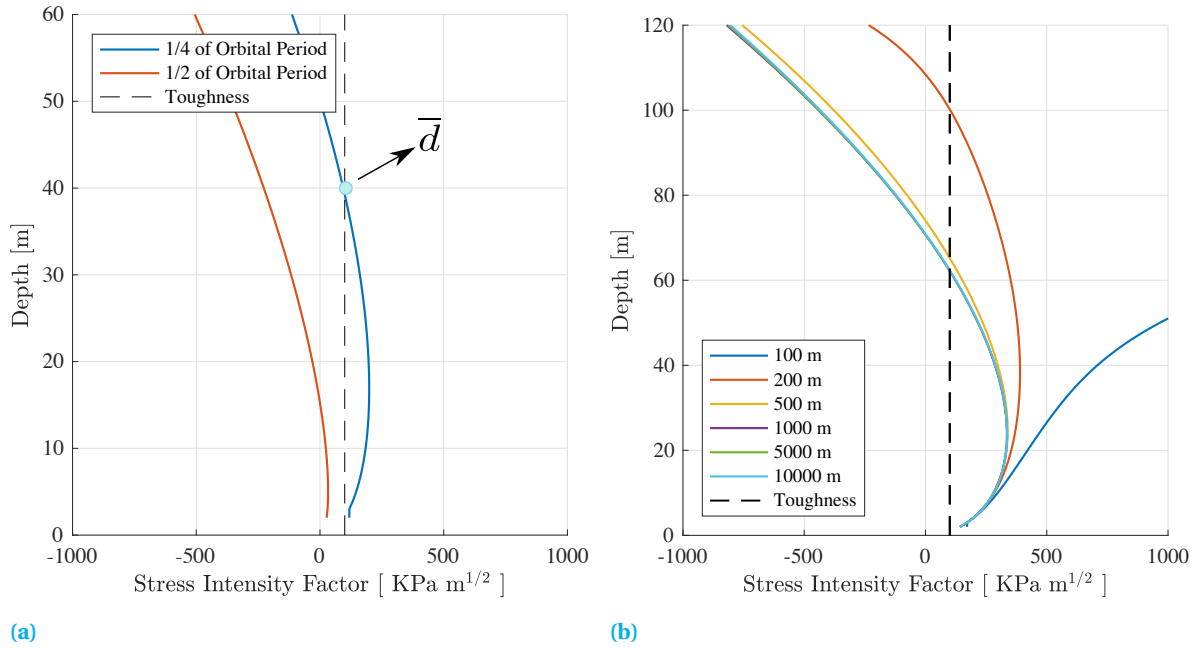
Figure 7.1: The two images represent the results of the stress intensity factor calculation for a specific location on the surface of Europa (in particular, the Pywill crater at longitude 90°E and latitude 15°S). Given the stress of non-zero eccentricity and obliquity coupled with NSR and together with overburden pressure, the curve of the stress intensity factor K_I with respect to the critical depth can be plotted. Figure (a) represents two K_I curves at two different orbital position of Europa. The blue curve at one quarter and the orange at half of the orbital period. The toughness threshold is reached only for the blue curve at around 40 m critical depth. Figure (b) represents the sensitivity of the stress intensity factor with respect to the ice thickness (different colours in the legend). At the same location of Figure (a) and at a fixed orbital position, for very shallow ice crust (lower than 150 m), the K_I is always higher than the toughness, meaning that the crack fractures the entire layer. For crusts thicker than 1 km, the sensitivity of the curve to the thickness itself is negligible. More details in the text.

for potential future works together with confronting the results obtained in the adequate literature contest.

7.1. VERTICAL PROPAGATION

This section represents the outcomes of the simulations that deal with the vertical propagation of crevasses. The routines that aim to find vertical depth for the crevasses are described in section 6.1.2. The current chapter is divided into two big sections that have the purpose of describing the two approaches used to investigate the vertical propagation: namely global and local view. Both the numerical models have as key routine the LEFM loop, presented in Algorithm 1 for surface crevasses and in Algorithm 2 for bottom crevasses. For both the cases the global ice layer is set as a 5 km purely elastic material. The characteristics the describe the physics of Europa and the LEFM routines are listed in Table 6.2 and 6.3. In particular, all the parameters that are needed to describe the physics of the ice layer belong to this latter table.

As section 5.2 already addressed in details, the LEFM approach of the current research is with the usage of the stress intensity factor. This element keeps track of the stress status around the tip of the crack together with the geometry of the fracture configuration. For crevasses on Europa, the background stress is formed by the tidal stress tensor of Jara-Orue and Vermeersen [42] and reported in Appendix B. The stress sources that are considered to deform the brittle crust are non zero eccentricity, non zero obliquity and non-synchronous rotation, being the key factors that act on the surface at two different time scales, diurnal and secular. This is better described in chapter 2. The model of Van der Veen [108] for surface crevasses and of Van der Veen [109] (also called VDV model, as abbreviation), expects that the ice overburden pressure, together with the pressure of the water, that entirely fills the bottom crevasses are included in the stress intensity factor analysis. The stress intensity factor for vertical crevasses K_I can be calculated as:

$$K_I = \sigma_I \sqrt{\pi d} F(d) \tag{7.1}$$

where d is the vertical length of the fracture. σ in case of the global approach is the most tensile principal stress σ_I, calculated as eigenvalue of the stress tensor of Jara-Orue and Vermeersen [42] and oriented with the eigenvector' direction. In case of the local approach, the term refers to the normal stress σ_n, rotated from the tensor. In the term σ it is possible to include the three different tidal components, the lithostatic pressure of the ice and the water pressure (for bottom crevasses only). The term $\sqrt{\pi d} F(d)$ describes the geometry adopted, in the case of the vertical propagation of a single notched test specimen the function F is written in Equation 5.28. The visual representations of the surface and bottom crevasses propagation for the VDV model are shown in Figure 5.4a and 5.4b, respectively. The vertical propagation routine of section 6.1.2 and in particular Algorithm 1 and 2 can be basically summarised in the monitoring of the K_I factor variating the depths and the orbital position of Europa (hence the time, hence the tidal stress amount), and in the determination of the reaching of the material toughness threshold K_{ic}. When this is reached, the critical depth $\overline{d}$ can be found from the stress intensity factor. Figure 7.1 shows the preliminary results for the K_I curve at a specific location for the surface crevasses of the moon[1]. In the specific, Figure 7.1a represents the same location at two different orbital positions of Europa, at a quarter (blue line) and at half (orange line) of the orbital period. Ice thickness is fixed at 5 km. It is interesting to notice that only for the first curve, the toughness (dashed line) is reached, with the possibility of finding a critical depth $\overline{d}$ of around 40 meters. The second curve does not touch the toughness vertical line, meaning that no vertical propagation occur. Conclusions extracted from Figure 7.1a is that this location on the moon is more prone to propagate a potential crevasse at one quarter of the orbital period. On the other hand, Figure 7.1b represent the dependance of the model with respect to the ice thickness, whose values range from 100 m to 10 km, as seen in the legend. Two main findings can be drawn by the current figure. First of all, for a very shallow ice crust (smaller than 150 m), the K_I curve is always higher than the toughness, meaning that the fracture reaches the bottom of the ice layer. Increasing the value of the thickness influences the a-dimensional geometry factor F and the results for the critical depth oscillates between 100 and 60 meters. Interesting to notice that after 1 km, the sensitivity of the critical depth with respect to the thickness seems to be negligible. This is due to the behaviour of the function F. As it can be seen in Figure 5.5, for large values of H, and small values of d/H the model assumes the aspect of a semi-infinite layer (dashed line) and the function $F(d)$ becomes 1.12 [100]. Therefore, for a valid description of the Europa's crust, a layer of 5 km is used in the rest of the simulations, value that is present in the literature of the moon several times [5].

7.1.1. GLOBAL VIEW

The adoption of the principal stresses allows the identification of a stress configuration that does not expect shear stress [102]. This is due to the fact that the tensor needs to be diagonalised in order to determine eigenvalues and eigenvectors. Using the principal stress in order to consider them as opening source for the LEFM theory can be considered as a first step in a global application of the code to the figure of Europa. The results of such a simulations produces a global contour map for the surface and for the bottom of the 5 km ice layer of Europa. The short term, or diurnal, time scale stress sources are a non-zero eccentricity of 0.0094 and a rotation axis tilt of 0.5°. These are the stress sources whose effects are seen to oscillate every orbital cycles (around 3.55 days, or 85 hours), because of the variation of the orbital distance between Europa and Jupiter, which varies every orbital cycle. On the other hand, a secular stress is assumed to form a background stress that increases its order of magnitude. It is the already addressed case of the crust's non-synchronous rotation. Nevertheless, depending on the rotation rate (or the rotation period), the effects to the stress can be seen at shorter or longer timescales. The NSR parameters is a key element in the LEFM simulations. Its influence to the stress (and as consequence to the stress intensity factor) is huge. Very fast rates of NSR, or very short rotation periods, increase the stress tensor's magnitude of several orders, leading to extremely large values for critical lengths of bottom and surface crevasses. Beside being very contested in the literature, very fast NSR could produce such trivial solutions for the critical depths. Therefore, for the rest of the simulations the NSR period is fixed at 10^7 years, as listed in Table 6.2. It is interesting to report the sensitivity of the LEFM depths to the rate of NSR. Figure 7.2 shows the dependance of the global critical depths, applied to surface crevasses, to the NSR period T_{ns}. The four plots are referring to a fixed position in time (PeriJove). White lines represent a set of selected target features directly shaped via GIS software. The list of the selected lineaments is reported in Table 3.1. As mentioned, the larger the NSR (smaller T_{ns}), the larger is the order of magnitude of the critical depth, which reaches orders of 4 km for a 0.1 million year rotation period. Slowing down the rotation till values of 100 million years produces depths that are around 60 m shallow. The order of magnitude was

---

[1]In particular, the Pywill crater was arbitrary selected. Its longitude is of 270°W and of latitude 15°S. Reference in Figure 3.2.
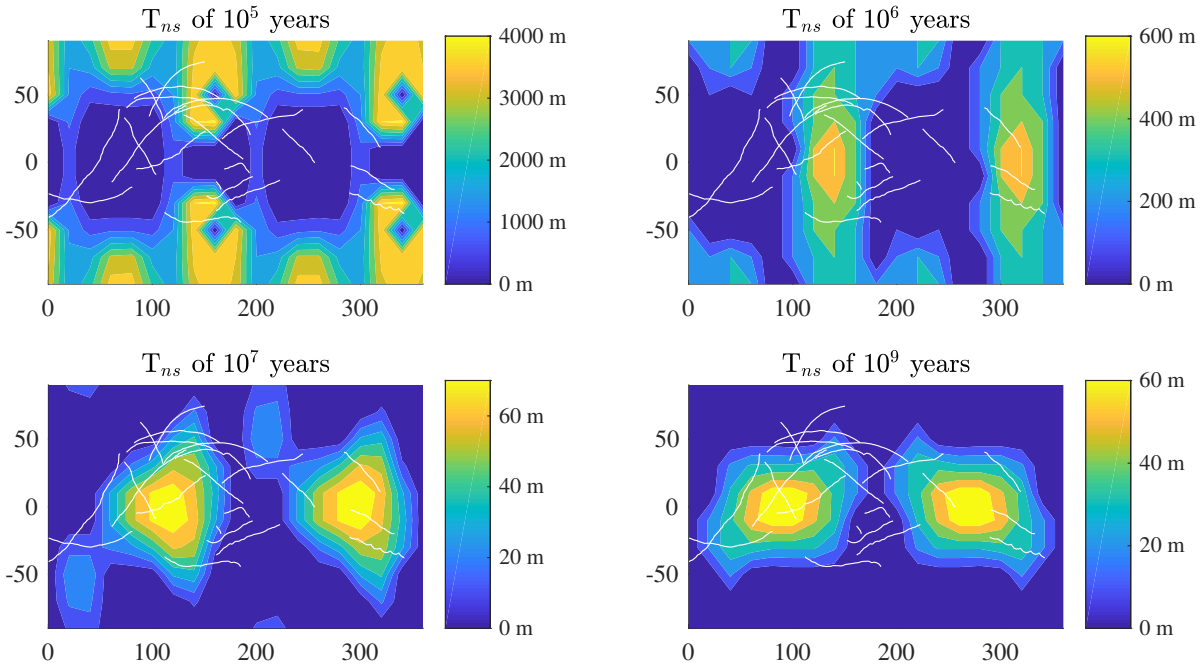
Figure 7.2: Global critical depth sensitivity to the non-synchronous rotation for surface crevasses. The faster the rotation period, the smaller the T_{ns} and the higher the values reached by the critical depths. The four contour maps are referring to a 5 km thick ice layer. The rate of NSR directly influence the stress tensor, which reaches maximum values that are orders of magnitude higher than the 100 KPa established as tensile strength of the material.

reduced of 100 times, which can determine whether or not the fracture propagates through the entire layer. The current research set the NSR period at 10^7 in order to find shallow depths, which are more probable to exist, as emerged in the literature. Nevertheless, the value of NSR, being completely unconstrained (e.g. see Table 2.2) can definitely play a important role in the estimation of crevasses total lengths. For sake of time and simplicity of the routines, some arbitrarily parameters needed to be chosen. Given the form of the tidal stress, NSR produces a constant background stress instead of a variating one, such as the ones generated by the diurnal components. The reason is that the timescales of the current simulations always limited to a few number of cycles. At this scale, NSR effects appears as a constant value throughout the all period. If the simulations were run for a longer time, the total effects of NSR would be a migration of the stress in the rotation direction, since the secular phenomenon expect a slightly faster rotation of the crust with respect to the locked interior [15, 17].

After the sensitivity of the NSR has been addressed and the final value for the rotation period has been chosen, it is possible to present the results for surface and bottom crevasses on Europa, according to the global point of view. Following the routines presented in Algorithm 1 and 2 it is possible to appreciate the contour maps for a full orbital cycle in Figure 7.3 and 7.4, respectively. Similarly to what shown in Figure 7.2, the global critical length of the crevasses, deformed by the most principal stress, are plotted. White lines still represent the target list of Table 3.1. Variating the position of Europa for a complete cycle around Jupiter, from PeriJove to PeriJove, a period of 3.55 days or 85 hours[2] passes and the stress reorient itself from the initial and reference status. The two figures shows the dependance of the critical depth for surface crevasse and of the critical height for the bottom crevasses with respect to the orbital position. Distance between surface and bottom of the ice layer is fixed at 5 km by assumption [5]. Considering the shape of the contour map, it is possible to identify that the two figures have the same aspects and their evolution in the orbital cycle is the same. This is principally due to the fact that the stress is assumed constant through the entire vertical dimension of the ice layer, as already assumed in the VDV model. Indeed the stress acting on the surface is assumed to keep the same value also at the bottom of the layer itself. As consequence, the tidal stress status is the same along the vertical dimension. Nevertheless, the introduction of lithostatic pressure that increase

---

[2]In the rest of the document, the terms orbital cycle, orbital period and Europa day refer to the 85 hours that Europa needs to complete a full revolution around Jupiter.
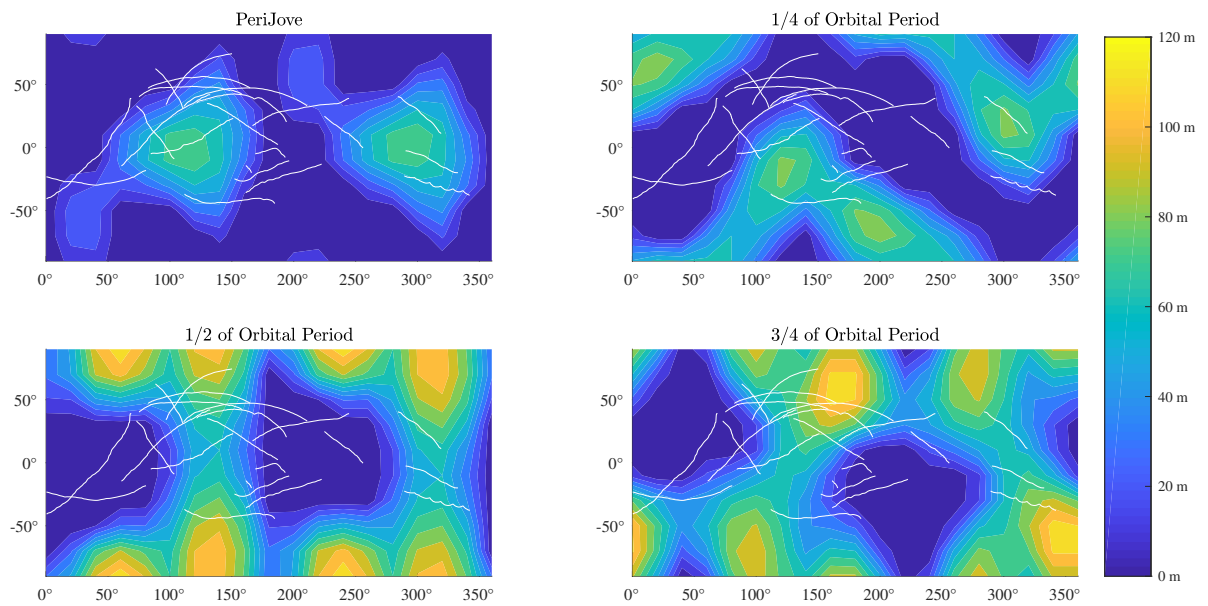
Figure 7.3: Representation of the LEFM results for the global surface of Europa for one orbital cycle. The equilibrium depth reached by every point composing the grid of the moon's surface is plotted. Depths are calculated from the surface of the ice layer. White lines are the lineament features that later on are shaped in the local approach. The opening stress source is the most tensile principal stress oriented as the calculated eigenvectors. It is already possible to appreciate that during one orbital cycle some areas are constantly presenting a positive value for the depth, while other areas are apparently always showing a 'closed' crack.
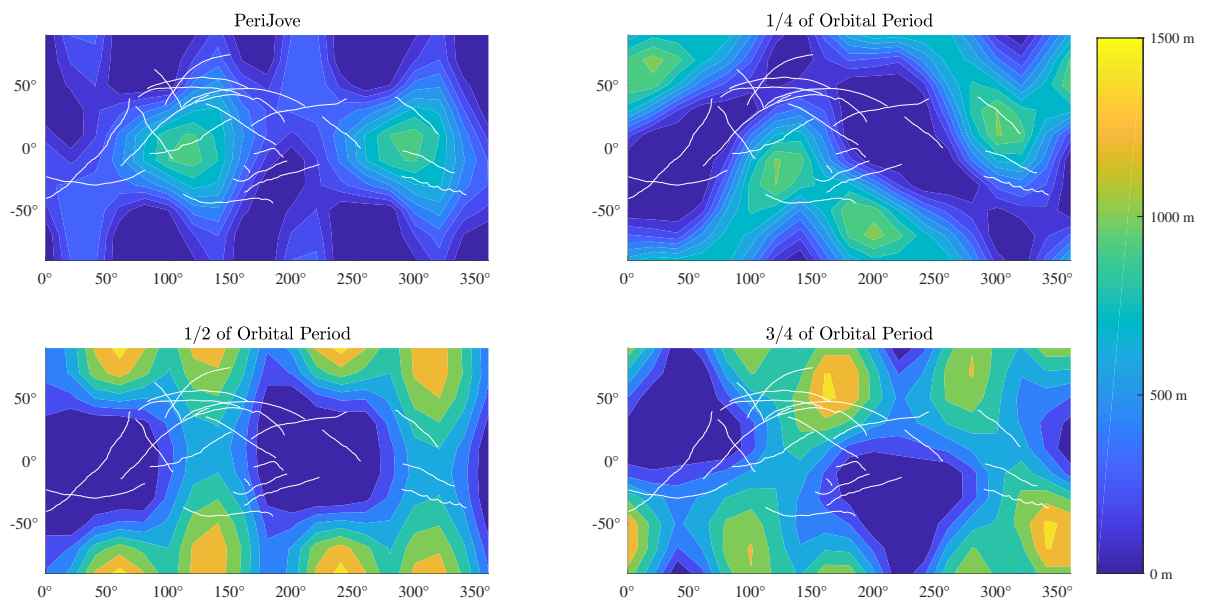
Figure 7.4: Same as Figure 7.3 but for the bottom of the 5 km ice layer. Instead of critical depths, the contour map measures height calculated from the bottom of the ice layer. The magnitude is 10 times higher than the one for the surface of the moon, because of the water that is filling the virtual fracture.

for deeper locations in the ice and of water pressure (for bottom crevasses), influence the values reached by the critical length. In particular, considering bottom crevasses, water is assumed to fill the fractures. As already mentioned in section 5.3, the introduction of water inside the crevasses counteracts the closing effects of the ice overburden pressure. This is the reason why critical heights for bottom crevasses reach magnitudes 10 times larger than the critical depths for the surface crevasses. Critical depths ranges from zero to 120 meters while the critical heights reaches maximum lengths of 1.5 km. Looking at the magnitude of the calculated critical lengths and referring it to the thickness of the ice layer, set at 5 km, no full fracture of the ice crust occurs. Indeed, considering the presence of both surface and bottom crevasses, one of the key questions that can be asked is whether or not these two can potentially meet. A combination of up-bottom and bottom-up propagation can potentially crack the entire layer. This is observed on terrestrial ice sheets and the comparison is interesting. For such thick ice layer, the surface crevasse are definitely shallow, especially if opened in vacuum. Bottom crevasses begins to be very prominent crossing 1/5 of the entire layer and the water pressure plays a key opening role here. The literature provided already with some numerical studies to determine whether or not the crevasses can fracture the entire layer. In particular, Walker [113] improved the analysis of Lee et al. [52], which adopted the LEFM in order to find the maximum propagation depth for surface crevasses in case and in the absence of a global subsurface ocean. Outcomes presented that in case of a global ocean underneath a 1 km thick layer, the fractures reaches values 50% larger than in the absence of the ocean, and these can easily propagate through the entire layer. Nevertheless, the estimations of Lee et al. [52] are contested by the work of Qin et al. [79], which found some inconsistencies in the geometrical representation of the crevasses by LEFM. On the other hand, Walker [113] produced a complete analysis of the penetration depths for different ranges of tensile stress, using the same VDV approach adopted in the current model. Results are defining a range of tensile stress that are needed to potentially fracture the entire ice layer. The aim of the current research is substantially different from the past works of Lee et al. [52] and Walker [113]. If these are studying the propagation depths in order to determine if the surface of the moon is in contact with the subsurface ocean, the built numerical model aims to investigate the propagation process itself, aiming to find areas of the moon that are more prone to host propagation of crevasses. Additionally, the objectives of former LEFM works for Europa are modelled in a very general approach, selecting a range of stresses that the literature provided and choosing a virtual target as location of the simulation. The current research puts the LEFM routine into perspective of the observed map of Europa. This approach is better explained in the next section and in section 7.2.

As it can be seen already from Figure 7.3 and 7.4, some areas of the moon are constantly showing a zero depth for the entire Europa day. On the other hand, for some other areas, the LEFM expects that the critical depth (or height), is constantly showing a value different than zero. Hence, the latter are called critical areas and the former non-critical areas. It is possible to visualise critical and non-critical areas by running the routines for several cycles and by averaging the obtained contour map in time. A global critical map for surface crevasses averaged over 5 orbital cycles is reported in Figure 7.5. Beside showing that the maximum average depth is of around 70 m, the critical and non-critical areas can be seen. The blue zones at the equator with central longitude of 30°E and 220°E are the non-critical areas, showing an average zero value for the critical depth. Alternatively, equatorial regions of longitude 110°E and 310°E generates average depths of 60-70 m. Critical areas imply that some zones to host vertical propagation. Beside the value found as average depth, this is the most important element to extract from the contour map. The possibility of determine whether or not an area is more prone to present propagation of feature is fundamental in the preliminary design of a potential lander in the future explorative missions of Europa. NASA's *Europa Clipper* is already defining the idea of hosting a lander which would be ejected from the spacecraft toward the more interesting zone on the surface [61]. The zones of interest could be selected after several flybys producing better images of the superficial features. According to the preliminary thoughts of the design team of scientists and engineers, a lander's payload could be potentially composed by a seismometer, among other instruments. Fractures that have spatial dimensions of thousand of kilometers (Table 3.1) would produce seismic signals that are orders of magnitudes higher than the ones detected on Earth. The positioning of a seismometer on areas that are more subjected to produce fracture propagation would allow a better recording, hence understanding, of the dynamic phenomena of the moon. in this sense, the current research and in particular the implications of Figure 7.5 can orient the landing site selection already.

Although the parameters that govern the LEFM routines and the physics of Europa were selected from the most recent and updated literature on the Jovian moon, the possibility of large diversity in the actual parameters needs to be taken into account. The limitations of the model introduced with the preliminary description of the numerical routines in chapter 6 are always considered. Additionally to the orbital parameters, the un-
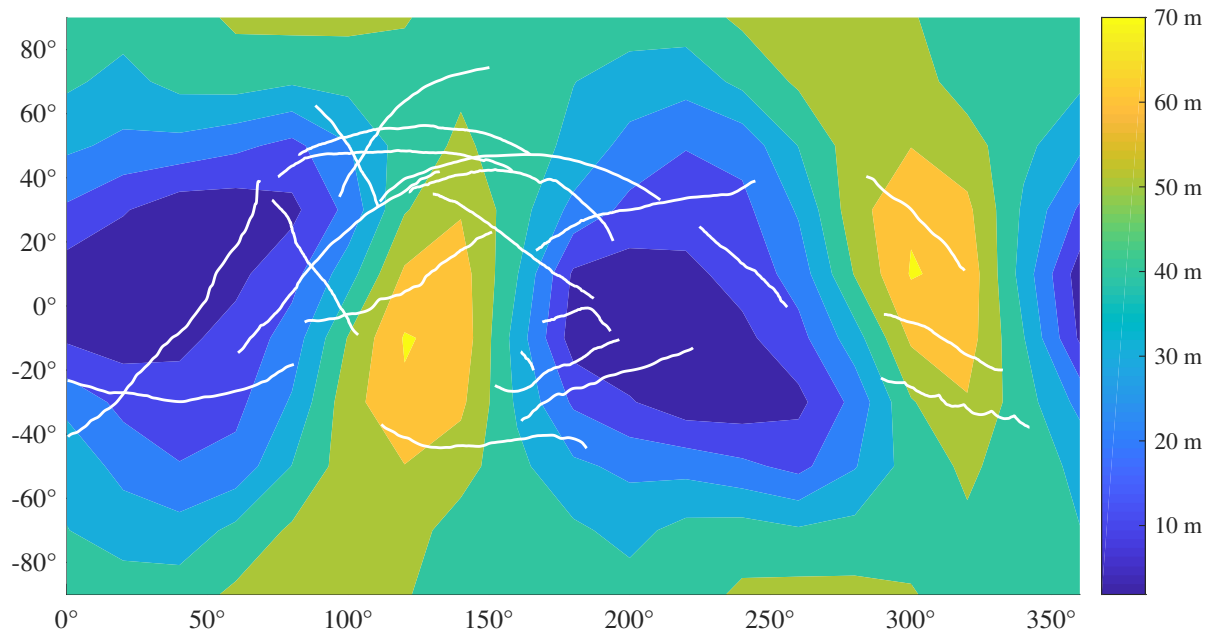
Figure 7.5: Global critical depths for the surface of the moon, averaged over 5 orbital cycles. White lines are the lineament features shaped along the local position of the crevasse. As it emerges from the figure, areas at the equator with a longitude central value of around 120° and 310° are more prone to observe a positive depth. On the other hand, longitudes of 25° and 220° seem to not be affected by interesting depth values. Critical and non-critical areas could potentially help the selection of target landing sites for the lander onboard of the *Europa Clipper* spacecraft.

known in the material properties of the ice investigated are a further element of uncertainties. In the current research, the ice is considered to be purely elastic with a density that follows a depth-profile. In reality, radar penetrating techniques allowed the identification of the Europa ice as a very porous material [7, 8, 52] which can be translated into a weaker status of the ice hence a crack grows easier.

7.1.2. Local View

The last section described the results obtained for the global approach to the calculation of the critical depths for surface crevasses and of critical heights for bottom crevasses. The global approach allowed the identification of critical and non-critical areas. In other words, the simulations allowed the emerging of some zones of the moon that are more favourable to host propagation events. Nevertheless, it is not possible to appreciate local depths of observed crevasses. The assumption of the most tensile principal stress as opening source does not consider the local geometry of the lineaments, given the framework of the routine. The principal stress evaluation allows the representation of the stress status in form of simple tension and/or compression, avoiding the arising of shear stress. The tensor is rotated of an angle that is calculated with the eigenvector orientation. The implications of global critical areas have been discussed in combination with the possible influence that they might have in the elaboration of a landing site for the future *Europa Clipper* lander.

Differently to what happened for the global approach, the current section aims to describe the application of the LEFM to observed crevasses in a localised view. It has been already addressed how the usage of a GIS software allowed the discretisation of continuous lineaments on the surface. In particular, Figure 6.3 shows that the lineament is discretised in form of nodes and segments. The rotation angle α that can be calculated with the introduction of spherical triangles (Equation 6.5 to 6.9) is used to rotate the stress tensor, firstly expressed by latitudinal and longitudinal components. Knowing the actual intensity of the normal stress σ_n that is acting on the crevasse's tip, allows the calculation of the critical depth of the crevasse itself. The normal stress σ_n can be substituted to the most principal stress σ_I in Equation 7.1. With this element taken into account, Algorithm 1 and 2 can be run for localised depths and heights. For bottom crevasses, it is assumed that a fracture has the same aspect (in terms of nodes and segments) of the one observed on the crust directly above. This is a very limiting assumption introduced to show consistency between the two simulations and in order to determine whether or not the two fractures eventually meet each other. In reality, it is naturally
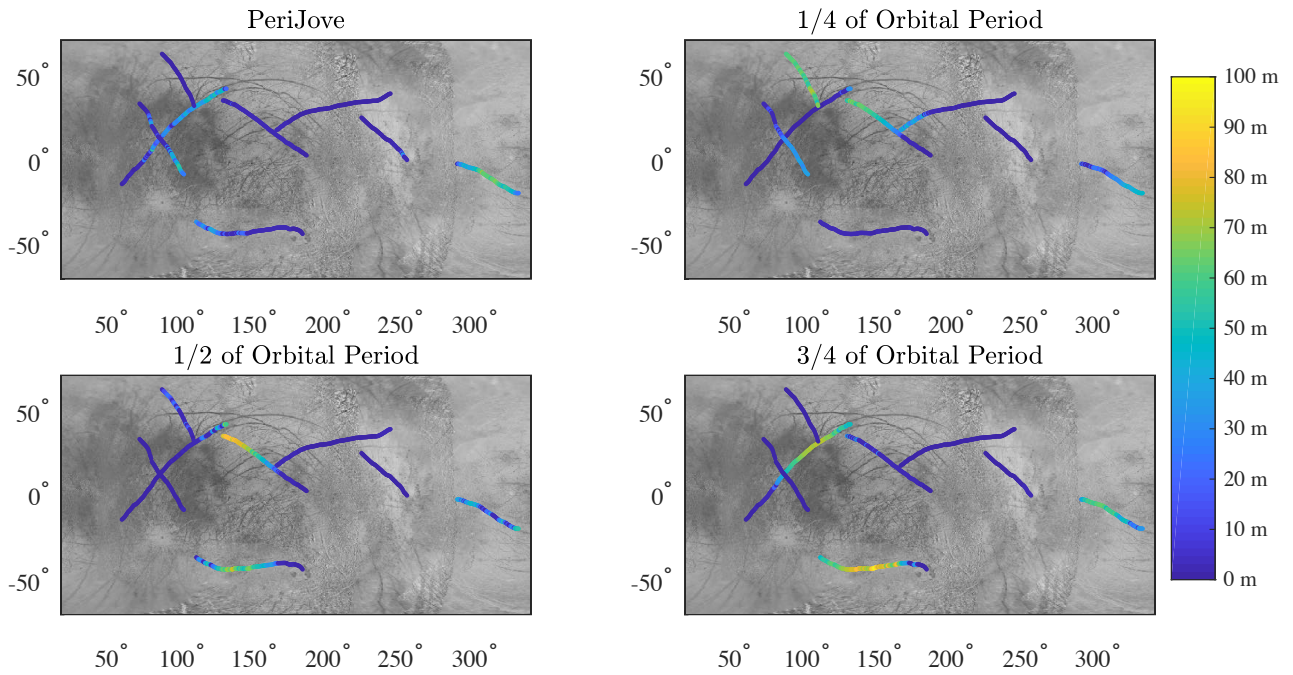
Figure 7.6: Results of the local application of the LEFM to specific surface crevasses. The depth value calculated with the routines is directly plotted along the shaped lineament and measured from the surface of the ice layer. A selection of 8 of the most representative lineament features of the list in Table 3.1 are reported. Generally speaking, it is possible to observe already that some features are showing a oscillating depth pattern, while other show a constant zero depth. More details in the text.
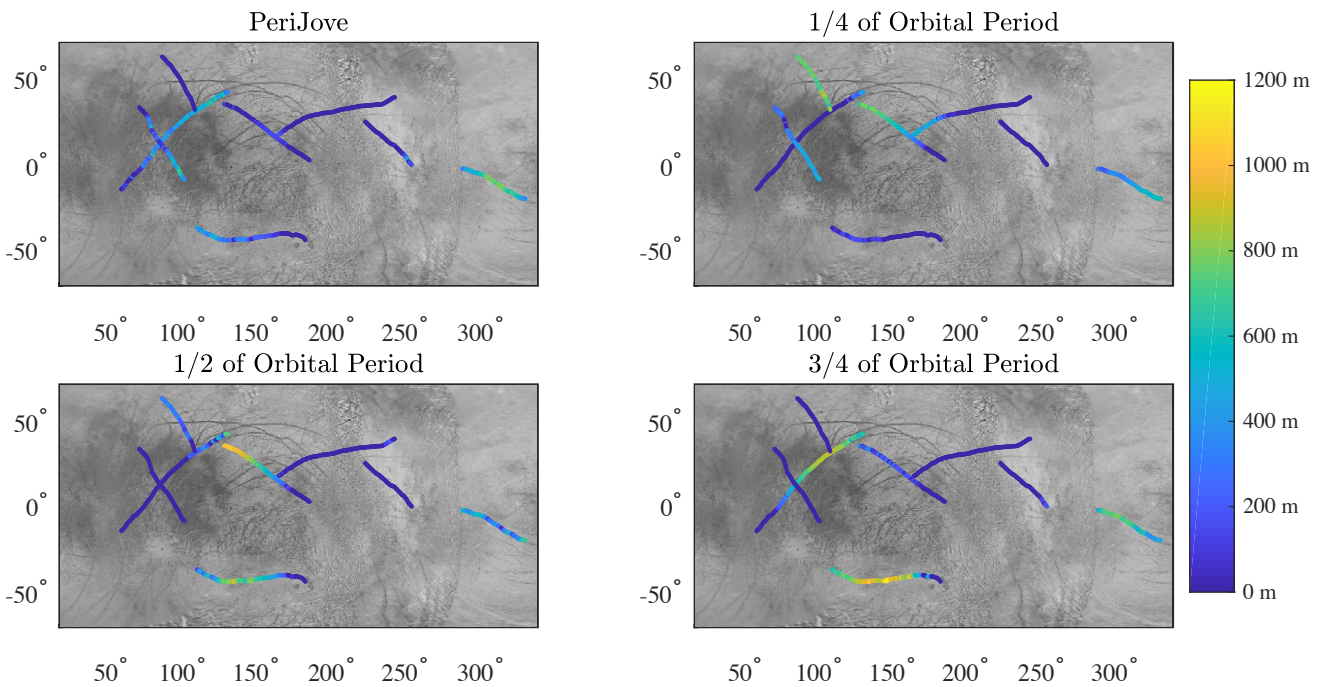
Figure 7.7: Same as Figure 7.6 but for potential crevasses formed at the bottom of the ice layer and directly below observed features. As before, the 8 chosen lineaments represent a selection taken from Table 3.1.

(a)   (b)
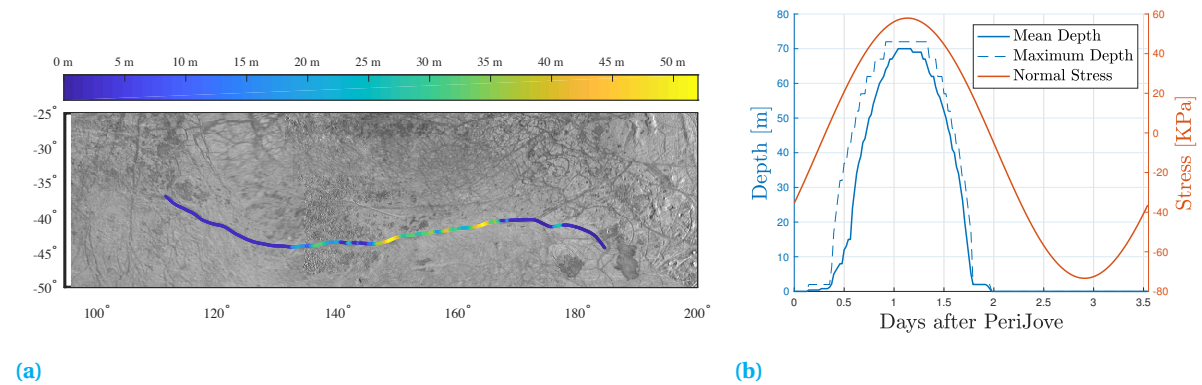
Figure 7.8: The image summarises the local approach of the LEFM to the Agenor Linea in the southern hemisphere of Europa. The loop is applied for the investigation of the surface crevasse propagation. In (a), a zoomed view of the Agenor Linea at half of the orbital period is elaborated from Figure 7.6. On the other hand, in (b) the blue curves represent the mean depth of the feature (solid line) and the maximum depth reached (dashed line), for the entire duration of one Europa day. The orange line represent the average normal stress acting on the crevasse. This oscillate from tension to compression within the cycle.

very hard that a bottom crevasse develops with the exact same aspect of the one above.

Similarly to the global approach results shown in Figure 7.3 and 7.4, the local application of the LEFM to existing surface and bottom crevasses is shown in Figure 7.6 and 7.7, respectively. In the figures, the output of the simulations are plotted directly over the observed lineaments. The background map is a re-elaboration of Figure 3.2 that digitalised images coming from three different exploration missions: *Voyager, Galileo* and *New Horizon*. The features that have been considered as target of the simulations are 8 of the more representative lineaments observed[3]. Already with a quick look at the two figures, one can already see that some of the features are showing a constant zero value for the crack's length. On the contrary, other features seem to present a sort of signal. Lineaments that are 'closed' for specific periods of time, are initiating their propagation at specific orbital position. This is due to the fact that, the feature is remaining in a stand-by status until the background stress re-orients itself in a more favourable configuration. When (if) this occurs, the crack eventually grows. Furthermore, it is possible to appreciate that in some cases, only specific parts of the crevasses are showing a depth variation during the orbital period. This distinction between sections of the same features is interesting when it is coupled with its implication in the history of the crack. Parts of a crevasse that are constantly showing a zero depth signal being observed imply that have been necessary generated in a stress configuration that is different from the one adopted in the current research. Hence, this might imply that the tidal stress that is composed by non-zero eccentricity, non-zero obliquity and NSR could be different at different periods in the history of Europa.

As mentioned, some features are apparently showing a oscillating critical value for the crack's length. It is possible to better appreciate this oscillating behaviour in Figure 7.8a, where the LEFM results are plotted only for the superficial propagation of Agenor Linea, in the southern hemisphere at around half of the orbital period. The inclusion of this zoomed version of Figure 7.6 for Agenor Linea only aims to show the variating critical depth reached by different parts of the features itself. At the same time, the most eastern part and the most western parts are not showing the occurrence of propagation while the central part does. Such curious behaviour could have not been observed by the previous global point of view. The localisation of the routines' application has the precise scope of investigating such oscillating behaviour for the depth. Figure 7.8b aims to represent the analysis of depths and stresses for the case of Agenor. In the graph, two different vertical axis are present. On the left and with the blue line, it is possible to measure depths while on the right the stress is plot with the orange line. Solid lines are referring to mean values for depths and for normal stress. As predictable, the mean normal stress for the lineament is a sinusoid, given the fact that this is the tidal potential (and the tidal stress) is formed by sinusoidal functions. The period is 3.55 days, the value of one orbital cycle, and the status passes from compression (negative stress), through tension (positive stress) till reaching the initial configuration. On the other axis, the mean depth shows the signal that was earlier mentioned several times.

---

[3]In the specific, the simulated lineaments are: Agave, Agenor, Asterius, Drizzlecomb, Euphemos, Harmonia, Rhadamanthys and Tormsdale Lineae. Characteristics of the features are listed in Table 3.1.

The feature seem to activate at around 10 hours after the PeriJove passage. Mean depth reaches values of 70 meters and then de-activate again. A value of zero for the depth means that the toughness is not reached, or a the tip belongs to a compressive status.

The most important outcome of the local application of the LEFM to existing crevasses is the emerging of oscillating signals for the critical length throughout the orbital cycle. Places on Europa are seeing a structural configuration that varies from compression to tension, while other are constantly in a single regime. The implications on the crevasses' depths and heights are that these changes magnitude in very unpredictable ways, given the sometimes strange geometrical configurations of the lineaments themselves. Knowing that some of the features are more 'active' and more prone to host vertical propagation can be a key input in the determination of potential target of the future exploration missions. A next step of the current research would be to produce a complete list of features that present potential activity of propagation.

7.2. Horizontal Propagation

This last section of the chapter deals with the outcomes of the application of LEFM techniques to horizontal propagation of Europa crevasses. So far, the geometry of the numerical analysis has followed the approach of the VDV model for terrestrial crevasses. Vertical propagation of fractures on ice are have been studied and validated by experimental works. The current numerical model has also been validated by fieldwork data (in section 6.2, using measurements of Mottram and Benn [60]). The direct measurement of stresses around the flanks of a crevasse and its depth seem to be a pretty straightforward process but in reality the dangerousness and the difficult accessibility of the locations where ice crevasses are observed definitely poses a serious risk in conducting experimental campaigns. For horizontal propagation, the issue of validating the rate calculation routines is a bit more complicated because of the difficulties in the detection of propagation events. Satellites investigations and a few fieldwork campaigns are the data that can help the understanding of the horizontal propagation. Probably the most interesting instruments that are surveying the surface of the Earth are satellites mounting SAR onboard. Radar and interferometric radar techniques allow the calculation of topography and of mass transport phenomena on Earth. One interesting proposal is to mount a SAR instrument on the payload of the future *Europa Clipper* mission. After multiple passages above the same areas of the moon, it would be possible to detect movement or flows of the icy crust and to record fracture propagations.

In the code, the analysis of horizontal propagation begins with the discretisation of an existing lineament on the surface. The shaping approach is the same of the local approach for vertical propagation but the geometrical representation of the crevasse in terms of the a-dimensional function F needs to be replaced by a new one, for instance the F_2 function of Equation 6.13. Doing so, the dependance to the ice thickness is now null, since the term does not appear in the stress intensity factor anymore. It is important to mention that the application of the LEFM in horizontal direction is only valid when dealing with surface crevasses, the application of the routine to bottom crevasses is not accounted in the current research. The numerical routine for the horizontal propagation is shown in Algorithm 4 and adopt the LEFM formulation of the displacement, coupled with the K_I factor. The time derivation of the displacement (Equation 6.14) and a further mathematical manipulation of the equations allows the identification of the propagation rate as function of stress, stress rate and length of the crack:

$$v(t) = f[\sigma_n(t), \dot{\sigma}_n(t), l(t)] \tag{7.2}$$

which is dependent on the orbital position of Europa with respect to Jupiter, via the temporal parameter t. The dependance of time is also present in the calculation of stress σ, stress rate $\dot{\sigma}_n$ and length l. As it has been presented already in the description of the model, the routine starts with the presence of a small crack on the surface, without which the LEFM is not applicable. This initial crack is represented by the first segment in Figure 6.5b. It is possible to run the LEFM routines for the tip of the second node in order to determine if propagation occurs. When the conditions are favourable to host crack's growth, the propagation rate can be calculated by Equation 7.2. Knowing the rate of growth, and the distance between two nodes, the calculation of the needed time step is straightforward. Applying the same scheme for the entire length of the feature allows the calculation of the total number of cycles that are needed to full develop[4] the lineament. A necessary note is that the shape of the lineament is directly modelled from the map of Figure 3.2 and, as consequence, is referring to the time when the pictures have been taken. An open argument of discussion

---

[4]The term development or completion is preferred to the term generation because of the latter is referred to a crack that is produced and initiated directly on a intact structure. Differently, the term development would suppose a crack that already exists.

(a)   **(b)**
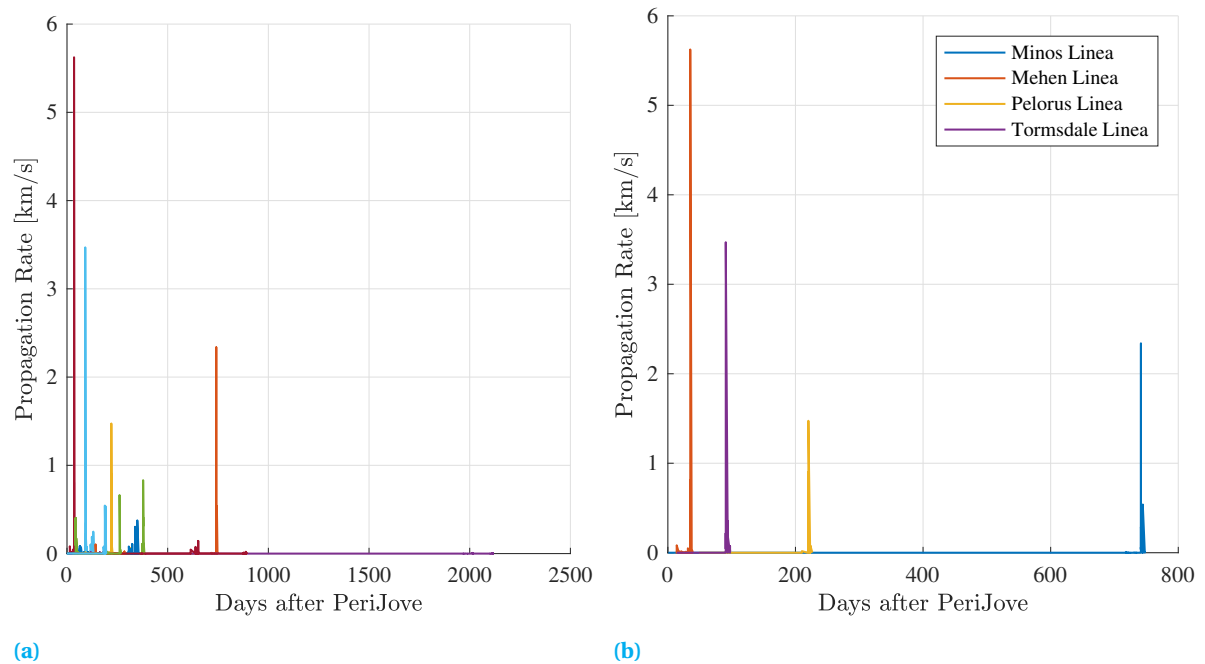
Figure 7.9: Representation of the simulations' results for the horizontal propagation rates of the features listed in Table 3.1, with respect to time after the reference PeriJove passage. (a) shows the 22 features in the same graph, while (b) presents a zoomed version for a restricted number of lineaments.

about Europa geology, is the appropriate consideration of the dynamical history of the moon in the contest. The determination of the age of the lineaments observed on Europa is one of the most difficult study that can be implemented, given the limited amount of observational data. The same features can be formed in completely different scenarios but in the current project, these are modelled as a single crevasse that is propagating in a precise and fixed direction. Additionally, sources of stress that are different from the tidal effects investigating here, can be the key perturbing elements that potentially trigger the crack's propagation. Past studies suggested the possibility of cryovolcanism whose extremely high pressurised vapors can also influence the fracture mechanics of the ice. Impacts of external bodies on the crust can be also accounted. Nevertheless, these considerations go beyond the scopes of the current research and the features are assumed to be propagating eastward.

The plot of the propagation rate with respect to the time from the reference PeriJove passage for the entire list of Table 3.1 is shown in Figure 7.9a, while a zoomed version of the same graph for four selected targets is reported in Figure 7.9b. The four lineaments have been chosen because they show the most interesting behaviour in terms of propagation. Probably the most important outcome of the simulations is that crevasses are growing through a set of propagation events, followed by standby periods. If the conditions are favourable and the toughness is reached, the crack grows experiencing almost instantaneous fracturing events. The adjective instantaneous can be used since the order of magnitude reached by the propagation event peaks is of kilometers per second. On Earth, such instantaneous events are seen in the propagation of ice sheets' crevasses, especially when these are observed at the extreme portions of glaciers. Example is the notorious Larsen C break in July 2017. A potential future application of the current model would be the adoption of data available for terrestrial crevasses (such as for the Larsen C) in order to study the same behaviour on Earth. At these extremely high rates and accounting the dimension of the lineaments observed on the surface of the moon, the fractures can be fully developed after a relatively short number of orbital cycles, as it can be seen from the temporal horizontal axis of Figure 7.9 (one Europa cycle is 3.55 days). In other words, the relatively short period of time needed for the full development is composed by periods of standby for the fracture. Anyhow, the conditions for the stress and for the length of the crack are continuously changing until the material threshold is reached and the fracture can eventually grow. A particular note concerning the length of the fracture needs to be recalled. The length of the fracture is one of the more influent elements in the evaluation of stress intensity factor. Large crack are more prone to continue the propagation respect to smaller ones. Therefore, a correct value for the term l needs to be taken into account. For this purpose, a specific routine
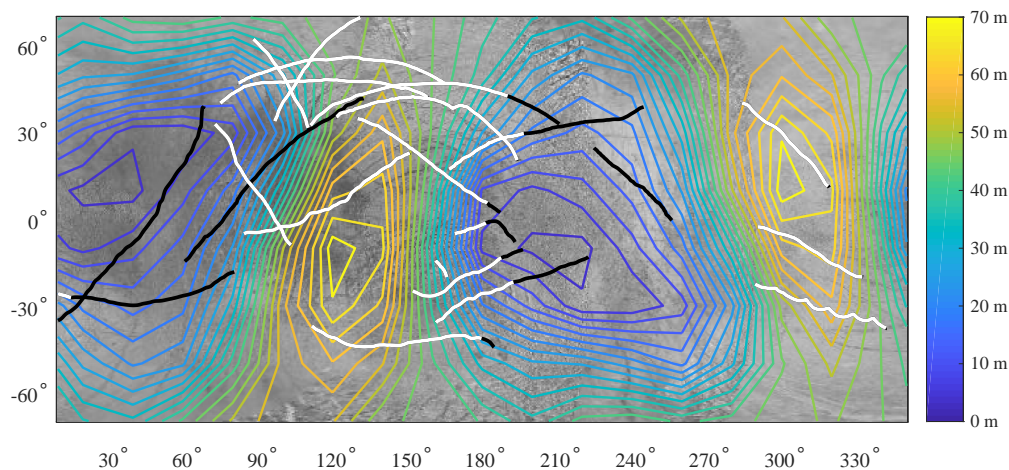
Figure 7.10: Representation of the completion of the features shape. White lines represent part of the lineaments that are propagated during the total time provided by the simulations. Black lines are the part of the features that are not developed or whose last surveyed node is in standby for at least 20 cycles. As consequence, full white lines are crevasses that are fully developed. Background image is the Europa global map of Figure 3.2, overlapped by a contour map showing the critical and non-critical areas for vertical propagation of Figure 7.5. Non-critical areas seem to trigger the arrest of the horizontal propagation, beside showing a zero average depth for superficial crevasses.

is analysing the stress status at all the nodes that are behind the one where the LEFM is focused. The routine goes back in the already analysed nodes in order to see how far the tensile configuration is observed for the specific time under investigation. As soon as the routine encounters a node that is experimenting compression, the calculation stops and the length of the crack is the sum of the segments under tension. More details in section 6.1.3 which describes the numerical code for horizontal propagation.

Beside all the considerations made so far, the model notices that some features are not experimenting a full development of their aspect. This means that the possibility that some crevasses are reaching areas not showing a favourable configuration for the propagation is accounted by the model in the total time provided by the simulations. Nevertheless, the numerical analysis is run for a maximum number of around 1000 cycles and the reorientation of the secular stress due to NSR is not appreciated at this relatively short timescales, being a constant offset in the stress background. The possibility that the (relatively) slow reorientation introduced by NSR can start to influence the standby tips of cracks after long time steps. In other words, given the timescale of the current routine, it is possible that some features are not showing a full completion of their shaped aspect. These reaches areas that are not prone to host propagation and they standby for a period that is larger than the threshold imposed to the simulation. This limit is set as 20 cycles. Such a relatively small time period is chosen while keeping in mind the possibility of detection via future in situ exploration missions. Features that are in standby for periods shorter than 20 cycles are more probable to be detected by potential lander's instruments (such as a seismometer). In order to present which features are reaching full completion and which are not, Figure 7.10 is reported. Here the shaped lineaments are plotted on the map of the moon in two different colours. Black lines are indicating the the full spatial dimension of the crevasse, as shaped by GIS software. The white lines that overlap the black ones, represent the part of the feature that has propagate in the timescale provided by the numerical routine. As consequence, the remaining black lines indicate line that are not yet developed, or whose last surveyed node was calculated to be in standby for more than 20 cycles. In this definition, for the two full black lines the propagation does not advance from the small assumed crack of the first node. The background image is the global map of Europa of Figure 3.2, which has been overlapped by the contour map of the average critical depth for surface crevasses of Figure 7.5. This contour map has been defined as the plot of the average value for surface critical depth at every point of the moon. Blue areas, where the mean critical depth is null, were defined as non-critical areas while the coloured zones are called critical, having a positive value for the depth that reaches a maximum of 70 meters. the rea-
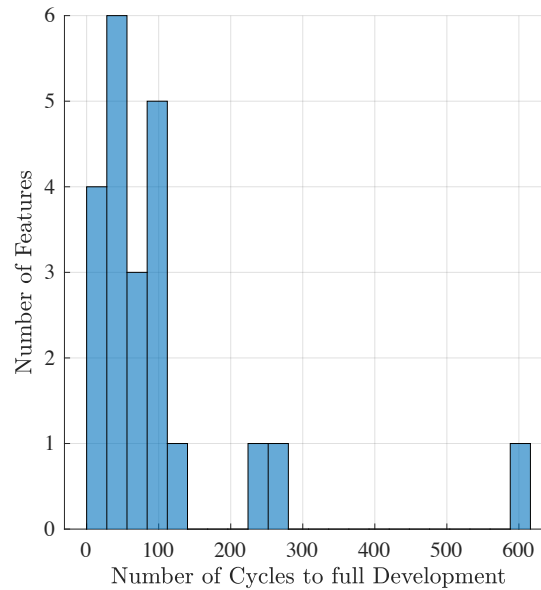
Figure 7.11: Histogram relating the number of features to the amount of orbital cycles needed to develop their shaped aspect. Partial developments are also included in the histogram. Data shown in Table 7.1.

son why the two different types of approach are coupled in the current figure is clear when looking at the locations where the feature's colour is black. Curiously, the non-critical areas seem to trigger the arrest of the horizontal propagation. As already mentioned, a couple of feature whose first node is found inside the non-critical area, the propagation does not even begin. For the majority of the not fully developed crevasses, the arrest node is found at a very advance position in the global dimension of the lineament. As logical deduction, being the length of the crack already at a large spatial dimension, the stress intensity factor should be relatively high. On the contrary, as soon as the crevasses enter the blue zones of Figure 7.5, propagation arrests also for large crevasses. The two approaches seem to reach the same conclusions, the critical and non critical areas can be referred to both horizontal and vertical propagation. The theoretical reason could be found in the fact that both the approaches are calculating stress intensity factor and this is naturally highly sensitive to the stress status, which is the same for the identical location. Apparently, the non-critical areas are subjected to a weak tensile effect, thus the K_I factor rarely reaches the material threshold, meaning that both horizontal and vertical propagation are limited. A further comment that can be done while studying Figure 7.10, is the determination of why features are actually observed even in non critical areas. Instead of saying that non-critical areas arrest the propagation, one can say that something needed to trigger the feature to reach locations that apparently are not prone to host fracture growth, in any direction. Other kind of stress source or geological processes should stimulate the propagating behaviour of crevasses in order to fully complete their shape.

As mentioned previously, knowing the propagation rate for the single nodes and the total length of the crevasse, it is possible to calculate the amount of time needed to complete the feature's shape. If this is divided by the duration of an orbital period, the amount of orbital cycles are needed for the completion. Numerical results are listed in Figure 7.11 where an histogram is showing the number of features that are completed in a specific amount of orbital cycles. The maximum number of cycles needed for a completion of a crevasse is of around 600, meaning around six terrestrial years. Minimum amount of cycles is of 11, around one month and 10 days. Although the number of surveyed features (20 out of 47 total lineaments tabulated by IAU) and despite the fact that it is not possible to implement a valid statistical analysis for such a few cases, the peak of around 50 cycles needed to completion can be visualised already. The order of magnitude of the cycles needed that has been found is a bit larger than the lifetime of the proposed *Europa Clipper*'s lander. The implication would be that the lander could hardly manage to detect a full propagation of a crack. Nevertheless, a large part of the propagation should be easily measured, given the extremely large values reached by crevasse's length and opening width. This last factor is nothing more than displacement term δ calculated by the LEFM in Equation 6.11. According to the numerical model, the opening width reaches values of several

meters, magnitude that is appropriate to a crevasse that can be several thousands of kilometers long.

A tabulated version of the numerical results of the routine is reported in Table 7.1, where the details for every analysed lineament feature have been reported. Together with the further indication of the crevasse' length, the table reports the number of cycles needed, the percentage of completion with respect to the full shape of the crevasse, the maximum opening width, and the maximum and mean horizontal propagation rate. A curious conclusion that can be drawn from the numbers in the table is that the implication that a large crevasse needs to be completed in an high number of cycles is not the current case. The dynamic propagation behaviour of every crevasse is intimately related to the geometry and, more in particular, to the location where the crevasse is found. Example is the Cadmus Linea that needs only 91 cycles to a full completion, even being a large 2993 km crevasse. The difference between the second columns of Table 7.1 and Table 3.1 is due to the fact that for the total features' length the latter are data directly taken from the IAU website while the former is calculated by the current routine. The discrepancies are due to the discretisation process via GIS softwares, that for some cases found difficulties in determining the exact location of the lineament, given the low resolution of some zones of the global map of Europa of Figure 3.2. Despite this, the order of magnitude is satisfied for the majority of the cases. Considering the maximum value reached by the propagation rate, the two features that are experimenting the faster events are also some of the most prominent, generally speaking. The smallest features of the list (Telephassa and Yelland Lineae) also presents some of the relatively slower propagation events. At the same time the opening widths of such crevasses reaches orders of a few meters, while bigger features such as Mehen Linea showing extremely large δ factors. As it can be seen in the fourth column, 9 out of 20 features reaches the full completion, while other 4 are completed at 75% or more. The remaining lineament present percentages of completion lower than around half of the full dimension, accounting the two features that do not start to propagate (Asterius and Drizzlecomp Lineae, for instance the total black lines of Figure 7.10). Finally, the last column of the table reports the average propagation rate which is directly linked to the amplitude of the propagating events. It is important to notice that the mean propagation rate is related to the single fracturing event and not the the ratio between total distance of the completed crack and the total time needed (number of cycles). These two types of values are intrinsically different in magnitude and in concept so it is important to express their different meaning. In particular, comparing the average rate of completion (total length over total time needed), the results are some orders of magnitude lower than the results of Hurford et al. [33], which assumed an estimation for cycloidal growth of around 4.8 km/hr. Average value of the current research is of around 500 m/hr. The last column of Table 7.1 is the mean propagation speed of the different fracturing events that form the crevasse. This value is particularly useful if coupled with the potential seismic signal that these events can generate. This application is not part o the current research but it is a good first step in development of future research. Generally speaking, the crevasses experience a mean propagation rate of meters per second with peaks of 55 m/s for Udaeus Linea and minimum values of around 2 meters per second. On average, these numbers can detected by future exploration mission that would orbit Europa.

Feature Name	Calculated Length [km]	Cycles to Development	Percentage of Completion	Maximum Opening Width [m]	Maximum Propagation rate [km/s]	Mean Propagation rate [m/s]
Agave Linea	1458	101	100%	48.019	0.376	23.143
Agenor Linea	2083	41	93%	42.986	0.084	17.764
Alphesiboea Linea	1817	75	51%	16.776	0.544	18.271
Asterius Linea	2541	-	-	-	-	-
Belus Linea	2041	34	100%	50.897	0.013	3.941
Cadmus Linea	2265	91	100%	33.506	0.062	5.902
Drizzlecomb Linea	1113	-	-	-	-	-
Euphemos Linea	1270	596	100%	32.466	0.008	1.975
Harmonia Linea	2256	129	38%	10.554	0.832	36.528
Hyperenor Linea	2993	63	14%	1.253	0.106	2.519
Mehen Linea	2339	11	100%	64.647	5.624	20.169
Minos Linea	2893	231	79%	26.824	2.337	30.163
Pelorus Linea	1332	84	80%	17.465	1.474	34.575
Phineus Linea	2276	96	18%	2.547	0.663	21.194
Rhadamantys Linea	1871	271	91%	21.773	0.144	5.238
Sparti Linea	1928	16	100%	48.728	0.404	17.400
Telephassa Linea	777	73	52%	1.899	0.017	1.756
Tormsdale Linea	1075	28	100%	26.838	3.47	55.472
Udaeus Linea	2361	39	100%	86.656	0.249	9.049
Yelland Linea	218	84	100%	3.61	0.023	1.841

Table 7.1: List of numerical results obtained for the horizontal propagation approach to the target features of Table 3.1. Note the difference between the second column of the current table and the one of Table 3.1. The latter directly taken from IAU data, the former calculated by the numerical routines of the model. Differences are due to the discretisation process which sometimes found difficulties in the interpretation of correct ending points. The two lineae whose values are labeled as '-' indicate the two features whose propagation do not begin.

8

CONCLUSIONS

Europa is one of the most fascinating planet observed in the Solar System. A global water layer is covering the moon, with an extreme outer frozen crust which is protecting the global ocean from the deadly radiation coming from Jupiter. The combination of these elements defines Europa as an habitable world, meaning that it can potentially host life. Nevertheless, the parameters and the physics that could be useful in categorising the life environment are poorly defined. The lack of observations is not permitting the numerical models to be validate and as consequence, there are completely different point of views regarding how to describe the various physical phenomena on the satellite of Jupiter. ESA and NASA are currently working on the design of future exploration missions with the main target set as Europa. More in the specific, NASA's *Europa Clipper* design team is trying to evaluate the feasibility of mounting a lander onboard of the interplanetary spacecraft. The possibility of having an active lander on the surface, even if for a small period of time, built to detect geological events, such as seismic activity, would be a fundamental improvement in the knowledge of Europa interior and of the effective moon's habitability. Therefore, knowing a priori which areas on the moon are more interesting to survey would be very helpful, in order to avoid the tremendously unfortunate scenario of landing on a region of no interest. The current research aims to preliminary determine which areas of the satellite are more favourable to host crevasse horizontal and vertical propagation. Additionally, the effective possibility of having a connection between the ocean and the outside of the surface, is an important aspect to take into account, given the potential biological material that can be reversed on the surface. Europa's outer surface shows an extremely large number of lineament features that are crossing the entire surface of the moon. These are assumed to be large fractures that, similarly to terrestrial crevasses found on large glaciers in Antarctica or in Greenland, are propagating on thick layers of ice floating on oceans. General aim of the current research is the better understanding of how these crevasses are propagating in order to put the results in the optic of future exploration missions, concerning their ability to detect such geological phenomena. The mathematical framework of the research is the model of C.J. Van Der Veen adopting linear elastic fracture mechanics tools.

The usage of linear elastic fracture mechanics techniques is a very simple but accurate approach to investigate the behaviour of crack propagation for elastic materials. Europa extreme outer layer can be considered to be a purely elastic ice crust, given the extremely low temperatures reached by the frozen surface. As consequence, the application of the fracture mechanics' selected tool is a valid approach with the avoidance of viscosity. The current research aimed to apply a LEFM-based model used to investigate the vertical propagation of terrestrial crevasses in order to determine the critical depth they potentially reach. The approach can be used for both bottom and surface crevasses and the theoretical basics are reported in Van der Veen [108, 109]. The analysis of the propagation environment at the tip of an existing crack is basically composed by different deforming phenomena that are acting on the crack. Opening and closing sources are combined in order to calculate the critical equilibrium length of the fracture. The stressing sources assumed by the current research are the ones calculated via normal mode theory in Jara-Orue and Vermeersen [42], namely: non-zero eccentricity, non-zero obliquity and non synchronous rotation. These are assumed to be the com-

ponents of the tidal stress which are deforming the brittle crust of Europa every orbital cycle. Additionally, a further purpose of the current research is the investigation of potential horizontal propagation events that can trigger the full development of the observed feature.

The current research produced a model based on a methodology derived from experimental works on test specimens. By the monitoring of the configuration status around the tip of an existing crack, it is possible to derive analytical function that describe the fracture behaviour. Being a model induced from the experimental works, it implies some limitations in the validity of its outcomes. First of all, the geometrical configurations adopted are referred to a finite plate, while in reality, the extremely large dimensions of the fracture would require a curvilinear geometry in order to correctly represent the correct shape of the lineaments. Lastly, the thickness of the ice is considered to be a constant 5 km, through the entire crust of the moon although several studies estimated that it is highly possible to have different moon's locations characterised by variating thicknesses.

The results for the application of linear elastic fracture mechanics to Europa crevasses consider both horizontal and vertical propagation. The next bullet list aims to summarise the most important findings found by the numerical analysis produced. Beside the numerical results that have been obtained, the model itself is a very important outcome of the research. Given its modular scheme, the application of physical characteristics of different planets would allow the identification of results also for completely diverse environments. A possible future development of the linear elastic fracture mechanics model is its implementation into larger and more complete ice flow models. This would allow an improvement of the mathematical understanding of complex glaciological problems also on Earth. Summarising, the six different outcomes of the routines allowed a better representation of the Europa crevasses by the usage of linear elastic fracture mechanics techniques.

- Surface crevasses reaches critical depths that reaches values up to 110 meters.

One of the first result of the linear elastic fracture mechanics, is the pure application of the VDV model to vertical crevasse on the surface of the Europa icy crust. The VDV model is a terrestrial numerical analysis implemented as one of the first historical attempts to find a valid calving law. It assumes a purely elastic material and the usage of the stress intensity factor approach. The extremely low temperatures (around 100 K) reached by the surface of Europa are one of the most relevant reasons that drove the selection of linear elastic fracture mechanics techniques for the current investigation of crevasse propagation. By the rotation of the stress tensor (found in Jara-Orue and Vermeersen [42]) to the local shape of single crevasses, the possibility of calculating the actual critical depth was possible. The ice thickness was chosen fixed at the value of 5 kilometers, consistently to the average estimations found in the review paper of Billings and Kattenhorn [5]. The results of the calculations are showing crevasses' critical depths that reaches maximum values of hundreds of meters. Relating this amplitudes with the thickness of the ice crust adopted, the fractures are definitely shallow and not able to reach the bottom of the ice layer, unless this is extremely thin (around 130 meters). The critical depth has been calculated throughout the completion of a full orbital cycle (around 3.55 days) in order to define whether or not a depth signal could be found. 20 lineament features have been investigated and different propagation scenarios have emerged. Specific features are showing an average null critical depth, meaning that are not propagating in the calculation of a full orbital cycle. On the other hand, other types of features are experiencing peculiar behaviours. For the majority of the surveyed crevasses the depth shows a signal of period as the orbital cycle, meaning that the crevasses are stimulate to initiate propagation every orbit of Europa around Jupiter. This would mean that a propagation should occur very often on the surface of Europa, hence its detection with orbiting or in situ instruments have to be very probable. If the outcomes of the current research are viewed with the optic of future exploration missions on the surface of the moon such as NASA's *Europa Clipper* and its potential lander or ESA's *JUICE*, the determination of preliminary estimations of crevasses depths could be a very interesting set of values to validate. As mentioned already, the results of the current simulations are deeply linked to the stress tensor adopted, which is related to the different stress sources considered. Even small variations in orbital parameters or in rheological behaviour of the ice, could largely affect the outcome of the model. In particular, the assumption of the material as purely elastic avoided the issue of representing viscosity, whose non-linearity is one of the major reason why ice is such a difficult material to model. Nevertheless, the extremely low temperatures for the crust of Europa allow the adoption of an elastic material in order to be able to host a linear elastic fracture mechanics analysis. One of the potential future development of the current research is the calculation of potential seismic signals that such fractures might generate. Given the large dimensions of the crevasses, the explosive amount of energy released in such a tiny moon are though to be tremendously high. Working in relation with seismometrical

technology would be a potential key aspect of the current research to further develop, especially if seen with respect to the possibility of the *Europa Clipper* to host a seismometer onboard. This would be the key in the understanding of the lithosphere phenomena on Europa.

- Bottom crevasses reaches critical heights that reaches values up to 1500 meters.

The same discussion presented before can be applied to the analysis of bottom crevasses. In particular, these have been shaped right below the actual observed surface crevasses, by assumption. Considering that the stress at the bottom of the ice layer is the same of the one at the surface, the VDV model was implemented and run. The only difference with the analysis of the surface crevasses is that, in this case, water from the underneath ocean is filling the fractures until the highest portion of the crevasse itself. As noticed in the VDV model, the water presence is deeply influencing the calculation of the crack's length. Indeed, the dimensions of the bottom crevasses are ten times larger than the surface ones, meaning magnitudes of 1500 meters. Although the initiation process of bottom crevasses is completely unknown and could be related to multiple dynamical effects that are potentially happening in the ocean[1], the extremely large amplitude reached by these fractures (around 1/4 of the total thickness) developed from below the crust are interesting phenomena to study and to better understand. For bottom crevasses, the problem of viscosity is even more important than for surface crevasses. Superficial temperature for Europa is estimated to be around 100 K while at the bottom the ice reaches the melting temperature, being in contact with the liquid water layer. As consequence, warmer section of the ice would be hardly modelled by a linear elastic fracture mechanics analysis.

- Consistently to what found in the literature, surface and bottom crevasses combined fracture the entire layer if this is thinner than 1.2 kilometers.

A various number of past works have been published with the main aim of determining whether or not the crust can be fully cracked, implying a connection between the subsurface ocean and the (almost null) atmosphere of Europa. This scenario is particularly interesting if looked in the perspective of the habitability of the water ocean. If organic or biological material is floating in the water layer, the eventuality of this connection with the extreme outer layer of the moon, would imply a probable presence of this material on the surface itself, where is easier to detect and to study. This has been the key motivation of applying calving theory to the Europa lineament features. Also linear elastic fracture mechanics analysis have been already adopted for this scope. It is the case of Lee et al. [52] and Walker [113] whose results are expecting that the ice layer can be fully cracked only if the thickness has dimensions of one kilometer. If this is the case, the existence of bottom crevasses would be a key element in the process, even more than the surface crevasses. The outcomes of the current research, although not precisely focused to this aspect, allowed a further corroboration of the past works. Surface and bottom crevasses are meeting each other only if the ice layer is thinner than around 1.2 kilometers. As already addressed multiple times, the bottom crevasses are reaching orders ten times larger than the surface crevasses, given the opening action of the water from below the crust.

- Specific areas of the crust are more prone to host vertical propagation.

The application of the linear elastic fracture mechanics vertical propagation routine to the global map of the moon, formed by a thin grid of selected locations, allowed the identification of crevasse's length contour maps for the surface and the bottom of the Europa crust. In order to simulate the general stress status at every point of the grid, the assumption of the most tensile principal stress has been adopted. The global critical depth, averaged over 5 orbital cycles, allowed the identification of two different types of area on the moon. The first, called critical areas, is showing an average positive depth while the second, named non critical areas, are experiencing a null depth on average. This means that some zones of the moon are more prone to host vertical propagation for crevasses. The identification of areas that are more subjected to present propagation phenomena can help the potential selection of the more interesting parts of the moon. When future exploration missions would need to strategically design potential landing sites, the results of the current model could present a preliminary investigation in the preliminary selection. Of course, the precise landing site would need a more complete process of identification that more likely will be provided after some flybys of the host spacecraft [61].

---

[1] For example cryovolcanism episodes, proposed several times in the literature about the moon.

- Other areas of the crust seem to lead both horizontal and vertical propagation to arrest.

The numerical analysis that aimed to model the horizontal propagation for crevasses allowed the identification of which features are experiencing a full completion of their aspect, given the final aspect of the lineament, the geometry of the problem and the stress sources taken as perturbing actors. The crevasses are shaped on the actual aspect observed on the global map of the moon, using GIS softwares. The features are extremely large and their dimension has the same order of magnitude of the radius of the moon itself. Beginning with the existence of a small fracture on the surface and accounting for the crack's dimension through the entire surveyed time, it is possible to calculate the propagation rate via a simple time derivation of standard linear elastic fracture mechanics equations. Furthermore, the actual possibility of a fracture to follow the observed shape with a eastward propagation is given. If the results of the horizontal propagation are combined with what was found for critical and non critical areas, a surprising behaviour occurs. Non critical areas which show an average zero depth for surface crevasses apparently arrest also the horizontal propagation of crevasses which enter the zone. Additionally, features whose first nodes are found inside the non critical areas are not even starting to present propagation events. The results of horizontal propagation corroborates what found already for vertical propagation scenarios. Areas of the moon apparently host more favourable conditions to facilitate crack propagation, while others are triggering the crevasses to arrest their growth. Again, these results are particularly interesting when seen in comparison with the potential purposes of the Europa future exploration missions. The cracking of such long and wide crevasses on a tiny moon such as Europa, would produce a tremendous amount of energy released in form of seismic activity. This also because of the extremely cold and fragile configuration of the superficial ice. Seismic activity are one of the most successful tools that can be used to investigate the interior structure of a planet. Knowing already which areas are more prone to present fracture propagation implies that the detection of such events is more probable to be issued in the areas that are more prone to host the phenomena. The current analysis could give preliminary recommendations for the more interesting superficial zones, that can also be considered in the preliminary design of the potential *Europa Clipper*'s lander's sites of analysis.

- Lineament features are formed by series of nearly instantaneous fracturing events.

As already mentioned, the horizontal propagation routine allows the identification of the propagation rate for every node of the discretised crevasse. The calculation methodology is pretty straightforward and can be found via time derivation of standard functions governing linear elastic fracture mechanics routines. As consequence, for every node and segment, the propagation scenario can be derived. One of the key outcome of the routine, is the calculation of the propagation rate's order of magnitude. Results reaches maximum values of kilometers per second, which is the definition of an almost instantaneous event. Something similar is observed while dealing with calving phenomena, such as the recent one of the Larsen C in Antarctica, in July 2017. Future application of the current model would be the application of the routines to terrestrial crevasses. For Europa, such tremendously fast events would imply an enormous amount of released energy, given the observed opening width and the total length of the feature. Knowing the propagation rate and the global dimension of the crevasse, the total time needed for the full completion of the fracture's shape can be calculated. This produced a first order estimation of the potential development scenario for 20 lineaments observed on the surface. Nevertheless, given the large uncertainties in the dynamical and geological history of the moon, these results have to be considered as a example of how much time such crevasses could need to fully develop in a specific and fixed direction. This does not mean that the time found is a precise estimation in the history of the fractures. More likely, the outcome of the research provided an estimation of the time needed to develop. Nevertheless, for the surveyed features the average time to full completion ranges from 10 to 600 orbital cycles (from a month to almost 6 years). *Galileo* surveyed the surface of Europa for 8 years and no apparent movement or crevasse propagation have been detected. Therefore, the claiming of a short completion time has to be seen in this optic. Of course, future and more precise observation of the icy crust will allow a better understanding of the crevasses' dynamics.

Concluding, the current research provided a new numerical representation of crevasses' propagation on the icy surface of Europa. Specific areas of the crust are more prone to host vertical and horizontal propagation, while other zones seem to trigger the arrest of fractures' growth. If surface and bottom crevasses exist at the same time, the ice layer is fully cracked for an extremely thin ice layer. Superficial fractures propagates at rates that can be considered quasi-instantaneous. The outcome of the simulations can be used with the preliminary design of future Europa missions that aim to capture crack growth's events in order to better constrain the physical description one of the more promising satellite of the Solar System, in terms of finding a biosphere.

IV

EXTRA

A

REPRESENTATION OF A FUNCTION

The current extra chapter is based on [9, 12], when not cited differently. It aims to describe the possibility of representing a function via a series of different analytical factors. Before starting the description, some preliminary mathematical tools need to be introduced. For instance, the definition of multiplication between function is a key aspect and it is here presented. The so-called L^2 inner product of two scalar functions $f(t)$ and $g(t)$, on a domain $t = [a, b]$ can be linked to the integral of the multiplications between the two functions. In symbols the inner product can be written as: $< f, g >$. After the L^2 inner product is shown, one can also define the L^2 norm $||f||$ of a scalar function f. The symbolical formulation of the two arithmetical operations is given in the following equations:

$$< f, g >= \int_a^b f(t)g(t)dt \tag{A.1a}$$

$$||f|| = \sqrt{< f, f >} = \sqrt{\int_a^b f^2(t)dt} \tag{A.1b}$$

The L^2 inner product can also be interpreted as a generalisation of the the scalar product between vectors. Pushing this analog for a step further than the simple scalar product between vectors, the concept of orthogonality can be claimed as well. Indeed, two scalar functions are said to be orthogonal if and only if:

$$< f, g >= 0 \tag{A.2}$$

Therefore, a set of N function $e_1(t), e_2(t), ..., e_N(t)$ is an orthogonal set if and only if their mutual L^2 inner products are null, in symbols:

$$< e_i e_j >= \delta_{ij} ||e_i||^2 \quad \forall i, j \in [1, N] \tag{A.3}$$

where δ_{ij} is the Kronecker delta. In the equation, the inner product of two distinct functions is zero while if the product is applied to the same function, the result is the L^2 norm, by definition.

A set of orthogonal function can be found in the so-called Lagrange polynomials. These are simple functions whose mutual L^2 product is always zero. The Lagrange polynomials are an useful set of functions that allows the representation of more complex such as the gravitational potential for example. These functions can be easily calculated with a bunch of algorithm such as the recursive method [12]. The following list gives the reader the first few polynomials of low orders and Figure A.1 represents the plot of the first 6 orders.

$$\begin{cases} P_0(t) = 1 \\ P_1(t) = t \\ P_2(t) = \frac{1}{2}(3t^2 - 1) \\ P_3(t) = \frac{1}{2}(5t^3 - 3t) \\ P_4(t) = \frac{1}{8}(35t^4 - 30t^2 + 3) \end{cases} \tag{A.4}$$
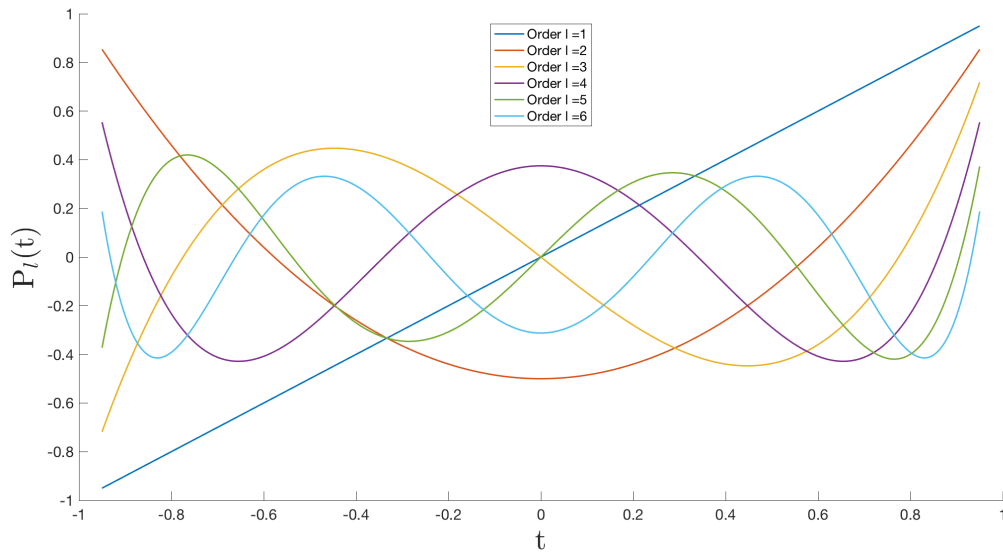
Figure A.1: Representation of the Lagrange polynomials P_l function of a variable t between -1 and 1. The order for the current graph is up to 6. An arbitrary L^2 inner product between each of these functions is null, meaning this set of functions is an orthogonal basis in the domain [-1,1].

It can be easily proved that these functions satisfy Equation A.3. A generalisation of the Legendre polynomials are the so-called associated Legendre functions, whose definition can be found in Equation 4.21. These are particularly useful in the determination of the tidal potential of Equation 4.34. The three different associate Legendre functions $P_{l,m}(\cos\theta)$, where l is the degree and m the order, that are used in the current research can be written as:

$$P_{2,0}(\cos\theta) = \frac{3\cos^2\theta - 1}{2} \tag{A.5a}$$

$$P_{2,1}(\cos\theta) = 3\sin\theta\cos\theta \tag{A.5b}$$

$$P_{2,2}(\cos\theta) = 3\sin^2\theta \tag{A.5c}$$

Among other orthogonal functions, it is important to mention the cosine and sine cases that will be used in the presentation of the Fourier series.

A further analog can be done between vectors and functions is the representation of a vector with an orthogonal basis. Linear algebra's theorems state that an arbitrary vector can be expressed by a linear combination of basis vectors. In particular, an interesting case is when this basis vectors are orthogonal. As a parallel to linear algebra, if a function can be represented as linear combination of some basis functions, the latter are called basis. In other words, every function can be represented by the linear combination of a set of basis function. This lemma is often named as superposition principle.

If one wants to represent a generic function $f(t)$, a possible way is to rewrite it as a linear combination of a set of orthogonal function $e_{1,...N}(t)$. The resulting series of functions can be expressed in symbols:

$$f(t) \approx \sum_{j=1}^{N} \xi_j e_j(t) \tag{A.6}$$

There are several ways to calculate the coefficients ξ_j. A possible attempt would be the assumptions of the ones that minimise the L^2 inner product of the difference between the left and the right member [101]. Differentiation of the equation obtained can be summarised into:

$$\xi_j = \frac{<f, e_j>}{||e_j||^2} \tag{A.7}$$

It is important to mention that there are other forms of writing the coefficients of the series, which are mainly based on different techniques of optimisation. By substituting Equation A.7 into A.6 the function $f(t)$ can be approximated by:

$$f(t) \approx \sum_{j=1}^{N} \frac{<f, e_j>}{||e_j||^2} e_j(t) \tag{A.8}$$

In the equation, the factors ξ_j are nothing more than the projection of the function $f(t)$ on the orthogonal basis. This is a further analog with a N-dimensional vectorial field, whose vector can be geometrically represented by its projection onto an arbitrary basis.

A generalised Fourier series is nothing more than a decomposition of a function as a linear combination of a set of orthogonal function, as it has been explained previously and summarised by Equation A.6. The selection of the coefficients ξ_j defines different types of series. In particular, an orthogonal set of functions is obeying the constraints of having mutual L^2 inner product null (Equation A.2).

An arbitrary function $f(t)$ can be re-written as the series from zero to infinity of some particular and orthogonal functions e_j:

$$f(t) \simeq \sum_{j=1}^{\infty} \xi_j e_j(t) \tag{A.9}$$

Formally speaking, the two members are not an identity and the residuals although depreciable are different than zero [12]. The representation of the function $f(t)$ as series of infinite function is called generalised Fourier series and the terms ξ_j are called generalised Fourier coefficient, while $e_j(t)$ are a set of orthogonal functions (basis). Theoretically, the linear combination can involve an infinite number of functions. Practically, the order is truncated and the Fourier series will involve a finite number of orthogonal functions.

The set of orthogonal function can be arbitrary. One might want to choose the Legendre polynomials for instance. In that case, the functions shown in Equation A.4 are valid as replacement of e_j. Nevertheless, in the classical formulation of the Fourier series the set of orthogonal function is represented by sinusoidal functions. It is important to notice that the selection of the basis is purely driven by the actual case. Sinusoidal functions are just an assumption made in the definition of the classical Fourier expansion.

In the classical formulation of the Fourier series, the orthogonal set is given by the following functions, which are often called Fourier harmonics:

$$\begin{cases} e_0(t) = 1 \\ e_n(t) = \cos n\omega t & \text{where } n = 1, ...\infty \\ e_n(t) = \sin |n|\omega t & \text{where } n = -\infty, ..., -1 \end{cases} \tag{A.10}$$

These functions are defined for a domain $t = [0, T]$, where T is the period of the sinusoidal functions and consequently ω is its angular frequency defined as $\omega = 2\pi/T$. The different values of n, which are all integer numbers lead to the identification of the so-called first, second, third, etc. harmonics, increasing the frequency to 1, 2, 3 or more times the value of ω.

By combining the Fourier harmonics with the decomposition of a general function $f(t)$, valid on a domain $t = 0, ...T$, one might write the following equation:

$$f(t) \simeq A_0 + \sum_{n=1}^{\infty} A_n \cos n\omega t + \sum_{n=1}^{\infty} B_n \sin n\omega t \tag{A.11}$$

where the three terms A_0, A_n, B_n are the Fourier coefficients that constraint the particular case under investigation.

The higher the values reached by n, the higher the accuracy for the description of $f(t)$ as a linear combinations of functions. The infinity value is idealistically meaning that Equation A.11 is an identity. As mentioned before, this case in not possible and the series needs truncation.

The Fourier coefficients can be evaluated with the usage of Equation A.7 and after some simple mathematical manipulations that includes the evaluation of the L^2 inner product for the terms of Equation A.10, the coefficients can be written as:

$$\begin{cases} A_0(t) = \frac{1}{T} \int\limits_0^T f(t)dt \\ A_n(t) = \frac{2}{T} \int\limits_0^T f(t) \cos n\omega t dt \\ B_n(t) = \frac{2}{T} \int\limits_0^T f(t) \sin n\omega t dt \end{cases} \tag{A.12}$$

The results of this sections will be particularly useful when dealing with the representation of the gravitational potential of a planet outside its surface. As it will become clear in the next chapter, the gravitational potential satisfy the Laplace equation whose solutions can be approximated by a set of harmonic functions. The classical Fourier series decomposition will represent the gravitational potential on the surface of the planet, and a particular function that is dependent on the distance from the centre of the planet will allow the extension of the approximation to every place in the space outside the planet. More details in chapter 4.

B

ANALYTICAL FUNCTIONS FOR THE TIDAL STRESS ON EUROPA

In this extra chapter, the equations used as background tidal stress are reported. The next equations are the outcome of the mathematical manipulation of the tidal potential expressed in Equation 4.34 through the usage of normal mode theory. The complete theoretical and practical formulation go beyond the scopes of the current document and it is reported in Jara-Orue and Vermeersen [42] or in Jara-Orue [41]. This part is only aimed to report the analytical functions used as background stress in the numerical routines. Diurnal stress is generated by non-zero eccentricity and non-zero obliquity while secular stress is due to the non-synchronous rotation. The physical characteristics governing the stress are the mean motion n of Equation 4.33 and the various parameters: radius of Europa R, orbital eccentricity e, superficial gravitational attraction g, axial tilt v and argument of pericentre w all listed in Table 6.2 and ice viscosity μ found in Table 2.1. The equations are time dependant via the term t which calculates the orbital position from a reference PeriJove passage, set as $t = 0$. The background stress is referred to spherical geographical coordinates that are longitude φ and colatitude θ. The stress tensor can be build from the identification of the following relations, where only the elastic part of the stress is considered. This is due to the fact that LEFM requires an elastic material in order to be applied. The short term stress tensor, whose timescale is the orbital period of Europa revolution around Jupiter T, is governed by the following relations:

$$\overline{\sigma}_{\theta\theta} = \frac{1}{2} \frac{n^2 R \mu}{g} \frac{1}{\sqrt{1+\Lambda^2}} \Big\{ -6e\beta_{2,0}^{\theta\theta}(\theta)\cos(nt+\arctan(\Lambda)) + e\beta_{2,2}^{\theta\theta}(\theta)\big[4\sin(2\varphi)\sin(nt+\arctan(\Lambda))$$
$$+3\cos(2\varphi)\cos(nt+\arctan(\Lambda))\big] + 4\cos(v)\sin(v)\beta_{2,1}^{\theta\theta}(\theta)\big[\cos(\varphi)\sin(w+nt+\arctan(\Lambda))\big]\Big\} \quad \text{(B.1)}$$

$$\overline{\sigma}_{\varphi\varphi} = \frac{1}{2} \frac{n^2 R \mu}{g} \frac{1}{\sqrt{1+\Lambda^2}} \Big\{ -6e\beta_{2,0}^{\varphi\varphi}(\theta)\cos(nt+\arctan(\Lambda)) + e\beta_{2,2}^{\varphi\varphi}(\theta)\big[4\sin(2\varphi)\sin(nt+\arctan(\Lambda))$$
$$+3\cos(2\varphi)\cos(nt+\arctan(\Lambda))\big] + 4\cos(v)\sin(v)\beta_{2,1}^{\varphi\varphi}(\theta)\big[\cos(\varphi)\sin(w+nt+\arctan(\Lambda))\big]\Big\} \quad \text{(B.2)}$$

$$\overline{\sigma}_{\theta\varphi} = \frac{1}{2} \frac{n^2 R \mu}{g} \frac{1}{\sqrt{1+\Lambda^2}} \Big\{ 2e\beta_{2,2}^{\theta\varphi}(\theta)\big[4\cos(2\varphi)\sin(nt+\arctan(\Lambda)) - 3\sin(2\varphi)\cos(nt+\arctan(\Lambda))\big]$$
$$+4\cos(v)\sin(v)\beta_{2,1}^{\theta\varphi}(\theta)\big[\sin(\varphi)\sin(w+nt+\arctan(\Lambda))\big]\Big\} \quad \text{(B.3)}$$

107

where the factor Λ is related to the Maxwell time τ_M and to the rigidity of the ice shell η as follows:

$$\Lambda = \frac{\mu/\eta}{n} = \frac{T}{2\pi\tau_M} \tag{B.4}$$

This dimensionless factor is related to the actual relaxation state of the diurnal stress on the icy surface of Europa.

Additionally to the diurnal stress of the previous equation, the secular components due to a non-synchronous rotation of period T_{ns}, also expressed in form of frequency $\Omega_{ns} = 2\pi/T_{ns}$, can be written as:

$$\hat{\sigma}_{\theta\theta} = \frac{1}{2}\frac{n^2 R\mu}{g}\frac{1}{\sqrt{1+\Delta^2}}\alpha_{2,2}^{\theta\theta}(\theta)\cos\left(2\varphi + 2\Omega_{ns}t + \arctan(\Delta)\right) \tag{B.5}$$

$$\hat{\sigma}_{\varphi\varphi} = \frac{1}{2}\frac{n^2 R\mu}{g}\frac{1}{\sqrt{1+\Delta^2}}\alpha_{2,2}^{\varphi\varphi}(\theta)\cos\left(2\varphi + 2\Omega_{ns}t + \arctan(\Delta)\right) \tag{B.6}$$

$$\hat{\sigma}_{\theta\varphi} = -\frac{1}{2}\frac{n^2 R\mu}{g}\frac{1}{\sqrt{1+\Delta^2}}\alpha_{2,2}^{\theta\varphi}(\theta)\sin\left(2\varphi + 2\Omega_{ns}t + \arctan(\Delta)\right) \tag{B.7}$$

where the term Δ represents the ratio between Maxwell time and non-synchronous rotation period as follow:

$$\Delta = \frac{\mu/\eta}{2\Omega_{ns}} = \frac{T_{ns}}{4\pi\tau_M} \tag{B.8}$$

In the six equations, the auxiliary functions $\alpha(\theta)$ and $\beta(\theta)$ can be written as:

$$\beta_{2,0}^{\theta\theta}(\theta) = \frac{3}{4}(3\overline{h}^e - 10\overline{l}^e)\cos(2\theta) + \frac{3}{4}(\overline{h}^e - 2\overline{l}^e) \tag{B.9}$$

$$\beta_{2,1}^{\theta\theta}(\theta) = \frac{3}{2}(3\overline{h}^e - 10\overline{l}^e)\sin(2\theta) \tag{B.10}$$

$$\beta_{2,2}^{\theta\theta}(\theta) = -\frac{3}{2}(3\overline{h}^e - 10\overline{l}^e)\cos(2\theta) + \frac{9}{2}(\overline{h}^e - 2\overline{l}^e) \tag{B.11}$$

$$\beta_{2,0}^{\varphi\varphi}(\theta) = \frac{3}{4}(3\overline{h}^e - 8\overline{l}^e)\cos(2\theta) + \frac{3}{4}(\overline{h}^e - 4\overline{l}^e) \tag{B.12}$$

$$\beta_{2,1}^{\varphi\varphi}(\theta) = \frac{3}{2}(3\overline{h}^e - 8\overline{l}^e)\sin(2\theta) \tag{B.13}$$

$$\beta_{2,2}^{\varphi\varphi}(\theta) = -\frac{3}{2}(3\overline{h}^e - 8\overline{l}^e)\cos(2\theta) + \frac{9}{2}(\overline{h}^e - 4\overline{l}^e) \tag{B.14}$$

$$\beta_{2,1}^{\theta\varphi}(\theta) = 3\overline{l}^e\sin(\theta) \tag{B.15}$$

$$\beta_{2,2}^{\theta\varphi}(\theta) = 3\overline{l}^e\cos(\theta) \tag{B.16}$$

$$\alpha_{2,2}^{\theta\theta}(\theta) = -\frac{3}{2}(3\hat{h}^e - 10\hat{l}^e)\cos(2\theta) + \frac{9}{2}(\hat{h}^e - 2\hat{l}^e) \tag{B.17}$$

$$\alpha_{2,2}^{\varphi\varphi}(\theta) = -\frac{3}{2}(3\hat{h}^e - 8\hat{l}^e)\cos(2\theta) + \frac{9}{2}(\hat{h}^e - 4\hat{l}^e) \tag{B.18}$$

$$\alpha_{2,2}^{\theta\varphi}(\theta) = 3\hat{l}^e\cos(\theta) \tag{B.19}$$

where the parameters $\overline{h}^e$, $\overline{l}^e$, $\hat{h}^e$ and $\hat{l}^e$ are the Love numbers for the elastic formulation of the ice crust, calculated via normal mode theory in Jara-Orue and Vermeersen [42]. Their values is reported in Table B.1

The total stress acting on the surface of the moon can be written, via superimposition principle, as sum of Equations B.1 to Equation B.3 with Equations B.5 to Equation B.7 in the following form:

$$\sigma_{\theta\theta} = \overline{\sigma}_{\theta\theta} + \hat{\sigma}_{\theta\theta} \tag{B.20a}$$

$$\sigma_{\varphi\varphi} = \overline{\sigma}_{\varphi\varphi} + \hat{\sigma}_{\varphi\varphi} \tag{B.20b}$$

$$\sigma_{\theta\varphi} = \overline{\sigma}_{\theta\varphi} + \hat{\sigma}_{\theta\varphi} \tag{B.20c}$$

which can be re-written as stress tensor related to longitude and latitude as follows:

$$\underline{\underline{\Sigma}} = \begin{bmatrix} \sigma_{\theta\theta} & \sigma_{\theta\varphi} \\ \sigma_{\varphi\theta} & \sigma_{\varphi\varphi} \end{bmatrix} \tag{B.21}$$

Love Parameter	Value
$\overline{h}^e$	1.15100×10^0
$\overline{l}^e$	3.07996×10^{-1}
$\hat{h}^e$	1.85155×10^0
$\hat{l}^e$	4.95366×10^{-1}

Table B.1: Tabularised values for the Love numbers for the elastic crust of Europa, calculated via normal mode theory from the tidal potential of Jara-Orue and Vermeersen [42].

which is the tensor used in Equation 6.1 and in the remaining of the document. This can also be rotated with respect of the actual geometry of a target crevasse, or derivate with respect to the time parameter t for the calculation of the stress rate. More details in chapter 6.

BIBLIOGRAPHY

[1] J. D. Anderson, G. Schubert, R. A. Jacobson, E. L. Lau, W. B. Moore, and W. L. Sjogren. Europa's differentiated internal structure: Inferences from four galileo encounters. *Science*, 281:2019–2022, 1998.

[2] A. Aydin. Failure modes of the lineaments on jupiter's moon, europa: Implications for the evolution of its icy crust. *Journal of Structural Geology*, 28:2222–2236, 2006.

[3] R.M. Baland, M. Yseboodt, and T. Van Hoolst. Obliquity of the galilean satellites: The influence of a global internal liquid layer. *Icarus*, 220:435–448, 2012.

[4] S. E. Billings and S. A. Kattenhorn. Determination of ice crust thickness from flanking cracks along ridges on europa. In *Lunar Planetary Science Conference XXXIII*, 2002.

[5] S. E. Billings and S. A. Kattenhorn. The great thickness debate: Ice shell thickness models for europa and comparisons with estimates based on flexure at ridges. *Icarus*, 177:397–412, 2005.

[6] B. G. Bills. Free and forced obliquities of the galilean satellites of jupiter. *Icarus*, 175:233–247, 2005.

[7] G. J. Black, D. B. Campbell, and P. D. Nicholson. Icy galilean satellites: Modeling radar reflectivities as a coherent backscatter effect. *Icarus*, 151:167–180, 2001.

[8] G. J. Black, D. B. Campbell, and S. J. Ostro. Icy galilean satellites: 70 cm radar results from arecibo. *Icarus*, 151:160–166, 2001.

[9] M. Bramanti, C. D. Pagani, and S. Salsa. *Matematica: Calcolo Infinitesimale e Algebra Lineare [in Italian]*. Zanichelli, 2004.

[10] J. H. Candice, L. Esposito, A.I.F. Stewart, J. Colwell, A. Hendrix, W. Pryor, D. Shemansky, and R. West. Enceladus' water vapor plume. *Science*, 311:1422–1425, 2006.

[11] M. H. Carr, M. J. S. Belton, C. R. Chapman, A. S. Davies, P. Geissler, R. Greenberg, McEwen A. S., B. R. Tufts, R. Greeley, R. Sullivan, J. W. Head, R. T. Pappalardo, K. P. Klaasen, T. V. Johnson, J. Kaufman, D. Senske, J. Moore, G. Neukum, G. Schubert, J. A. Burns, P. Thomas, and J. Veverka. Evidence for a subsurface ocean on europa. *Nature*, 391:363–365, 1998.

[12] P. Ditmar. Cie4610 mass transport in the earth systems, lecture notes. Technical report, Technical University Delft, 2016.

[13] P. H. Figueredo and R. Greeley. Geological mapping of the northern leading hemisphere of europa from galileo solid-state imaging data. *Journal of Geophysical Research*, 105:22,629–22,646., 2000.

[14] P. Geissler, R. Greenberg, G. V. Hoppa, B. R. Tufts, and M. Milazzo. Rotation of lineaments in europa's southern hemisphere. In *Lunar Planetary Science Conference XXX*, page 1743, 1999.

[15] P. E. Geissler, R. Greenberg, G. Hoppa, P. Helfenstein, A. McEwen, R. Pappalardo, R. Tufts, M. Ockert-Bell, R. Sullivan, R. Greeley, M. J. S. Belton, T. Denk, B. Clark, J. Burns, J. Veverka, and Galileo Imaging Team. Evidence for non-synchronous rotation of europa. *Nature*, 391:368–370, 1998.

[16] R. Greenberg. *Europa, The Ocean Moon, Search for an Alien Biosphere*. Springer, first edition, 2005.

[17] R. Greenberg and S. Weidenschilling. How fast do the galilean satellites spin? *Icarus*, 58:186–196, 1984.

[18] R. Greenberg, P. Geissler, G. Hoppa, B. R. Tufts, D. D. Durda, R. Pappalardo, J. W. Head, R. Greeley, R. Sullivan, and M. H. Carr. Tectonic processes on europa: Tidal stresses, mechanical response, and visible features. *Icarus*, 135:64–78, 1998.

[19] R. Greenberg, P. Geissler, B. R. Tufts, and G. V. Hoppa. Habitability of europa's crust: The role of tidal-tectonic processes. *Journal of Geophysical Research-Planets*, 105:17551–17562, 2000.

[20] R. Greenberg, G. V. Hoppa, P. Geissler, A. Sarid, and B. R. Tufts. The rotation of europa. *Celestial Mechanics and Dynamical Astronomy*, 83:35–47, 2002.

[21] A.A. Griffith. The phenomenon of rupture and flow in solids. *Philosophical Transactions of the Royal Society of London*, 1920.

[22] J. M. Groenleer and S. A. Kattenhorn. Cycloid crack sequences on europa: Relationship to stress history and constraints on growth mechanics based on cusp angles. *Icarus*, 193:158–181, 2008.

[23] P. Helfenstein and E. M. Parmentier. Patterns of fracture and tidal stresses due to nonsynchronous rotation - implications for fracturing on europa. *Icarus*, 61:175–184, 1985.

[24] R. W. Hertzberg. *Deformation and Fracture Mechanics of Engineering Materials*. Wiley, second edition, 1983.

[25] S. A Holmes and W.E. Featherstone. A unified approach to the clenshaw summation and the recursive computation of very high degree and order normalised associated legendre functions. *Journal of Geodesy*, 76:279–299, 2002.

[26] R. L. B. Hooke. *Principles of glacier mechanics*. Cambridge University Press, second edition, 2005.

[27] G. Hoppa, B. R. Tufts, R. Greenberg, and P. Geissler. Strike-slip faults on europa: Global shear patterns driven by tidal stress. *Icarus*, 141:287–298, 1999.

[28] G. V. Hoppa, R. Greenberg, G. Geissler, B. Plassmann, and R. Tufts. Rotation of europa: Constraints from terminator positions. In *Proc. Lunar Planet. Sci. Conf*, volume 28, pages 597–598, 1997.

[29] G. V. Hoppa, B. R. Tufts, R. Greenberg, and P. E. Geissler. Formation of cycloidal features on europa. *Science*, 285:1899–1902, 1999.

[30] G. V. Hoppa, R. Greenberg, B. R. Tufts, C. Geissler, P.and Phillips, and M. Milazzo. Distribution of strike-slip faults on europa. *Journal of Geophysical Research*, 105:22,617–22,627, 2000.

[31] C. L Hulbe, C. . LeDoux, and K. Cruikshank. Propagation of long fractures in the ronne ice shelf, antarctica, investigated using a numerical model of fracture propagation. *Journal of Glaciology*, 56:459–472, 2010.

[32] T. A. Hurford and K. M. Brunt. Antarctic analog for dilational bands on europa. *Earth and Planetary Science Letters*, 401:275–283, 2014.

[33] T. A. Hurford, A. R. Sarid, and R. Greenberg. Cycloidal cracks on europa: Improved modeling and nonsynchronous rotation implications. *Icarus*, 186:218–233, 2007.

[34] T. A. Hurford, B. G. Bills, P. Helfenstein, R. Greenberg, G. V. Hoppa, and D. P. Hamilton. Geological implication of a physical libration on enceladus. *Icarus*, 2009.

[35] T. A. Hurford, A. R. Sarid, R. Greenberg, and B. G. Bills. The influence of obliquity on europan cycloid formation. *Icarus*, 202:197–215, 2009.

[36] H. Hussmann and T. Spohn. Thermal-orbital evolution of io and europa. *Icarus*, 171:391–410, 2004.

[37] H. Hussmann, T. Spohn, and K. Wieczerkowski. Thermal equilibrium states of europa's ice shell: Implications for internal ocean thickness and surface heat flow. *Icarus*, 156:143–151, 2002.

[38] H. Hussmann, D. Shoji, G. Steinbrugge, A. Stark, and F. Sohl. Constraints on dissipation in the deep interiors of ganymede and europa from tidal phase-lags. *Celestial Mechanics and Dynamical Astronomy*, 126:131–144, 2016.

[39] K. Hutter. *Theoretical glaciology: material science of ice and the mechanics of glaciers and ice sheets*. D. Reidel Publishing Co., Dordrecht, Netherlands, 1983.

[40] G. R. Irwin. Analysis of stresses and strains near the end of a crack transversing a plate. *Journal of Applied Mechanics*, 24:361, 1957.

[41] H. M. Jara-Orue. State of stresses at europa's icy surface: a strong case for the existence of a subsurface ocean. Master's thesis, Technical University Delft, 2009.

[42] H. M. Jara-Orue and B. L. A. Vermeersen. Effects of low-viscous layers and a non-zero obliquity on surface stresses induced by diurnal tides and non-synchronous rotation: The case of europa. *Icarus*, 215:417–438, 2011.

[43] S. D. Kadel, S. A Fagents, and R. Greele. Trough-bounding ridge pairs on europa. considerations for an endogenic model of formation. In *Lunar Planetary Science Conference XXIX*, 1998.

[44] S. A. Kattenhorn. Nonsynchronous rotation evidence and fracture history in the bright plains region, europa. *Icarus*, 157:490–506, 2002.

[45] S. A. Kattenhorn and S. T. Marshall. Fault-induced perturbed stress fields and associated tensile and compressive deformation at fault tips in the ice shell of europa: implications for fault mechanics. *Journal of Structural Geology*, 28:2204–2221, 2006.

[46] S. A. Kattenhorn and L. M. Prockter. Evidence for subduction in the ice shell of europa. *Nature Geoscience*, 7:762–767, 2014.

[47] W.M. Kaula. *Theory of Satellite Geodesy: Applications of Satellites to Geodesy.* Blaisdell Publishing Company, 1966.

[48] K. K. Khurana, M. G. Kivelson, D. J. Stevenson, G. Schubert, C. T. Russell, R. J. Walker, and C. Polanskey. Induced magnetic fields as evidence for subsurface oceans in europa and callisto. *Nature*, 395:777–780, 1998.

[49] M. G. Kivelson, K. K. Khurana, C. T. Russell, M. Volwerk, R. J. Walker, and C. Zimmer. Galileo magnetometer measurements: A stronger case for a subsurface ocean at europa. *Science*, 289:1340–1344, 2000.

[50] E. Larour, E. Rignot, and D. Aubry. Modelling of rift propagation on ronne ice shelf, antarctica, and sensitivity to climate change. *Geophysical Research Letters*, 31, 2004.

[51] E. Larour, E. Rignot, and D. Aubry. Processes involved in the propagation of rifts near hemmen ice rise, ronne ice shelf, antarctica. *Journal of Glaciology*, 50, 2004.

[52] S. Lee, R. T. Pappalardo, and N. C. Makris. Mechanics of tidally driven fractures in europa's ice shell. *Icarus*, 177:367–379, 2005.

[53] A. C. Leith and W. B. McKinnon. Is there evidence for polar wander on europa? *Icarus*, 120:387–398, 1996.

[54] J.J. Lissauer and I. De Pater. *Fundamental Planetary Science.* Cambridge University Press, 2013.

[55] A. E. H. Love. *A Treatise on the Mathematical Theory of Elasticity.* Cambridge University Press, 1927.

[56] M. Manga. Formation of bands and ridges on europa by cyclic deformation: Insights from analogue wax experiments. *Journal of Geophysical Research*, 109, 2004.

[57] S. T. Marshall and S. A. Kattenhorn. A revised model for cycloid growth mechanics on europa: Evidence from surface morphologies and geometries. *Icarus*, 177:341–366, 2005.

[58] A. S. McEwen. Tidal reorientation and the fracturing of jupiter's moon europa. *Nature*, 321:49–51, 1986.

[59] H. Moritz. *Advanced Physical Geodesy.* Herbert Wichmann Verlag Karlsruhe, 1980.

[60] R. H. Mottram and D. I. Benn. Testing crevasse-depth models: a field study at breioamerkurjokull, iceland. *Journal of Glaciology*, 55:746–752, 2009.

[61] C.S. Niebur, J.S. Salute, J.L. Green, and D. C. Schurr. Europa lander study. Technical report, NASA, Jet Propulsion Laboratory, 2017.

[62] F. Nimmo. Causes, characteristics and consequences of convective diapirism on europa. *Geophysical Research Letters*, 29:24, 1–4, 2002.

[63] F. Nimmo. Stress generated in cooling viscoelastic ice shells: applications to europa. *Geophysical Research Letters*, 109, 2004.

[64] F. Nimmo, R. T. Pappalardo, and B. Giese. On the origins of band topography, europa. *Icarus*, 116:21–32, 2003.

[65] G. W. Ojakangas and D. J. Stevenson. Thermal state of an ice shell on europa. *Icarus*, 81:220–241, 1989.

[66] G. W. Ojakangas and D. J. Stevenson. Polar wander of an ice shell on europa. *Icarus*, 81:242–270, 1989.

[67] R. Pappalardo and M. D. Coon. A sea analog for the surface of europa. In *Lunar Planetary Science Conference XXVII*, volume XXVII, pages 997–998, 1996.

[68] R. T. Pappalardo and A. C. Barr. The origin of domes on europa: The role of thermally induced compositional diapirism. *Geophysical Research Letters*, 31, 2004.

[69] R. T. Pappalardo, J. W. Head, R. Greeley, R. J. Sullivan, C. Pilcher, G. Schubert, W. B. Moore, M. H. Carr, J. M. Moore, M. J. S. Belton, and D. L. Goldsby. Geological evidence for solid-state convection in europa's ice shell. *Nature*, 391:365–368, 1998.

[70] R. T. Pappalardo, M. J. S. Belton, H. H. Breneman, M. H. Carr, C. R. Chapman, G. C. Collins, T. Denk, S. Fagents, P. E. Geissler, B. Giese, R. Greeley, R. Greenberg, J. W. Head, P. Helfenstein, G. Hoppa, S. D. Kadel, K. P. Klaasen, J. E. Klemaszewski, K. Magee, A. S. McEwen, J. M. Moore, W. B. Moore, G. Neukum, C. B. Phillips, L. M. Prockter, G. Schubert, D. A. Senske, R. J. Sullivan, B. R. Tufts, E. P. Turtle, R. Wagner, and K. K. Williams. Does europa have a subsurface ocean? evaluation of the geological evidence. *Journal of Geophysical Research-Planets*, 104:24015–24055, 1999.

[71] R. T. Pappalardo, W. B. McKinnon, and K. K. Khurana. *Europa*. The University of Arizona Press, 2009.

[72] W.S.B. Paterson. *The Physics of Glaciers*. Pergamon/Elservier, 1994.

[73] S. J. Peale. Generalised cassini's laws. *The Astronomical Journal*, 74, 1969.

[74] W. R. Peltier. Glacial-isostatic adjustment-i. the forward problem. *Geophysical Journal International*, 46:605–646, 1976.

[75] C.B. Pilcher, S.T. Ridgway, and T.B. Mccord. Galilean satellites - identification of water frost. *Science*, 178:1087–1089, 1972.

[76] B. Preblich, R. Greenberg, J. Riley, and D. O'Brien. Tidally driven strike–slip displacement on europa: Viscoelastic modeling. *Planetary and Space Science*, 55:1225–1245, 2007.

[77] L. M. Prockter and R. T. Pappalardo. Folds on europa: Implications for crustal cycling and accommodation of extension. *Science*, 289:941–943, 2000.

[78] L. M. Prockter, J. W. Head, R. T. Pappalardo, R. J. Sullivan, A. E. Clifton, B. Giese, R. Wagner, and G. Neukum. Morphology of europan bands at high resolution: A mid-ocean ridge-type rift mechanism. *Journal of Geophysical Research-Planets*, 107, 2002.

[79] R. Qin, W. R. Buck, and L. Germanovich. Comment on "mechanics of tidally driven fractures in europa's ice shell" by s. lee, r.t. pappalardo, and n.c. makris [2005. icarus 177, 367-379]. *Icarus*, 189:595–597, 2007.

[80] N. Rambaux, T. Van Hoolst, and Ö Karatekin. Librational response of europa, ganymede, and callisto with an ocean for a non-keplerian orbit. *Astronomy and Astrophysics*, 2011.

[81] J. A. Rathbun. Ice diapirs on europa' implications for liquid water. *Geophysical Research Letters*, 25: 4157–4160, 1998.

[82] A. R. Rhoden, B. Militzer, E. M. Huff, T. A. Hurford, M. Manga, and M. A. Richards. Constraints on europa's rotational dynamics from modeling of tidally-driven fractures. *Icarus*, 210:770–784, 2010.

[83] A. R. Rhoden, T. A. Hurford, and M. Manga. Strike-slip fault patterns on europa: Obliquity or polar wander? *Icarus*, 211:636–647, 2011.

[84] A. R. Rhoden, T. A. Hurford, L. Roth, and K. Retherford. Linking europa's plume activity to tides, tectonics, and liquid water. *Icarus*, 253:169–178, 2015.

[85] M. A. Rist, P. R. Sammonds, S. A. F. Murrel, P.G. Meredith, H. Oeter, and C.S.M. Doake. Experimental fracture and mechanical properties of antarctic ice: Preliminary results. *Annals of Glaciology*, 23:284–292, 1996.

[86] L. Roth, J. Saur, K. D. Retherford, D. F. Strobel, P. D. Feldman, M. A. McGrath, and F. Nimmo. Transient water vapor at europa's south pole. *Science*, 343:171–174, 2014.

[87] R. Sabadini and B. L. A. Vermeersen. *Global Dynamics of the Earth: Application of Normal Mode Relaxation Theory to Solid-Earth Geophysics*. Kluwer Academic Publisher, first edition, 2004.

[88] R. Sabadini, B. Vermeersen, and G. Cambiotti. *Global Dynamics of the Earth: Application of Viscoelastic Relaxation Theory to Solid-Earth and Planetary Geophysics*. Springer, second edition, 2016.

[89] S. Salsa, F. M. G. Vegni, A. Zaretti, and P. Zunino. *A primer on PDEs: Models, Methods, Simulations*. Springer, 2013.

[90] A. R. Sarid, R. Greenberg, G. V. Hoppa, T. A. Hurford, B. R. Tufts, and P. Geissler. Polar wander and surface convergence of europa's ice shell: Evidence from a survey of strike-slip displacement. *Icarus*, 158:24–41, 2002.

[91] P. Schenk and R. T. Pappalardo. Topographic variations in chaos on europa: Implications for diapiric formation. *Geophysical Research Letters*, 31, 2004.

[92] P. Schenk, I. Matsuyama, and F. Nimmo. True polar wander on europa from global-scale small-circle depressions. *Nature*, 453:368–371, 2008.

[93] E. Schrama. Lecture notes on planetary sciences and satellite data processing. Technical report, Technical University Delft, 2015.

[94] E. M. Schulson. On the origin of a wedge crack within the icy crust of europa. *Journal of Geophysical Research-Planets*, 107, 2002.

[95] J. Souchay, S. Mathis, and T. Tokieda. *Tides in Astronomy and Astrophysics*. Springer, 2013.

[96] W. B. Sparks, K. P. Hand, M. A. McGrath, E. Bergeron, M. Cracraft, and S. E. Deustua. Probing for evidence of plumes on europa with hst/stis. *Astrophysical Journal*, 829, 2016.

[97] N. A. Spaun, R. T. Pappalardo, and J. W. Head. Evidence for shear failure in forming near-equatorial lineae on europa. *Journal of Geophysical Research*, 108:14,1–14,21, 2003.

[98] J. R. Spencer, L. K. Tamppari, T.Z. Martin, and L.D. Travis. Temperatures on europa from galileo photopolarimeter–radiometer: Nighttime thermal anomalies. *Science*, 284:1514–1516, 1999.

[99] S.W. Squyres, R.T. Reynolds, and P.M. Cassen. Liquid water and active resurfacing on europa. *Nature*, 301:225–226, 1983.

[100] H. Tada. *The Stress Analysis of Cracks Handbook*. Aeronautics Library, 2000.

[101] B. D. Tapley, B. E. Schutz, and G. H. Borne. *Statistical Orbit Determination*. Elsevier Academic Press, 2004.

[102] S. Timoshenko and D. H. Young. *Theory of Structures*. McGraw-Hill, second edition, 1965.

[103] B. R. Tufts. A san andreas-sized strike-slip fault on europa. In *Lunar Planetary Science Conference XXVIII*, 1996.

[104] B. R. Tufts, R. Greenberg, G. Geissler, G. Hoppa, R. Pappalardo, R. Sullivan, and the Galileo Imaging Team 1997. Crustal displacement features on europa. *Bull. Am. Astron. Soc.*, 29:983, 1997.

[105] B. R. Tufts, R. Greenberg, G. V. Hoppa, and P. Geissler. Astypalaea linea: A large-scale strike-slip fault on europa. *Icarus*, 141:53–64, 1999.

[106] B. R. Tufts, R. Greenberg, G. Hoppa, and P. Geissler. Lithospheric dilation on europa. *Icarus*, 146:75–97, 2000.

[107] R. H. Tyler. Strong ocean tidal flow and heating on moons of the outer planets. *Nature*, 456:770–773, 2008.

[108] C. J. Van der Veen. Fracture mechanics approach to penetration of surface crevasses on glaciers. *Cold regions science and technology*, 27:31–47, 1998.

[109] C. J.an Van der Veen. Fracture mechanics approach to penetration of bottom crevasses on glaciers. *Cold regions science and technology*, 27:213–223, 1998.

[110] B. L. A. Vermeersen. Planetary volcanism-lecture notes. Technical report, Technical University Delft, 2015.

[111] J. Wahr, Z. A. Selvans, M. E. Mullen, A. C. Barr, G. C. Collins, M. M. Selvans, and R. T. Pappalardo. Modeling stresses on satellites due to nonsynchronous rotation and orbital eccentricity using gravitational potential theory. *Icarus*, 200:188–206, 2009.

[112] K. F. Wakker. Fundamentals of astrodynamics. Technical report, Technical University Delft, 2015.

[113] C. C. Walker. *Fracture of Antarctic ice shelves and implications for the icy satellites of the outer solar system*. PhD thesis, The University of Michigan, 2013.

[114] J. R. Wertz. *Orbit and Constellation Design and Managment*. Springer, 2001.

[115] H. M. Westergaard. Bearing pressures and cracks. *Journal of Applied Mechanics*, 66:49, 1939.

[116] K. L. Zahnle, L. Dones, and H.F. Levison. Cratering rates on the galilean satellites. *Icarus*, 136:202–222, 1998.